Exploiting the Thermoresponsive Properties of Poly(2-oxazoline)s for Biofabrication

Anwendung der Thermoresponsivität von Poly(2-oxazolin) für die Biofabrikation

Doctoral thesis for a doctoral degree
at the Graduate School of Life Sciences,
Julius-Maximilians-Universität Würzburg,
Section: Biomedicine

submitted by
Matthias Ryma
from Würzburg

Würzburg 2021

Submitted on:

Members of the Thesis Committee

Chairperson:

Primary Supervisor: Prof. Dr. Jürgen Groll

Supervisor (Second): Prof. Dr. Süleyman Ergün

Supervisor (Third): Prof. Dr. Iwona Cicha

Date of Public Defence:

Date of Receipt of Certificate

Table of Contents

List of Figures

List of Tables

Chapter 1

Aims and Motivation

Biofabrication is the generation of biologically relevant products based on the combination of living cells, materials and fabrication methods for improved applications in medicine.[1] The scientific field of biofabrication is rapidly evolving with increasing numbers of publications each year. There is a continuous development of materials and fabrication processes, which involves e.g., chemical improvements of hydrogels and biopolymers or increasing resolution of additive manufacturing approaches. Because of these steady advances, the scientific objectives naturally become more and more specialized, leading to very complex approaches for only small improvements. For example, biocompatible polymers like polyethylene glycol (PEG) need to be functionalized to generate hydrogels for 3D cell culture. However, the encapsulated cells are not able to attach to and spread inside of the matrix, which prevents biological function.[2] Therefore, another functionalization like the addition of peptides must be introduced to circumvent this effect and finally create a biocompatible matrix. The same property that fibrin hydrogels[3] or hydrogels based on gelatin crosslinked with transglutaminase[4] provide naturally without chemical modification.

This trend - Increasing chemical complexity for small biological improvements.[5,6] - can also be observed in other branches of biofabrication, like bioprinting or electrospinning. Based on this development, two questions remain:

1. Is further modification always necessary to create new applications?
2. Are the intrinsic properties of different materials already fully exploited?

Driven by these questions, this thesis aims to make use of basic non-modified materials to create new applications for biofabrication. However, materials used in a biological and medical context need to fulfill several requirements: First, materials must be biocompatible and therefore not cytotoxic. Second, materials must be stable and express their unique effects in the physiological range. Especially exceeding the optimal temperature of 37°C for longer incubation times must be avoided, as it would lead to the death of cells and tissues.

A polymer class fulfilling these requirements are poly(2-oxazoline)s (POx). POx are an emerging polymer class, which mainly stand out because of their biocompatibility, modification potential and thermoresponsive behavior in aqueous solutions.[7] In case of POx,

thermoresponsiveness means the ability to dissolve in water below a certain temperature, the Lower Critical Solution Temperature (LCST).

There are 3 homopolymers from the POx family, which express their LCST in the physiological range between room and body temperature: poly(2-*n*propyl-2-oxazoline) (P*n*PrOx), poly(2-*cyclo*propyl-2-oxazoline) (P*cyclo*PrOx) and poly(2-*iso*propyl-2-oxazoline) (P*i*PrOx). Depending on the chain length and composition of the aqueous solution, P*n*PrOx exhibits its LCST at ~20° C and P*cyclo*PrOx at ~25° C, while the LCST of P*i*PrOx is at ~35° C.[8] With its higher LCST, P*i*PrOx would dissolve quickly outside of the incubator and therefore does not provide a sufficient timeframe for handling in cell culture related studies. In contrast, the LCST of P*n*PrOx and P*cyclo*PrOx is near room temperature, therefore extending the handling timeframe significantly. For this reason, the following studies focused on P*n*PrOx and P*cyclo*PrOx.

In this thesis, three different applications of P*n*PrOx and P*cyclo*PrOx were developed that utilize their unique characteristics: A coating for cell sheet creation, the fabrication technique Melt Electrofibrillation and a prevascularization approach (**Figure 1**).

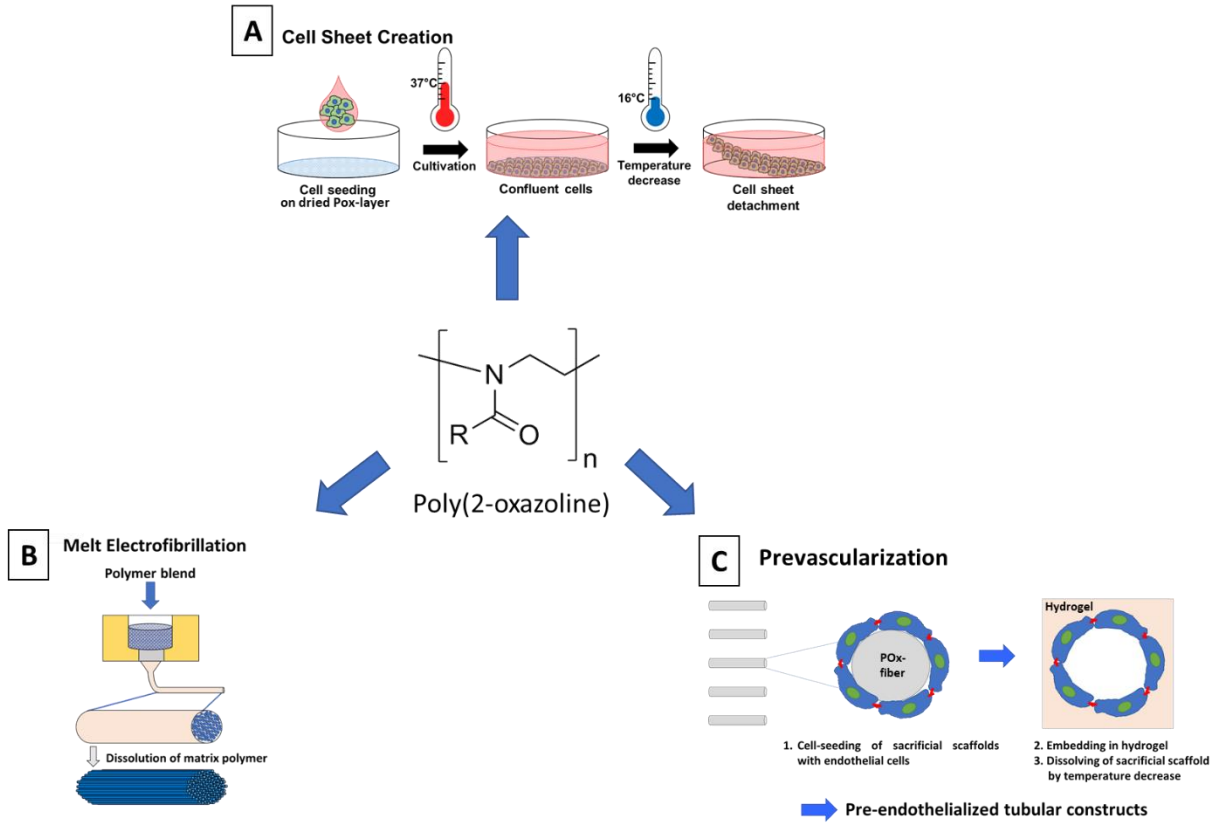

Figure 1: Methodological summary of this thesis. *A: Easy-to-apply POx-coating for cell sheet creation. B: Melt electrofibrillation for the creation of polymer fibril bundles. C: A prevascularization approach based on melt electrowritten POx-fibers.*

Chapter 2 provides an overview of current methods, materials, and strategies in the field of biofabrication. Especially the role of biomaterial inks and thermoresponsive materials is highlighted here.

In **Chapter 3** P*n*PrOx was established as an easy-to-use coating for cell sheet engineering.[9] To usually introduce cell sheet technology in biological laboratories, expensive precoated cell culture plastics can be acquired commercially. As an alternative, the cell culture plastics can be coated in the lab to avoid high costs. However, this requires specialized equipment and competent personnel with a chemical background, which are usually not part of conventional biological labs. Therefore, P*n*PrOx was used to develop an easy-to-use coating procedure to enable simple generation of a functional coating for cell sheet engineering.

Chapter 4 provides the establishment of a new technique, which was termed "Melt Electrofibrillation". It is based on Melt Electrowriting (MEW), a fabrication method that allows the directed deposition of up to submicron polymer filaments by introducing voltage. Instead of using only one polymer as melt, compatible polyblends are fabricated with MEW. The electrohydrodynamic stretching of the fiber during fabrication leads to a flow-induced directed phase separation. By subsequent dissolution of the matrix polymer, nano-fiber bundles with a remarkable structural similarity to native collagen I fibril bundles are created. In this project, the following polymer blends with 30% fibrilling and 70% matrix polymer were used: P*n*PrOx + P*cyclo*PrOx and PCL + PVAc, respectively. Scaffolds created via Melt Electrofibrillation were further applied for polarization of human macrophages to a pro-healing, anti-inflammatory M2-like phenotype.[10] Altough many studies indicated a differentiation and polarization of different cell types on aligned topographies[11-13], they lacked efficiency compared to differentiation by soluble factors. However, here the induction of polarization was as efficient as by IL-4 cytokine treatment.

Chapter 5 shows the advances in the establishment of P*n*PrOx and P*cyclo*PrOx scaffolds as sacrificial materials for biofabrication constructs. The main bottleneck for tissue engineering and biofabrication is the need for a perfusable vascular system to keep artificial tissues exceeding size of >1 mm alive by providing oxygen and nutrition.[14] At the time of submitting this thesis, no method allows the creation of perfusable channels in tissues with sizes below 200 µm and only a few studies demonstrated diameters below 500 µm to this day.[15] Furthermore, the standard procedure for endothelialization is perfusion with endothelial cells after generation of the channels. Due to inefficient attachment, this requires a high number

of cells and takes at least 7 days to fully endothelialize the channel.[16,17] Therefore, a method was developed within this thesis called “inverse engineering”, where cells are seeded onto sacrificial scaffolds, grown to confluency, and embedded into a biocompatible hydrogel matrix. After a short dissolution time of 2 minutes, the sacrificial scaffolds were removed, and the endothelial cell layer remains attached to the channel wall of the hydrogel.

In detail, the polymers were first printed into scaffolds resembling the shape of vascularization with its branches and interconnections. Embedding them into hydrogels led to swelling of the fibers, with adjacent fibers lastly fusing. By reducing the temperature below their respective LCST, the polymers dissolve, leaving a natural interconnecting channel depending on the design of the printed scaffolds behind. The material and its dissolution process were further proven not to affect cell viability negatively.

The next step was the addition of endothelial cells before embedding the scaffolds into a hydrogel. The main challenge to further establish inverse biofabrication was the insufficient stability of P*n*PrOx and P*cyclo*PrOx scaffolds in aqueous solutions, which is a prerequisite for cell culture. To overcome this issue, P*n*PrOx was partially crystallized to allow an increased stability for the cost of reduced dissolution capabilities. With the endothelial cell line HMEC-1 the proof-of-concept was given. However, primary endothelial cells showed no attachment, and it was not possible to flush out crystalline P*n*PrOx residues out of more complex structures. To overcome this issue, dip coating with the biocompatible and biodegradable polymer poly(lactid-co-glycolid) (PLGA) (50:50) was used as another way to improve stability. However, the dipcoating solvents lead to crystallization of P*n*PrOx and the amorphous P*cyclo*PrOx was used instead. Using this approach, good stability of the scaffolds was achieved, and after air plasma treatment, primary cell attachment succeeded.

Chapter 6 provides a concluding discussion of all three applications of POx and their position in the field of biofabrication.

Chapter 7 is a summary of the established methods and results of the thesis.

Chapter 2

Introduction

2.1 Biofabrication

2-dimensional (2D) cell culture was and is still the status quo of biological and pharmaceutical research in universities, institutes, and industry. The reason is mainly the simplicity of this method and the unavailability of 3D alternatives. However, 2D cell culture has obvious limitations.[18,19] First, except for specialized tissue like endothelium and epithelium, cells do not naturally grow in a 2D environment. They are embedded in a 3D matrix with several other cell types, which interact with each other. The matrix composition itself and factors embedded within are influencing the cells in a way, which is not possible to mimic in 2D. This significantly impacts cell proliferation, differentiation, mechano-responses, and cell survival.[20] Therefore, much research conducted in 2D cannot be correlated to the natural state in 3D tissues. This is also a reason, why pharmaceutical testing of potential new drug candidates in 2D often leads to false-positive results, that fail in eventual animal tests, increasing the costs of drug development.[21] Furthermore, advances in 3D cell culture could ultimately lead to the generation of replacement organs, covering the shortage of donor organs for patients in need of transplants while circumventing the immune system without immunosuppressive.[22]

3D cell culture, or tissue engineering, is the combination of cells with a biocompatible matrix.[23] However, the functionality of a 3D tissue is not given by merely mixing cells and matrix for cultivation. Instead, the hierarchical positioning of cells, matrix and other components are decisive to mimic tissues and their function correctly. The science of creating these functional structures of biocompatible materials combined with living cells is called biofabrication. Biofabrication in the context of tissue engineering and regenerative medicine has recently been defined as “the automated generation of biologically functional products with structural organization from living cells, bioactive molecules, biomaterials, cell aggregates such as micro-tissues, or hybrid cell-material constructs, through Bioprinting or Bioassembly and subsequent tissue maturation processes.”[1]

The main goal of biofabrication is, therefore, the creation of biologically functional products. This means per definition: if a fabrication method leads to the structural organization of living cells, it is considered a biofabrication method.

2.2 The critical role of hierarchy and vascularization for the biofabrication of larger constructs

An important aspect of biofabrication is the creation of hierarchical structures, mimicking the allocation of cells and the macro- and microstructural features of the extracellular matrix (ECM). Depending on the tissue, different hierarchical structures with specific functionalities are present. Accordingly, as the main component of the connective tissue, collagen is hierarchically structured as highly ordered and aligned fibers.[24] For example, muscle[25] and tendon tissues[26] consist of their respective cells embedded in a 3D fibrous matrix, where these collagen fibers are highly aligned to resist tensile stress. Even cartilage, which seems to be a simple tissue at first glance, provides a complex hierarchical structure comprised of three zones with different fiber and cell distribution.[27] A further type of hierarchical structures are epithelial and endothelial tissue. Here, cells grow on 2D surfaces either within monolayers (endothelium)[28] or multilayers (epidermis).[29]

Especially the vasculature has a complex branched structure, ranging from large multilayered arteries like the aorta to tiny microvascular capillaries, which ensure nutrition and oxygen supply throughout the whole body.[30] This leads to the complete supply of every cell *in vivo*, where the highest distance between single capillaries is no more than 200 µm.[31] However, this density is only needed due to the high cell number and the complex ECM with different soluble and solid components. Despite the *in vivo* situation, it has been shown that cells also survive in developing artificial 3D tissues with a size of even above 1 mm.[32,33] Furthermore, the self-organization capabilities of endothelial cells caused by stimuli like soluble factors and hypoxia lead to vessel sprouting[34] and to neovascularization of the surrounding tissue in later stages of the tissue maturation. This simplifies the required complexity of hierarchical tissue generation via biofabrication methods, where resolution is a big challenge to overcome.

Nevertheless, vascularization remains the most crucial hurdle to overcome for the generation of functional, reasonable sized artificial tissues, which can be used for accurate *in vitro* tissue models for pharmaceutical testing or even organ replacement in patients. The mimicry of bigger arterial structures with diameters above 500 µm has been shown in several studies.[35-

[37] However the biofabrication community is still struggling with the generation of perfusable channels with diameters below 200 µm and is still far away from actual biomimetic channel networks comparable to vascular branching.

Therefore, the mimicry of these hierarchical features is the main challenge as well as the main opportunity in the field of biofabrication. Although cells intrinsically provide the properties to create and shape their surrounding matrix[38], they are not able to recreate complex tissue with macroscopic features in a sufficient timeframe. Nonetheless, biofabrication methods provide the tools to mimic these macroscopic features and to improve tissue engineering.

Currently, there is no omnipotent biofabrication method, which can facilitate and fulfil the requirements for the creation of every artificial tissue type. In the next paragraph two examples of biofabrication methods with obvious disadvantages are given. However, the employment of these methods for the generation of tissues with specific features has led to useful, interesting, and applicable results.

A very thoroughly studied method is cell sheet engineering, which allows harvesting and stacking of intact cell layers to create various tissues.[39] Although stacking of cell sheets to create 3D tissue is possible, but highly complex, the creation of cell sheets from epithelial tissue like cornea has been effectively used as a biological implant. [40] Since corneal tissues typically grow in a 2D manner, the cells can proliferate, differentiate, and create their own matrix in a more natural way than 3D cell culture. Furthermore, the newly formed matrix is kept intact during harvesting of the cell sheet. This method was even successfully utilized to reconstruct cornea in human trials with cell sheets composed of oral mucosal epithelium.[40] No other biofabrication method can recreate these epithelial structures as exact as cell sheet engineering. However, this method is not easily transferable to other applications like vascularized tissue with a more complex 3D-hierarchy and cell distribution, which exceeds the potential of stacked 2D layers.

Another suitable approach is the creation of scaffolds for heart valve tissue engineering based on MEW.[41] Here, the functionality was mimicked by introducing fiber orientation, which resembles the orientation of collagen fibers in heart valve leaflets. The advantages of MEW, namely direct fiber deposition and resolution, were easily adaptable for the flat leaflets. The clever utilization of the advances offered by the technique lead to the development of a study with very interesting results. However, since MEW is limited in stacking height of the fibers, it

cannot be used for 3D tissue engineering approaches, which include artificial tissues with sizes above ~1 mm.

Although increasing progress was made, and different methods and materials were developed, so far, only a few useful biological approaches were identified. Moreover, although the field of bioprinting is evolving rapidly, there are only a few clinical successes up until now. Each method seems to lack either resolution[42], accuracy[43] or upscalable volume.[44] Therefore, more research should be conducted focusing on the creation of relevant biological products, by exploiting the specific advantages of biofabrication methods in combination with specialized materials. In this context, especially the lack of adequate biofabrication methods for sufficient vascularization in micrometer scale is the most significant bottleneck for current developments to evolve their results into applicable, clinically relevant products.

2.3 Bioinks and biomaterial ink scaffolds

Biofabrication methods can be mainly divided into 2 categories (**Figure 2**):

1. Bioprinting of bioinks

Bioprinting is the selective distribution of cells, biomaterials and growth factors to manufacture living 3D tissues via additive manufacturing (AM) technologies.[1] Here, cells are directly embedded in hydrogels and are therefore part of the processed biomaterial, resulting in the so-called bioink.[45]

2. Biomaterial ink scaffolds for post-fabrication cell seeding

Compared to bioinks, biomaterial inks do not incorporate cells as part of the processed biomaterial. Since the cells are seeded post-fabrication, the requirements for processing are much lower than in bioinks, where cells need to be kept alive during and after fabrication. Therefore, material processing of biocompatible thermoplastic polymers like polycaprolactone (PCL), biopolymers like alginate and gelatin, metals, cements, or lithography-based resins are included in the group of biomaterial inks.

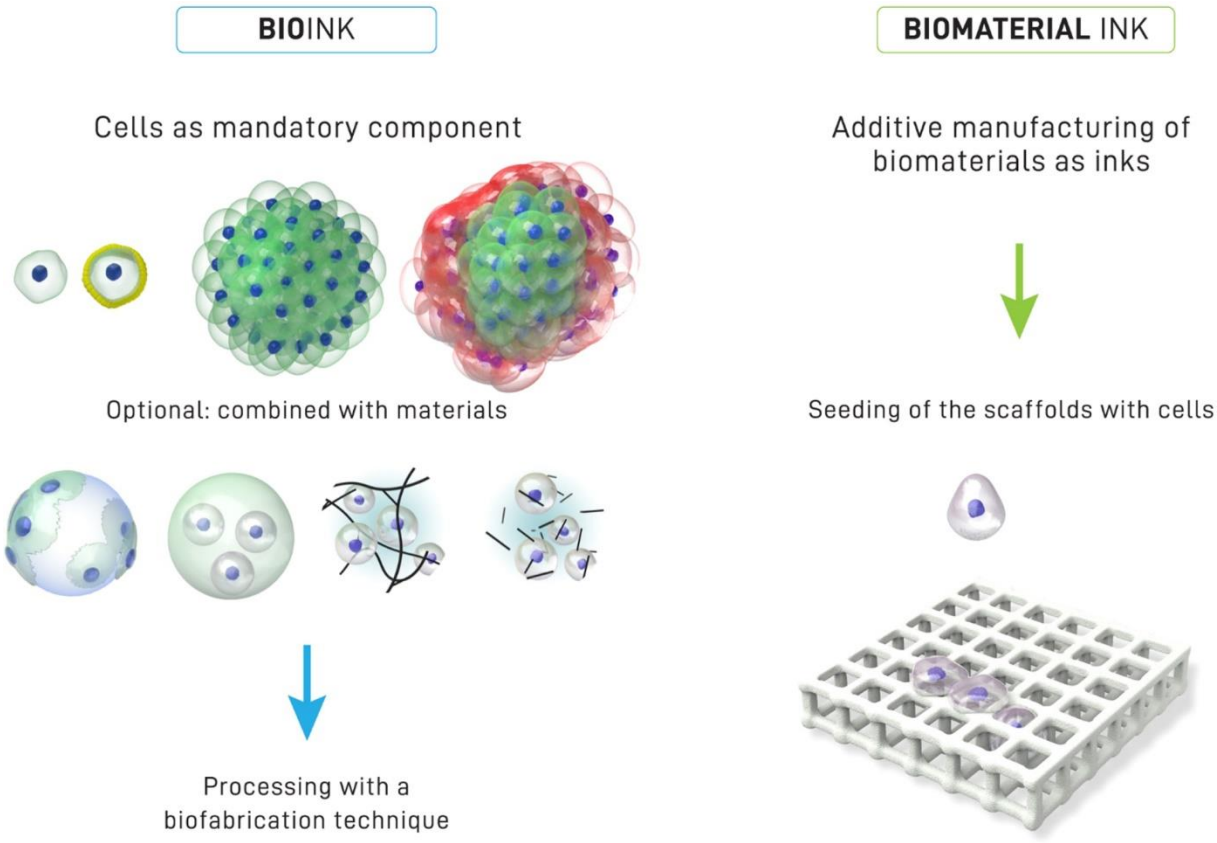

Figure 2: Distinction between bioinks and biomaterial inks. *Bioinks involve cells as a mandatory component, which is then processed with a biofabrication technique. Biomaterial inks are fabricated without cells during the fabrication process, but cells are seeded post generation. Taken from Groll et al. (2018) "A definition of bioinks and their distinction from biomaterial inks"*[45]

In the following section, more details will be given about several bioprinting methods for bioinks and the generation of fibrous scaffolds based on biomaterial inks. Furthermore, the general role of thermoresponsive materials in the light of biofabrication, especially cell sheet engineering, will be stated. Since poly(2-oxazoline)s (POx) are the main material used within this thesis, their role in biofabrication will be especially highlighted.

2.2 Bioprinting

The term "bioprinting" was first introduced by Vladimir Mironov in 2003 within the context of organ printing.[46] In general, bioprinting can be divided into several technologies, with pressure-assisted systems being the most prominent ones because of their low costs and abundant availability (**Figure 3** A, B).[47,48] Here, a syringe is filled with a bioink and extruded as a filament by applying gas pressure. The resolution is defined by bioink viscosity, pressure, nozzle diameter, and deposition speed. The limiting factor is the shear stress induced cell viability issue, which increases due to a decreased nozzle diameter, leading to average strand thicknesses between 200 µm to 1 mm.[42]

Another technology is Inkjet or droplet-on-demand bioprinting. Here, droplets of bioinks are produced by thermal, piezo, electromagnetic, or even acoustic triggers.[49] With this, droplets in micro- to picolitre range can lead to the generation of strands within 100 µm resolution. However, this technique is limited by bioink viscosity and the strong impact on cell viability.[49] Light-assisted bioprinting, also termed stereolithography (SLA), is an emerging technique which utilizes light to crosslink hydrogels. Laser-based SLA is used for voxel-precise crosslinking in a photosensitive resin at specific points, where the light is focused with enough energy input for the reaction.[47] Another variant is digital light processing (DLP). Instead of focusing light on one specific point in the resin, a dynamic mirror array selectively projects light into areas to crosslink all points in each layer.[50] This leads to an increase in processing speed, resulting in enhanced cell viability. Two-photon polymerization is another alternative with very high resolution, where voxels are selectively irradiated. Because of the high accuracy, the processing time is increased and only small constructs can be created in a sufficient timeframe.[51] A very recent technology is volumetric SLA, enabling the user to create 3D objects in a resin within 1 minute (**Figure 3** C, D). For this, a cell-laden photocrosslinkable hydrogel resin is rotated and tomographic images are projected into the resin.[52] Another current technique which should be mentioned is SLATE (stereolithographic apparatus for tissue engineering), which leads to the fast generation of hydrogels by using projection stereolithography.[53] Here, the speed of hydrogel creation is very fast and enables the generation of complex structures for mimicking organ morphology. Although processing speed challenges have been overcome by methods like DLP or volumetric SLA, one big challenge remains: The controlled distribution of different cell types is not possible with the conventional technologies based on light-assisted bioprinting.

A very recently developed technology is printing into support baths based on FRESH-technology (freeform reversible embedding of suspended hydrogels) [54] or jammed microgels (**Figure 3** E, F)[55], allowing to generate highly defined structures in 3D. Additionally, soft bioinks, which do not have printable properties with conventional printing methods, can be used for bioprinting, leading to the generation of thick organ-like structures with high resolution.[32] However, support bath printing is very slow since fast printing speeds can deform the initially printed structures.

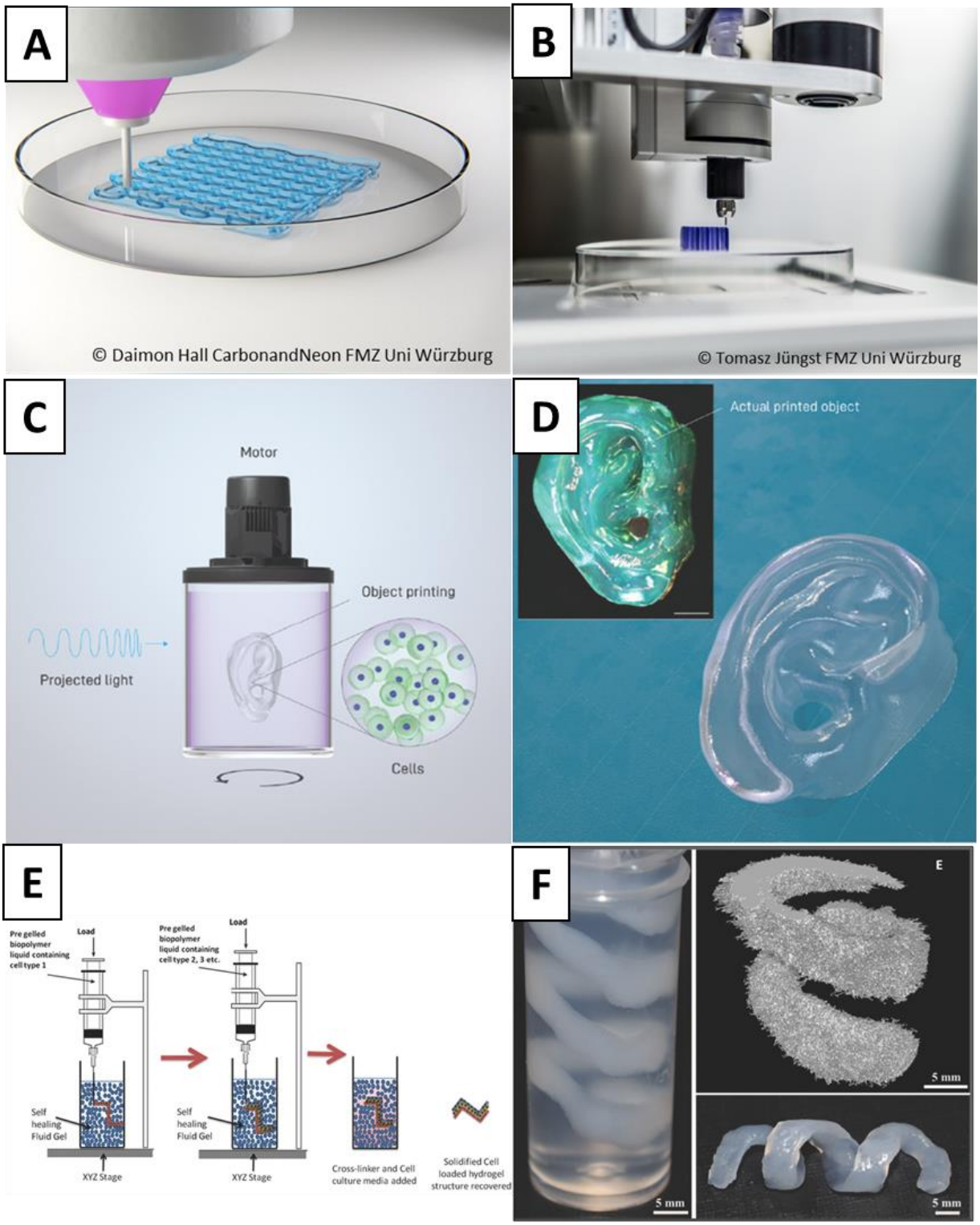

Figure 3: Examples of current bioprinting techniques. *A, B: Schematic and example of FDM-printed biological hydrogels. C, D: Schematic and example of light-assisted bioprinting. Taken from Bernal et al. (2019) "Volumetric Bioprinting of Complex Living-Tissue Constructs within Seconds"[52] E, F: Schematic and example biological hydrogels printed in a support bath. Taken and adapted from Moxon et al. (2017) "Suspended Manufacture of Biological Structures"[44]*

2.3 Biomaterial Ink Scaffolds

An important aspect of biofabrication is the generation of scaffolds, which can be post-seeded with cells. Since cells cannot be incorporated directly during biomaterial ink scaffold fabrication due to certain requirements such as high temperature, solvents and other bioincompatible processes, these scaffolds must exhibit a certain porosity for cell infiltration.

2.3.1 Solvent casting/particle leaching

The most basic and conventional ways to create scaffolds are solvent casting/particle leaching.[56] Here, dissolvable porogens like gelatin or salts are mixed with a dissolved polymer. After solvent casting, the solvent evaporates and forms a composite of the polymer and the porogens. The porogens are leached by embedding the composite in a selective solvent, which does not dissolve the polymer. In case of gelatin or salts, water leads to the dissolution of the porogens and the creation of the final porous scaffold.[57]

Furthermore, non-miscible polymer blends can be used for this method instead of porogens.[58] By dissolving the polymers in different concentrations in a common solvent, blends can be created. The selective leaching of one polymer then creates the porous structure and by changing the polymer ratios, the resulting pore sizes can be influenced.

2.3.2 Fiber-based scaffolds

The next category is fiber-based scaffolds. Compared to solvent casting/particle leaching, an AM method is used to create polymer fibers, that can be stacked for the generation of scaffolds. Besides conventional 3D printing, there are currently two main fabrication methods: Solution Electrospinning (SES) (**Figure 4**) and Melt Electrowriting (MEW) (**Figure 5**).

2.3.2.1 Solution Electrospinning (SES)

SES is a widely used technique for the fabrication of nanofibers into scaffolds[43] that requires a syringe pump, a collector, and a high-voltage power source. In brief, a syringe is filled with a dissolved polymer. A droplet is extruded at the syringe tip, which forms a so-called Taylor cone by the electrostatic force of the high-voltage source (**Figure 4** A). This leads to the generation of a jet, that is deposited randomly on a flat collector (**Figure 4** B) or aligned on a rotating cylindrical one (**Figure 4** C). During and after deposition, the solvent evaporates, leading to the creation of polymeric nanofibers.[59]

An essential aspect of SES is the range of materials, which can be utilized. Synthetic materials, like poly(ε-caprolactone) (PCL)[60], polyvinyl alcohol (PVA)[61], poly(lactide-co-glycolide) (PLGA)[62], and polyethylene oxide (PEO)[63] have been established for this system. Additionally, even natural polymers like collagen[64], gelatin[65], hyaluronic acid[66], and chitosan[67] were used for electrospinning and have been enhanced by crosslinking afterwards. Compared to natural ones, artificial polymers are often cost-effective and tunable regarding desired mechanical and morphological requirements. However, natural polymers provide cell recognition signals, which would need an additional modification in synthetic polymers.[68]

Since SES is solvent-based, it is also possible to mix synthetic and natural polymers to produce composite fibers with mechanical stability and cell adhesion motifs.[69,70] Moreover, it is possible to functionalize the fibers to improve specific properties like biocompatibility, e.g., by co-electrospinning with additives like inorganic nanoparticles[70], by post-modification of the surface with plasma-treatment[71] or by mimicking natural patterns like fiber alignment via electrospinning on a cylindrical collector rotating at high speeds.[72] Therefore, the versatility of SES led to several applications in the field of tissue engineering[68], like vascular[73], neural[74], bone[75], cartilage[76] and tendon tissue engineering[77]. Although products based on SES have been developed by different companies[78], none have yet been approved by the Food and Drug Administration (FDA).[79,80] The main reasons for this are safety issues, low productivity and lack of robust process and quality control.[81]

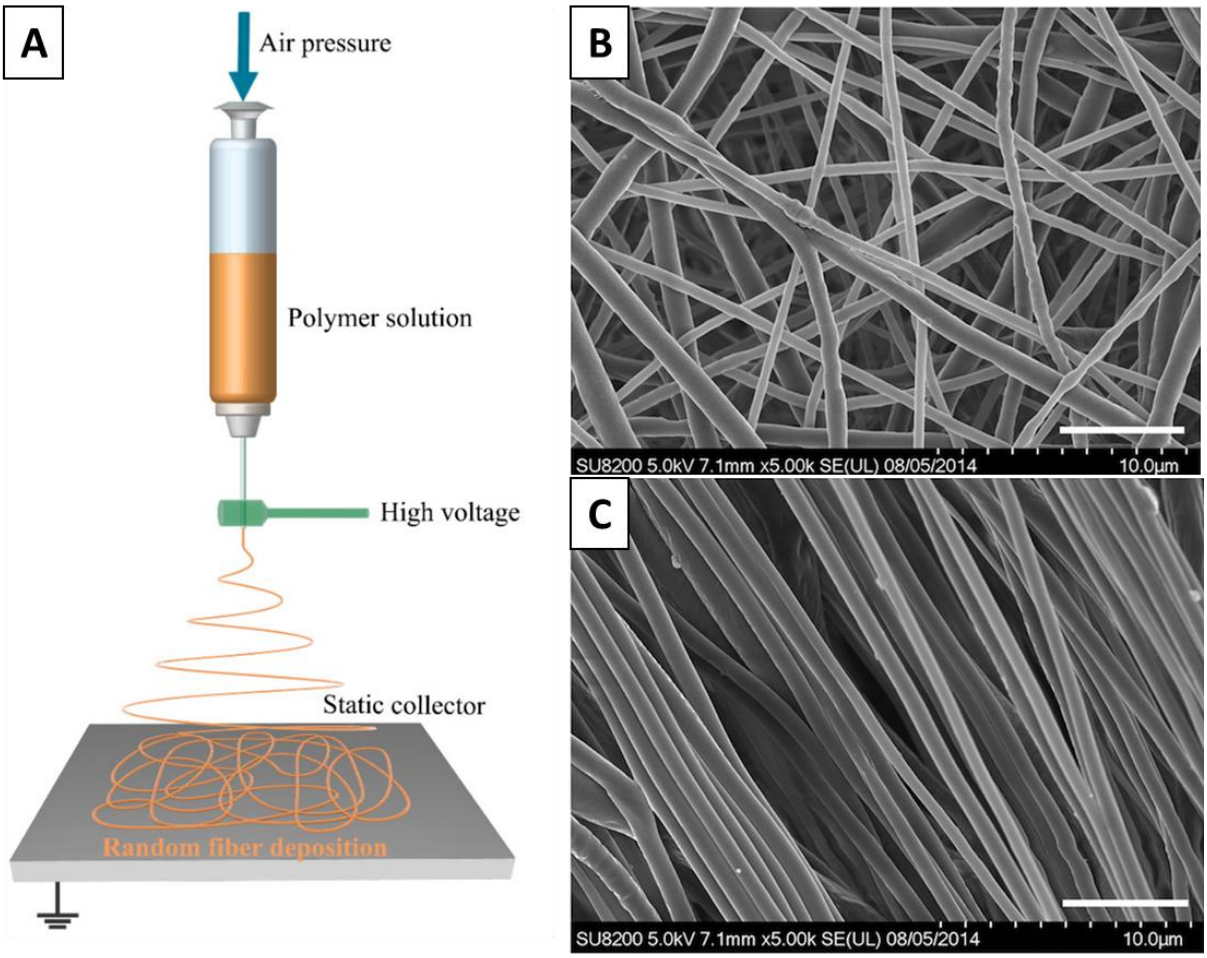

Figure 4: Fibrous scaffolds created by Solution Electrospinning (SES). *A: Schematic of SES. Taken from Afghah et al. (2019) "Biomimicry in Bio-Manufacturing: Developments in Melt Electrospinning Writing Technology Towards Hybrid Biomanufacturing "(2019).[82] Random (B) and aligned (C) scaffolds created via SES. Taken from Han et al. (2016) "Cell alignment induced by anisotropic electrospun fibrous scaffolds alone has limited effect on cardiomyocyte maturation".[83]*

2.3.2.2 Melt Electrowriting (MEW)

Another emerging technique for the creation of fiber-based scaffolds is Melt Electrowriting (MEW). It was first described in 2011[84] and has gained increased interest in the scientific community since 2016.[85] In short, a polymer is heated in a syringe and extruded through a nozzle via pneumatic pressure. By applying high voltage, the melt forms a Taylor cone at the tip of the nozzle leading to the generation of a molten polymer jet. Compared to SES, the jet is stable and can, therefore, be directly deposited on a translating collector plate to create scaffolds (**Figure 5** A).[84] Besides the standardized box-structures, this technology allows the generation of different geometries like triangular designs[86], sinusoidal architectures[87], and even tubular scaffolds by exchanging the flat collector plate with a cylindrical one.[88] Furthermore, by mainly changing pressure and collector speed, Hrynevich et al. (2018) were

able to create multimodal scaffold structures (**Figure 5** B).[89] Even the minimum porosity of melt electrowritten scaffolds was reduced to 40 µm.[90]

Most primary research in the field of MEW was conducted with PCL as material, because of the abundancy, simple printing parameters, and FDA approvement. However, with the increased interest, different materials have been established for MEW like poly(urea-siloxane)s[91], poly(vinylidene difluoride)[92] or polypropylene.[93] In contrast to SES, natural polymers are not processable because of their inability to melt without degradation. However, post-modification to improve the biocompatibility of the scaffolds has also been studied with proteins like antibodies[94] or decellularized matrix of adipose tissue[95] and inorganic coatings of calcium phosphate.[96]

MEW scaffolds have been applied in several ways including drug delivery, with studies investigating the drug release properties of e.g. dipyridamole[97], daunorubicin hydrochloride[98] and ciprofloxacin.[99] The most prominent MEW applications are in the context of tissue engineering, where melt electrowritten scaffolds have been used as fiber reinforcements for matrices. In this context, Castilho et al. (2018) designed an injectable hexagonal scaffold, which can support high tensile strains when placed on a contracting heart.[100] Also, by combining a specially designed scaffold with cells and fibrin hydrogels, Saidy et al. (2019) were able to mimic the morphology and function of a heart valve.[101] Furthermore, many studies were performed that prove the compatibility of MEW scaffolds with mono-[102,103] and co-culture[104,105], spheroid culture[106], *in vitro* tumor culture and humanized *in vivo* models.[107] The scaffolds have even been used as sacrificial materials for hydrogels[108] and silica glass[109], however not in a biocompatible way with cell consisting matrices. MEW is, therefore, a technique with many applications, especially in biofabrication. However, it is mainly limited by the materials applicable for this fabrication process, pore size resolution, and stacking height.

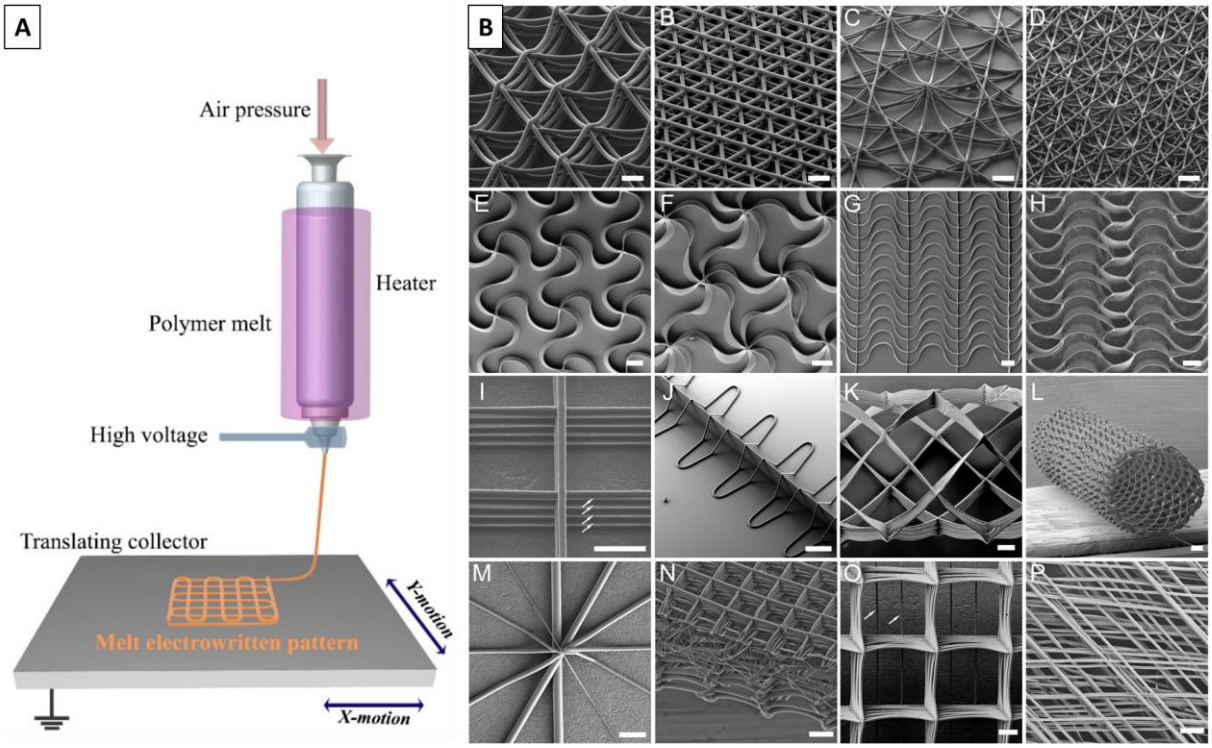

Figure 5: Fibrous scaffolds created by Melt Electrowriting (MEW). *A: Schematic of MEW. Taken from Afghah et al. "Biomimicry in Bio-Manufacturing: Developments in Melt Electrospinning Writing Technology Towards Hybrid Biomanufacturing ".[82] B: Examples of scaffolds which can be created via MEW. Taken from Robinson et al. "The Next Frontier in Melt Electrospinning: Taming the Jet ".[85]*

In conclusion, especially fiber-based biofabrication techniques have a great impact in the field of tissue engineering and regenerative medicine. Scaffolds have been adapted concerning material, morphology, mechanical strength, biocompatibility, and other properties to fulfill the requirements of specific tissues.

2.4 Thermoresponsive Materials

For biofabrication, the choice of materials is of great importance. Therefore, the development of new or improved polymers with specialized properties is always ongoing. The polymers are especially tailored to have enhanced biodegradability, biocompatibility, stability, and mechanical properties. This also led to the increased development of "smart" or "stimuli-responsive" biomaterials in the last decades.[110] Among those, the most abundant polymer types are thermoresponsive polymers, which exhibit a thermally induced phase-transition.[111] They can be divided into polymers exhibiting a Lower Critical Solution Temperature (LCST), Upper Critical Solution Temperature (UCST) and shape-memory effects. LCST- and UCST-type thermoresponsive polymers exhibit a temperature-dependent miscibility or solubility gap in aqueous solutions (**Figure 6**). This leads to a phase separation above (LCST) or below (UCST) a

certain temperature, which occurs due to reversible change from a hydrophilic coil to a hydrophobic globule state.[112]

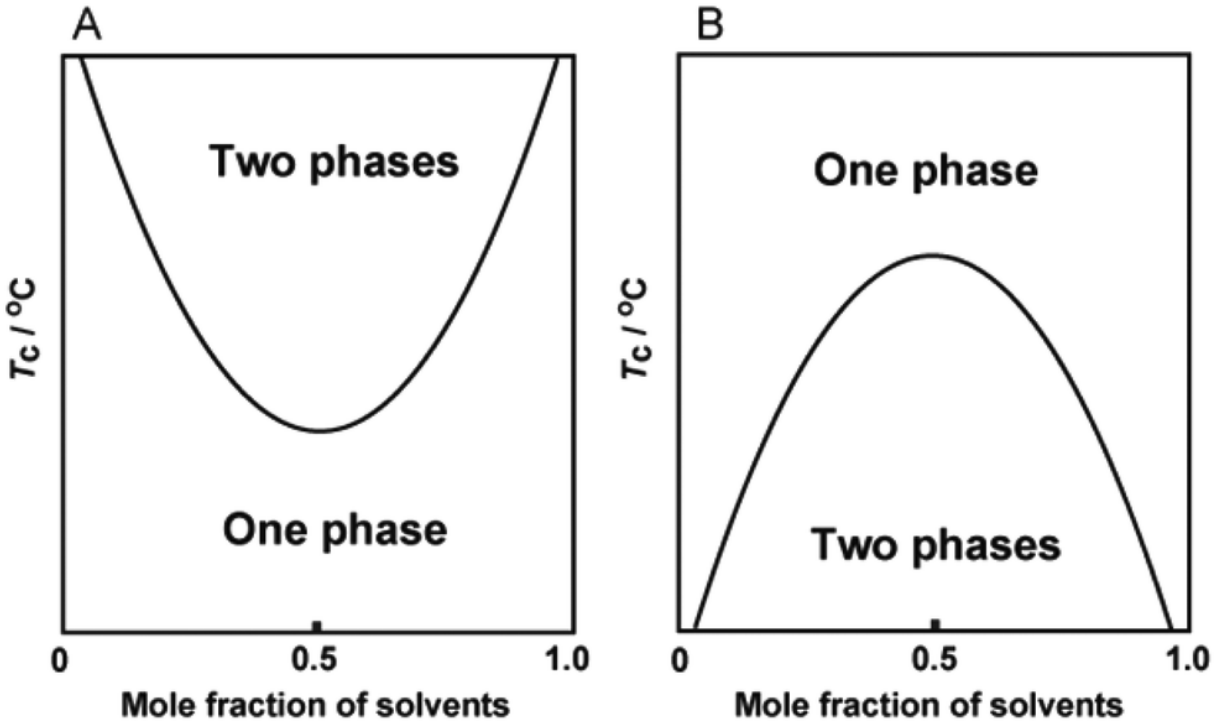

Figure 6: Mole fraction and temperature dependency phase diagram of LCST (Lower critical solution temperature) and UCST behavior. *A: Temperature-dependent miscibility of LCST-polymers. Decreasing the temperature below their respective LCST leads to dissolution of the thermoresponsive polymers. B: Temperature-dependent miscibility of UCST-polymers. Increasing the temperature above their respective UCST leads to dissolution of the thermoresponsive polymers. Taken from Kohno et al. "Thermoresponsive polyelectrolytes derived from ionic liquids" [113]*

2.4.1 LCST-type polymers

The most common and extensively studied thermoresponsive polymers are of the LCST-type. These thermoresponsive polymers exhibit solubility in water below their respective LCST, also known as "cloud point", since increasing the temperature above the LCST leads to the phase transition from a clear to a cloudy state. Poly(N-isopropylacrylamide) (PNIPAM) is the most studied polymer of this group, exhibiting an LCST in the range of 30-35°C, which is very close to the human physiological temperature.[114,115] Additionally, the LCST can be finetuned by adding further functionalization[116,117] or copolymerization.[118] Besides the synthetic PNIPAM, natural polymers like methylcellulose[119] and several derivatives[120,121] also show thermoresponsive LCST-behavior. Further thermoresponsive polymers are poly(N,N-diethylacrylamide)[122], poly(methyl vinyl ether)[123] or poly(N-vinylcaprolactam).[124]

The most common application of thermoresponsive polymers with an LCST is cell sheet engineering. Here, PNIPAM was covalently bound to polystyrene cell culture surfaces, which,

enabled cell attachment and proliferation in aqueous solutions at 37°C. By temperature reduction, the grafted polymer surface changed to a hydrophilic state leading to the detachment of whole cell sheets.[125] Compared to conventional cell detachment methods, no enzymes are required and extracellular matrix proteins as well as membrane bound proteins are preserved. Moreover, by stacking of several cell sheet layers, tissues can be created. Hence, cell sheet engineering has been applied to various types of tissues like cornea[126], periodontal tissue[127], cartilage[128], bone[129], myocardium[130] or vascular grafts[131].[132]

Another application is the creation of smart nanofibers via LCST-polymers. Here, in aqueous solutions, fiber mats created from PNIPAM nanofibers were able to shrink below and swell above the LCST.[133] Additionally, it has been reported that thermoresponsive polymers were used to create bundles of aligned gel microfibers by using a co-flow microfluidic device with phase-separated aqueous precursor solutions of alginate.[134] It was also shown that cells could attach to these fibrous gel bundles and elongate into the direction of the aligned fibrils.[134]

It is possible to further functionalize and crosslink LCST-polymers for the creation of hydrogels. In detail, hydrogels were based on PNIPAM[135] or cellulose[136] and exhibited thermoreversible characteristics that led to either swelling behavior or could be used for the creation of cell sheets. Furthermore, the sol-gel properties of thermoresponsive polymers dissolved in aqueous solution enable the use as injectable hydrogels. While being in an injectable state at room temperature, the solution solidifies after injection into the body.[137]For this approach, natural[138] as well as synthetic polymers[139] can be used for biocompatible and biodegradable drug delivery. Injectability and drug-loading of thermoresponsive hydrogels were also enabled by the creation of nanogels.[140]

2.4.2 Poly(2-oxazoline)s (POx)

An emerging family of polymers exhibiting LCST behavior are poly(2-oxazolines) (POx), which have been reported for the first time in 1966.[141,142] The number of publications per year concerning POx increased in the last decade[143], which also led to increased utilization in the field of biofabrication and biomaterials.

POx are synthesized via cationic ring-opening polymerization of oxazoline monomers.[144] Because of their structural similarity to natural polypeptides, they are also called bioinspired polymers or pseudopeptides.[145] The two main features of POx are the LCST-behaviour, which is mainly dependent on the side-chain composition, chain length and architecture[146,147], the

intrinsic biocompatibility[148], and the stealth behavior[149], enabling the application in cell culture. Moreover, POx homopolymers with propyl sidechains exhibit LCST behavior in physiological range[150], making them especially interesting regarding biofabrication. Therefore, POx polymers have been used in a variety of applications. Utilizing POx as hydrogels has been achieved via thiol-ene "click" chemistry[151] or as thermogelling hydrogel for the use as bioink.[152] Even microgels as cell carriers[153] and nanogels for drug delivery[154] have been developed in the community. However, most hydrogel and bioprinting studies in the context of tissue engineering still have not been adapted from a proof-of-concept to application-oriented studies. In accordance with other artificial polymer-based hydrogels, cells are not able to attach to the hydrogel intrinsically, which inhibits their elongation and leads to a nonnatural spherical cell shape. It has been shown that the modification of these hydrogels with RGD-sequences or peptides promote cell adhesion.[155,156] By adding RGD to POx-based hydrogels, they can be modified to combine the intrinsic biocompatibility of POx with cell attachment and improved biodegradation.[157]

Besides hydrogels, POx have been applied as conjugates for nanoparticles[158], peptides[159], proteins[160], and lipids.[161] Also, covalent POx-coatings led to the creation of antifouling[162] and antimicrobial[163] surfaces and were even applied as a surface for cell sheet engineering.[164,165] Additionally, an initial study utilizing POx as biomaterial ink for MEW was reported by Hochleitner et al.[166] (2014), where scaffolds of poly(2-ethyl-2-oxazoline) were created. Later, extrusion and electrospinning of gradient copolymers of 2-isopropyl- with 2-*n*-propyl-2-oxazoline has been shown.[167] In both cases, however, no biological application has been reported.

The most interesting development, and by far the most successful in proving the biocompatibility of POx, is a study reporting about the clinical trial of the POx-conjugated rotigotine, a treatment drug for Parkinson's disease.[168] Here, the authors reported the preclinical and early clinical safety and tolerability from patient data of the Phase I study. By linking rotigotine to the polymer, they were able to create a sustained release over the course of 7 days, after applying one subcutaneous injection. With this, the potential of the POx family has been clearly brought to the next level, especially in terms of biocompatibility and linking of active substances.

In summary, the utilization of POx provides a potent platform for a variety of applications. The modification potential, as well as the biocompatibility and thermoresponsive properties, led

to an increasing number of studies and an increased interest among several communities, including pharmaceutical research, tissue engineering and biofabrication.

Chapter 3

Easy-to-prepare Coating of Standard Cell Culture Dishes for Cell Sheet Engineering using Aqueous Solutions of Poly(2-npropyl-oxazoline)

Chapter 2 was published as original research article. Reprinted with permission from Matthias Ryma, Julia Blöhbaum, Raminder Singh, Ana Sancho, Jasmin Matuszak, Iwona Cicha, Jürgen Groll. "Easy-to-prepare Coating of Standard Cell Culture Dishes for Cell Sheet Engineering using Aqueous Solutions of Poly(2-n-propyl-oxazoline)". Copyright 2019 American Chemical Society. The original text was modified to exclude the experiments conducted by coauthors and improve readability.

The author contributions to the original research article are as follows:

Contributor	**Contributions**
Matthias Ryma	Designed research; development of the method; performed and analyzed data of coating establishment and cell sheet detachment of HMEC-1 cells
Julia Blöhbaum	Performed synthesis and analysis of Poly(2-npropyl-2-oxazoline)
Raminder Singh	Performed cell sheet creation and stainings with fibroblasts
Ana Sancho	Performed and analyzed data of cell substrate adhesion forces
Jasmin Matuszak	Performed cell sheet creation and stainings with HUVECs
Iwona Cicha	Conceived the research; revised and provided feedback on the manuscript
Jürgen Groll	Conceived the research; revised and provided feedback on the manuscript

3.1 Abstract

Cell sheet technology is a well-known method where cells are grown on thermoswitchable substrates that, upon cooling, become non-adhesive so that the complete layer of adherent cells including the produced extracellular matrix detaches as sheet. Usually, polymer exhibiting a lower critical solution temperature (LCST) in water below physiological temperature, commonly poly(N-isopropylacrylamide) (PNIPAM), are covalently grafted or, in form of block-copolymers, physisorbed onto substrates in a monomolecular thin film to achieve this effect, so that such substrates or the polymers needed for film-formation can only be prepared in a chemical lab with profound macromolecular expertise.

In this study I present a method to coat standard cell culture dishes with aqueous solutions of commercially available poly(2-*n*propyl-2-oxazoline) (P*n*PrOx), a polymer also exhibiting LCST behavior, in an easy and robust way. Different standard cell culture dishes were repeatedly coated with 0.1 wt% aqueous solution of P*n*PrOx and dried in the oven to create a fully covered thermoresponsive surface. A variety of cell types including endothelial cells, mesenchymal stem cells and fibroblasts were seeded and cultured until confluency on P*n*PrOx-covered surfaces. By decreasing temperature to 16 °C viable cell sheets were detached within time frames that are cell type dependent and could be harvested for biological analysis. It is shown that the cytoskeleton rearranges, leading to a more contracted morphology of the cells in the detached cell sheet. The cellular junctions between single cells within the sheet were detectable using immunostainings, which indicates that strong and intact intracellular contacts are preserved in the harvested sheets.

3.2 Introduction

Cell sheet technology is an established method to create multicellular sheets developed by Okano and co-workers. The method was originally based on culture dishes grafted with a thermoresponsive polymer, poly(N-isopropylacrylamide) (PNIPAM). PNIPAM exhibits a lower critical solution temperature (LCST) in water at 32 °C, meaning that above 32 °C, PNIPAM chains are dehydrated, leading to hydrophobicity of the grafted dish surfaces. Below 32 °C, the polymer reversibly changes to hydrophilic [169]. Under standard cell culture conditions, cells are able to adhere and proliferate on the surface and, upon simply decreasing temperature, whole cell sheets can be detached [170]. Compared to standard cell harvesting methods via trypsinization, cell sheet technology allows non-invasive harvesting, which is important for rapid colonization of cells on biomatrices and engineering 3D cellular constructs. Until now, many different cell types, e.g., epithelial[171-173] and endothelial cells[174], cardiomyocytes[175,176], or hepatocytes[176], have been shown to adhere to PNIPAM, enabling the application in cell sheet technology.

Apart from PNIPAM, other polymers also show LCST behavior in water. One example are polymers based on poly(2-oxazolines) (POx). POx have attracted increasing interest because of their tunable thermoresponsive properties and biocompatibility, which is based on their structural relation to polypeptides [7,177]. Compared to PNIPAM, POx-based polymers exhibit minimal thermal hysteresis and by exchanging side-chains, copolymerization or functionalization, the LCST of the polymer can be fine-tuned [178]. Due to this fact, many potential applications of POx have been developed. Among others, it was shown that the conjugation of proteins and small molecule drugs to POx helps to preserve their activity [179] and POx micelles have also been used as a drug carrier system [180]. Furthermore, by immobilizing poly(2-*iso*propyl-2-oxazoline) (P*i*PrOx) on surfaces, thermoresponsive nanolayers that allow non-invasive detachment of fibroblasts were created [181]. Compared to P*i*PrOx, poly(2-*n*propyl-2-oxazoline) (P*n*PrOx) has not been studied as extensively and has not been utilized in the field of life sciences thus far. Nevertheless, having its LCST at 20 °C in 1x Dulbecco's phosphate buffered saline (PBS) [182], makes it a promising candidate for applications in this field.

Currently, creating cell sheets for tissue engineering requires either purchasing of commercially available pretreated dishes, or effort- and time-consuming grafting of a thermoresponsive polymer on cell culture dishes, which requires pre-defined materials and

established methods. However, easy-to-apply coatings have been examined by different groups before. Schmidt S. et al. created PNIPAM microgels and deposited closely packed films by solvent evaporation resulting in a thermoresponsive surface for cell sheet engineering[183]. Also, block copolymers of PNIPAM and poly(butyl methacrylate) were used to cover standard cell culture dishes with a thermoresponsive polymer layer by physical deposition[184]. Furthermore, to prevent cell adhesion in defined patterns for precise and long-term control of neurite outgrowth, POx-based triblock copolymers were used to create easy-to-apply coatings[185]. Although these methods share the simplicity of application, the preparation of the applicable thermoresponsive polymers is more complex and requires special knowledge. The only exception was an extensive study reported by Nash et al., where an ethanolic PNIPAM solution was used to create thermoresponsive culture substrate via spin coating in order to create an easy and straightforward preparation method[186].

In this study, I aimed to establish an easy-to-apply and especially easy to prepare coating procedure purely based on aqueous solutions that can be transferred to standard cell culture plates and utilized in each biological laboratory in possession of standard equipment. I have developed a simplified and cheap method to create thermoresponsive polymer layers in cell culture dishes without the use of grafting techniques. By coating the dishes with aqueous solution of P*n*PrOx a thermoresponsive surface for cell growth was prepared. Different cell types were able to adhere and proliferate on P*n*PrOx in a manner similar to non-treated culture dishes. By reducing the temperature below the LCST of P*n*PrOx, the polymer became hydrophilic and the detached cell sheets could be harvested for further processing. I showed that the cytoskeleton rearranges, leading to a more contracted morphology of the cells in the detached cell sheet. The cellular junctions between single cells within the sheet were detectable using immunostainings, which indicates that strong and intact intracellular contacts are preserved in the harvested sheets. Taken together, an easy, user-friendly and low-cost technique of creating thermoresponsive P*n*PrOx surface was established, applicable for cell sheet technology and tissue engineering purposes, in each cell biology lab.

3.3 Materials and Methods

3.3.1 Chemicals

Synthesized and characterized P*n*PrOx has been kindly provided by Julia Blöhbaum. Ultroxa® poly(2-*n*propyl-2-oxazoline) (Mn 10,000, PDI ≤1.2) was used as a commercial reference to the self-synthesized polymer.

3.3.2 Coating of cell culture dishes with P*n*PrOx

P*n*PrOx was dissolved at 4 °C in ultrapure water to a final concentration of 0. 1 wt%. Wells of PS-treated (polystyrene) standard cell culture dishes (Thermo Fischer Scientific) were fully covered with P*n*PrOx-solution (Table 1). Evaporation of water was performed in an oven at 60 °C. After the initial drying process, the coating could be seen by eye as a thin film. Nevertheless, the coating in the central region was noticeably thinner after the drying, due to capillary effects. Therefore, another drop of P*n*PrOx-solution was added to the center and placed again in the oven for the complete evaporation of water. As a result, the entire surface was covered with a layer of P*n*PrOx (Figure 7).

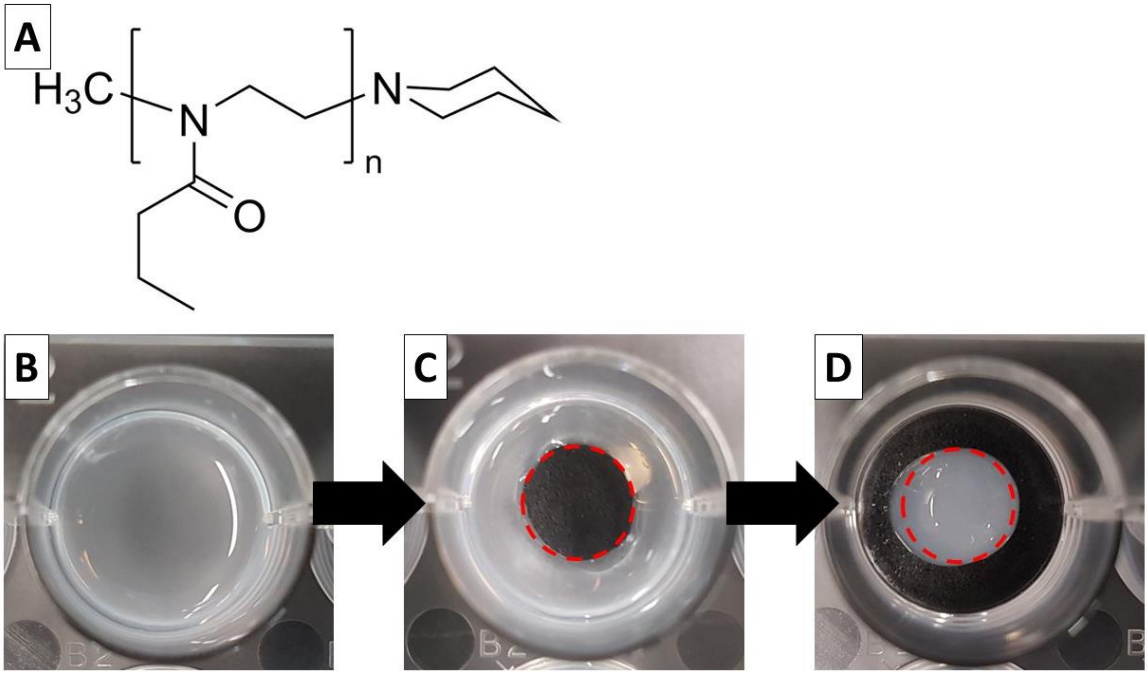

Figure 7: Formula of poly(2-npropyl-oxazoline) (A) and coating procedure of a standard cell culture dish with aqueous 0.1 wt% PnPrOx solution. *The culture dish is filled with aqueous 0.1 wt% PnPrOx solution until the whole well is covered and dried in the oven at 60 °C (B). During the drying process, water evaporates from the inside of the well to the outside (B). After evaporation of the residual water, the middle of the well is less coated with polymer than the outside. To counteract the uneven coating, the middle of the well is again covered with aqueous 0.1 wt% PnPrOx solution (C). Since the solution does not*

touch the walls of the well, the water evaporates from the outside to the inside covering the previously less coated part of the well.

3.3.3 Contact angle measurement

Contact angle measurement was performed with the Contact Angle System OCA (DataPhysics Instruments, Filderstadt, Germany) and the corresponding software SCA20. The drop volume was 3 µl and the contact angle was calculated via Laplace-Young Fitting.

3.3.4 Cell culture

Human microvascular endothelial cell line isolated from human dermal microvascular endothelium (HMEC-1) was acquired from ATCC. The cells were cultivated in MCDB 131 media (Thermo Fischer Scientific) with additional 10 ng/mL Epidermal Growth Factor (EGF), 1 µg/mL hydrocortisone, 10 mM glutamine, fetal calf serum (FCS) (Thermo Fischer Scientific) to a final concentration of 10% and Pen/Strep to a final concentration of 1%.

Primary human mesenchymal stem cells (hMSCs) from trabecular bone were isolated via plastic adherence from the femoral heads of patients undergoing total hip arthroplasty [187]. Cells were cultured in DMEM F´12 media (Thermo Fischer Scientific,) with additional FCS, 1% Pen-Strep (Thermo Fischer Scientific) and 50 µg/ml L-ascorbic-acid-2-phosphate (Sigma-Aldrich,) in 175 cm^2 cell culture flasks (Greiner Bio-One). Undifferentiated hMSCs in passage 2 were used for the experiments. All experiments were approved by the Local Ethics Committee of the University of Wuerzburg and each donor gave the informed consent.

Primary human umbilical vein endothelial cells (HUVECs) were isolated from freshly collected umbilical cords by a standard technique [188] and grown in endothelial cell growth medium (Promo Cell) with endothelial cell growth supplement containing 5% FCS, 4 µL/mL heparin, 10 ng/mL epidermal growth factor and 1 µg/mL hydrocortisone, at humidified 7.5% CO_2 atmosphere. The use of human material was approved by the Institutional Ethical Committee on Human Research at the University Hospital Erlangen (ethical review number 85_14 B) and all donors have given an Informed Consent according to the ethical guidelines. In all experiments, HUVECs at passage 1-2 were used.

Commercially available normal human dermal fibroblasts (PromoCell, Heidelberg, Germany) were cultured in DMEM supplemented with 10% (v/v) FCS and 1% (v/v) antibiotic-antimycotic, at 37 °C with a controlled atmosphere of 5% CO_2 and 95% relative humidity.

Murine fibroblast cell line (L929) was acquired from ATCC. L929 cells were cultivated in DMEM (Dulbecco's Modified Eagle medium) (Thermo Fischer Scientific) with additional HEPES Buffer, FCS to a final concentration of 10% and Pen/Strep to a final concentration of 1%.
Passaging of the cells was executed via 5 minutes of incubation with PBS/EDTA (0.45M EDTA) and afterwards trypsinization with 0.05% Trypsin-EDTA 1X (Thermo Fischer Scientific), unless otherwise stated. Cells were cultivated in 75 cm^2 and 175 cm^2 cell culture flasks (Greiner Bio-One, Kremsmuenster, Germany).

3.3.5 Cytocompatibility

L929 cells (40000 cells/cm^2) were seeded in P*n*PrOx-coated and uncoated wells of standard PS-treated 96-well-plates. Cell viability was examined via CellTiter-Glo® Luminescent Cell Viability Assay (Promega, Germany) by quantification of the presence of ATP, indicating cell viability, for 24, 48 and 72 hours.
Additionally, L929 cells (25,000 cells/cm^2) were seeded in wells of 24-well-plates. Proliferation was examined via cell counting for 24, 48 and 72 hours.

3.3.6 Temperature dependent detachment of cell sheets

After the cells reached confluency the medium was exchanged with 16 °C cold medium and the culture dish was also kept at 16 °C for 30-90 minutes, depending on the cell type. Layers of Fibroblasts and hMSCs detached after 30 minutes spontaneously from the outside to the inside, while endothelial cell layer detached after 90 minutes. If the monolayer did not detach by itself, simple shaking and soft agitation with the pipette improved the detachment.

3.3.7 Immunofluorescent analysis

Cell sheets were fixed with 4% phosphate buffered formaldehyde and permeabilised with 0.2% Triton X-100 (Sigma-Aldrich) in PBS. Samples were then stained with rhodamine phalloidin (PromoKine, Heidelberg, Germany), which selectively binds F-actin.
The samples were subsequently stained with Hoechst 33342 (Life Technologies GmbH, Darmstadt, Germany) to visualize nuclei of cells. Images were obtained via fluorescence microscopy (Zeiss AxioObserver) at different magnifications.

3.4 Results

3.4.1 P*n*PrOx coating

P*n*PrOx was dissolved in water to a final concentration of 0.1 wt%. Using lower concentrations of P*n*PrOx in water, led to difficulties with cell detachment (data not shown). Therefore, 0.1 wt% was determined as the minimum effective concentration. Different culture dishes were filled with the solution until the whole well was covered (using volumes indicated in Table 1). After drying, another layer of coating was applied in order to fully cover the whole bottom of the well.

Table 1: Volumes of aqueous PnPrOx solution used to coat cell culture dishes of different sizes

Volume per dish	**48-Well-Dish**	**24-Well-Dish**	**12-Well-Dish**	**6-Well-Dish**
1. Coating	100 µL	200 µL	400 µL	800 µL
2. Coating	100 µL	100 µL	100 µL	200 µL

Thermoresponsive capabilities of the dried surface coating were examined via contact angle measurement (Table 2) on standard cell culture dishes. Contact angle measurement of P*n*PrOx-coating at 37 °C revealed hydrophobic surface with a contact angle of 65°, whereas the measurements at temperatures at 16 °C resulted in a decreased contact angle of 39°, indicating a more hydrophilic surface. The contact angle of the uncoated culture dish was also hydrophobic at both temperatures.

Table 2: Contact angles of cell culture dishes coated with PnPrOx at 37 °C and 16 °C. Uncoated dishes were used as control surfaces (n=3).

	37 °C	**16 °C**
P*n*PrOx-coated dish	64.6° ± 5.9°	39.9° ± 3.2°
Uncoated dish	73.1° ± 1.1°	69.5° ± 1.2°

Furthermore, 6-Well-Plates were coated with 10 mg of P*n*PrOx and incubated in 2 ml dH_2O for 72 hours at 37 °C. After decreasing the temperature to 16 °C, dissolved P*n*PrOx was collected past 30, 60, 90 and 120 minutes and subsequently freeze-dried and weighted (Figure 8).

Longer incubation in water at 16 °C lead to increased amount of dissolved P*n*PrOx with most of the polymer being dissolved after 120 minutes.

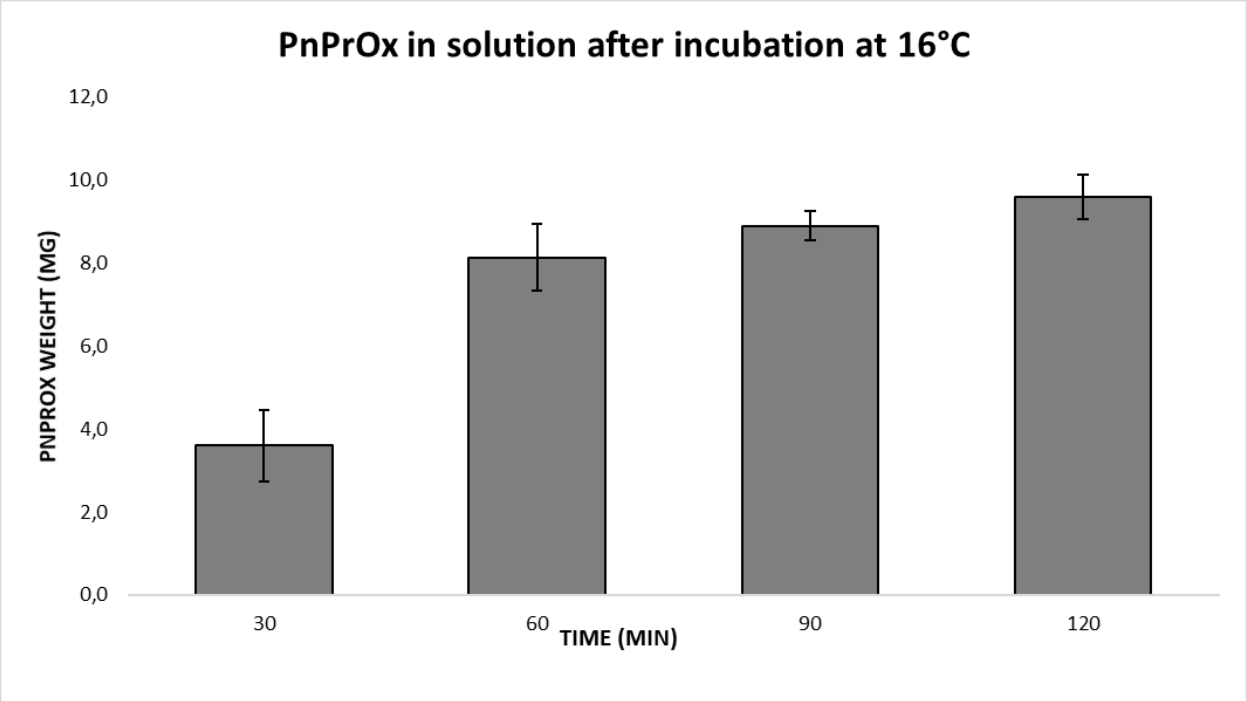

Figure 8: 6-Well plates were coated with 10 mg PnPrOx and incubated for 72 hours at 37°C. *The weight of PnPrOx in solution was determined after decreasing the temperature to 16°C for 30, 60, 90 and 120 minutes. Error bars refer to standard deviation with n=3 separate samples.*

3.4.2 Cytocompatibility

The casted P*n*PrOx coating was tested by determining proliferation and viability to ensure cytocompatibility. Compared to PS-treated uncoated wells, cell growth on P*n*PrOx-coated dishes was slower at the beginning. This effect was observed for all tested cell types. However, cells proliferated over time, reaching numbers comparable to the PS-control within 72h, indicating comparable cytocompatibility. Cell proliferation tested on L929 cells seeded on PS and P*n*PrOx is shown in Figure 9A. Furthermore, the results obtained with CellTiter-Glo® Luminescent Cell Viability Assay confirmed equal performance in terms of viability and metabolic activity of cells grown on P*n*PrOx compared with standard PS control dishes (Figure 9B).

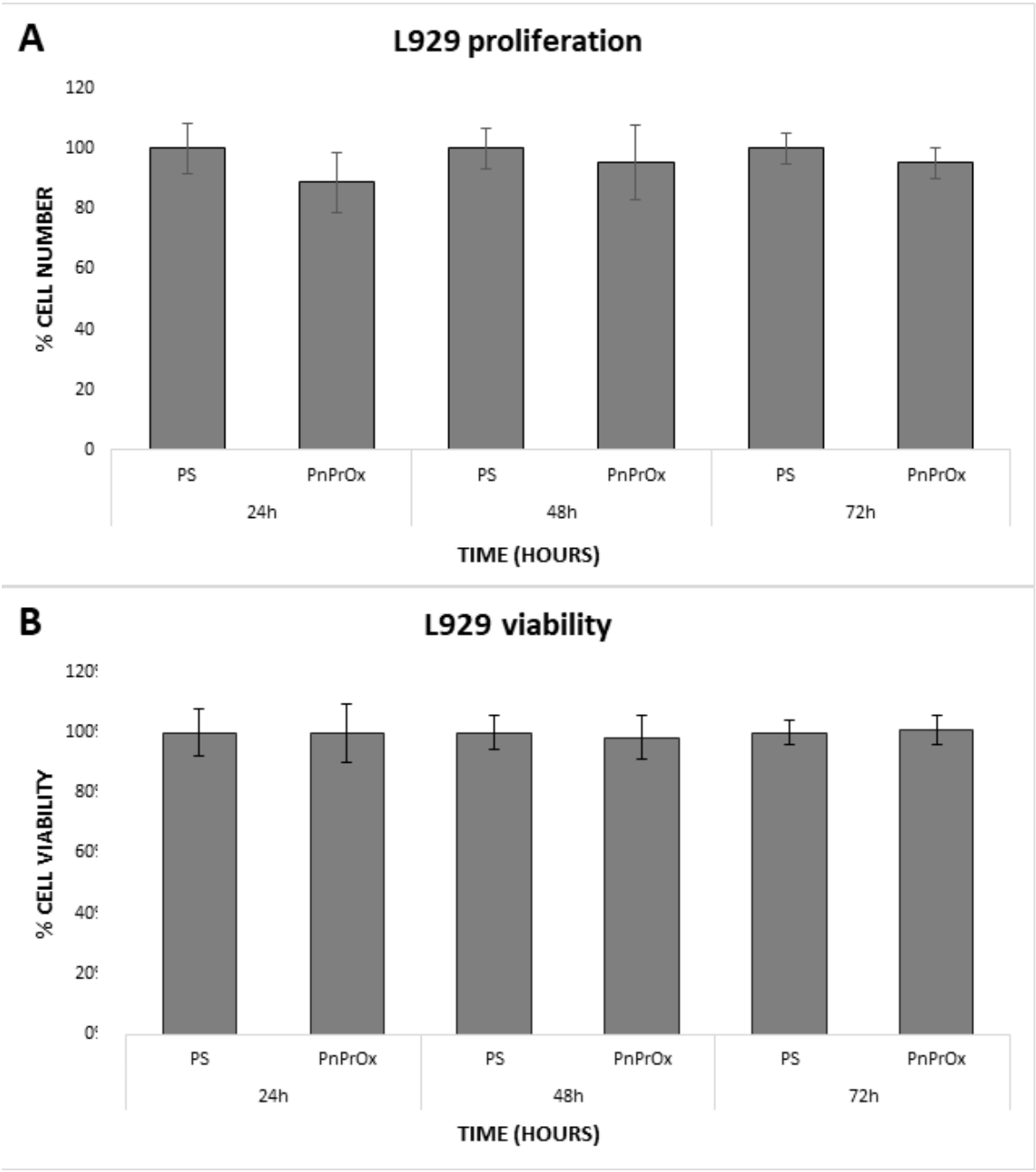

Figure 9: Cell proliferation (A) and viability (B) results of L929 cells *; n=3. L929 cells were cultivated on standard PS culture dishes or PnPrOx-coated dishes. Cell viability was estimated using CellTiter-Glo® Luminescent Cell Viability Assay. Error bars refer to a standard deviation of n=3 independent samples with N=5 technical replicates each.*

3.4.3 Temperature-dependent detachment of cell sheets

To confirm the temperature-dependent detachment of cell sheets, different types of cells were seeded on dishes pre-coated with 0.1 wt% aqueous solution of P*n*PrOx and grown until 100% confluency. Subsequently, the temperature was decreased to 16 °C and cells grown on the P*n*PrOx coating were incubated for 30-90 minutes, depending on the cell type. After the specific incubation time, most cell sheets began to detach spontaneously starting from the

periphery of the well. If cell-monolayers did not detach by themselves, slow shaking, or soft agitation of medium on the sides of the well, led to faster detachment of the whole monolayer. No differences in detachment were seen by varying the size of the culture dish (Figure 10). In order to corroborate that detachment of cell sheets is caused by alterations in the underlaying polymer and not due to the state of cells, confluent cells seeded on uncoated culture dishes were incubated then at 16 °C for 30-90 minutes. After testing it with every cell type, no cell sheet detachment occurred on uncoated dishes.

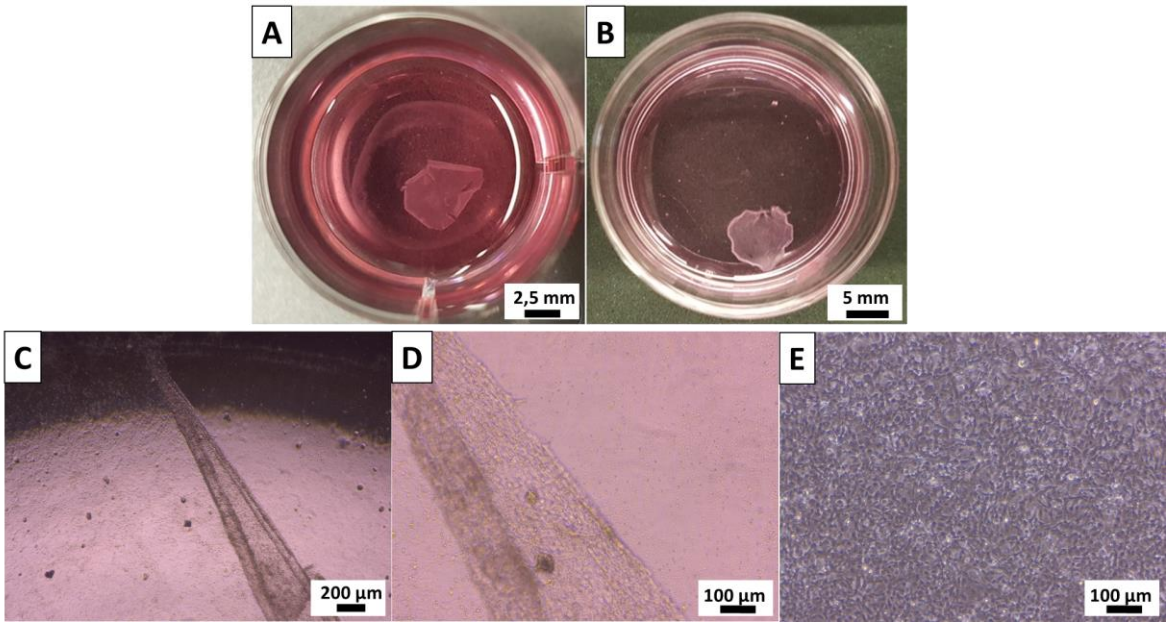

Figure 10: HMEC-1 cell sheets. *(A) Macroscopic images of spontaneously detached and contracted cell sheet of HMEC-1 in a PnPrOx-coated well of a 12-well-plate after 60 minutes incubation at 16 °C; (B) Spontaneously detached hMSC cell sheet in a PnPrOx-coated 30 mm Petri dish after 30 minutes incubation at 16 °C; (C), and (D): Representative microscopic images of spontaneously detaching cell sheet of HMEC-1 after 60 min incubation at 16 °C in a well precoated with PnPrOx; (E) Control HMEC-1 cells grown on uncoated dish. Incubating for 60 minutes does not lead to spontaneous cell sheet detachment*

The system was first tested with microvascular endothelial cell line HMEC-1[189]. HMEC-1 were seeded at a density of 150,000 cells/cm² and cultivated for 48 hours, before exchanging the medium and cooling the dish down to 16 °C for 60 minutes. After this cooling step monolayers already started to detach, going from the edges of the coated wells towards the central region (Figure 10). The detached monolayer shrunk to around 10% of its initial size but could be further used for tissue engineering purposes: By transferring it to another uncoated well and incubating for 1 hour at 37 °C, the monolayer reattached again. Monolayers grown in uncoated control dishes did not detach during this time period.

To validate this method in different cell types, I tested the thermosensitive coating using primary hMSCs, isolated from bone tissue of the femoral head. The hMSCs were seeded at a

density of 100,000 cells/cm² and cultivated until a confluent monolayer was obtained. Then, the temperature was reduced to 16 °C and after less than 30 minutes, the monolayer detached spontaneously.

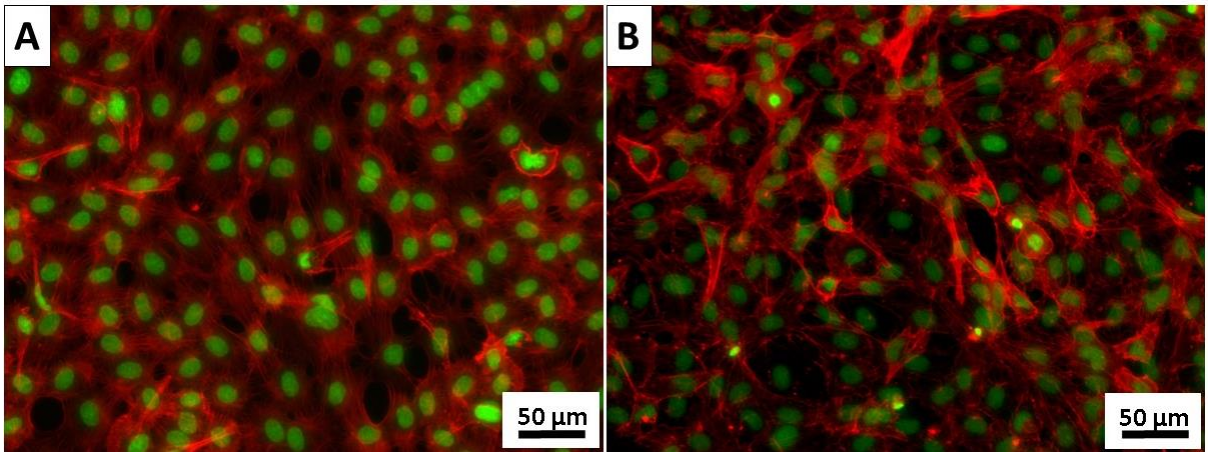

Figure 11: Phalloidin-staining of primary HUVEC monolayer *cultured in (A) a standard cell culture dish (attached cells); (B) Phalloidin staining of HUVEC monolayer grown on PnPrOx after detachment. F-actin, red; nuclei, green.*

For further testing, primary HUVECs were seeded at a density of 150,000 cells/cm² and cultivated on P*n*PrOx coated wells. Phalloidin staining was performed to visualize intracellular F-actin. As shown in Figure 11 A, attached HUVECs had spread cell bodies and formed a monolayer with typical cobblestone morphology. In the cells grown on control dishes F-actin was uniformly distributed. By contrast, in the detached cell sheet, HUVEC monolayer showed a more contracted cell morphology and F-actin was localized at the edges of the cell. This localization of F-actin indicates its rearrangement to cortical region and to cell-cell junctions linking neighboring cells upon detachment from focal adhesions (Figure 11 B). This method has further been successfully tested for non-monolayer forming fibroblasts.

This protocol to create cell sheets was further used with the commercially available P*n*PrOx by Ultroxa®, which differs in terms of molecular weight from the synthesized polymer. The synthesized P*n*PrOx has a molecular weight of about 50 kDa, while it is 10kDa for the commercially available alternative. After seeding and cultivating with HMEC-1 and following temperature decrease, cell sheets were obtained as well. However, the concentration was increased from 0.1 wt% to 0.2 wt% (Figure 12 C-D). When using only 0,1% aqueous P*n*PrOx, the cell sheet only detached from the outside, but did not continue to detach fully (Figure 12 A-B).

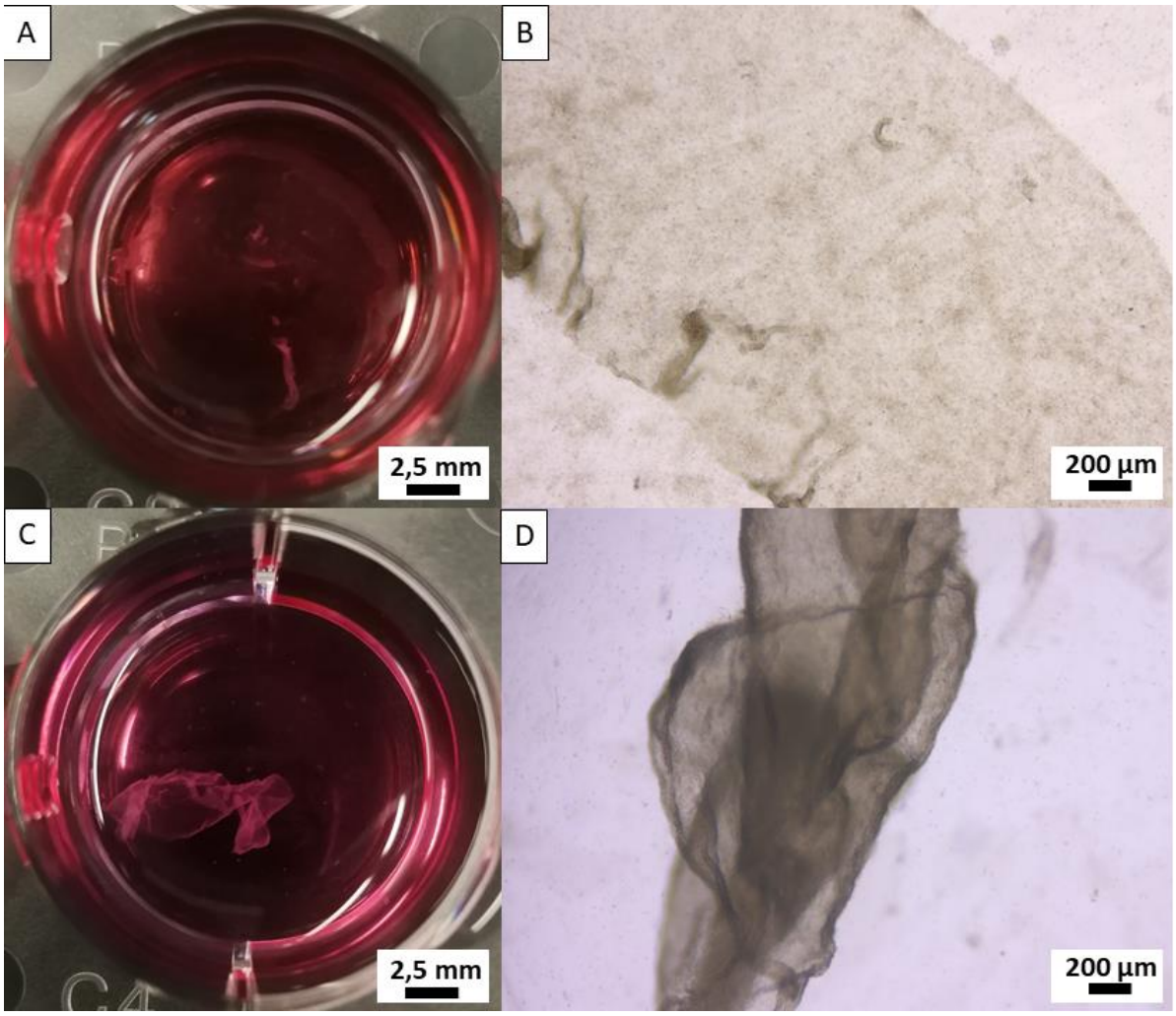

Figure 12: Cell sheets of HMEC-1 created with surface coating of Ultroxa® PnPrOx. *(A) Macroscopic overview of non-detaching HMEC-1 cell sheet seeded on 0.1 wt% Ultroxa® PnPrOx, (B) Microscopic image of non-detached cell sheet at x10 magnification. (C) Macroscopic overview of detached HMEC-1 cell sheet seeded on 0,2 wt% Ultroxa® PnPrOx, (B) Microscopic image of detached cell sheet at x10 magnification.*

3.5 Discussion

In this study, I successfully produced an easy-to-use thermoresponsive polymer coating for cell sheet technology that is applicable to standard cell culture dishes. In the first step, poly(2-*n*propyl-2-oxazoline) was synthesized via cationic ring-opening polymerization and characterized. The LCST of P*n*PrOx determined in ultrapure water (21 °C) was reduced to 19 °C in PBS, as previously shown by Boerman et al [182]. Concentration of salts and various ions is known to affect the LCST of different POx, a phenomenon termed as "salting in or out" [190]. Consequently, a decrease of the LCST of P*n*PrOx is observed in the presence of PBS and cell culture medium. Therefore, to achieve the change in the polymer chains to a hydrophilic conformation, which is necessary to create cell sheets, I selected the temperature of 16 °C for cell detachment.

Contact angle measurement was used to determine the thermoresponsive capabilities of the coating. During the measurement at the standard cell culture temperature of 37 °C, which is above the LCST of POx, a hydrophobic contact angle of 64.6° was obtained as expected. With the decrease of temperature, hydrophilic interactions of the polymer chains become more influential and water molecules interact with the polymer sidechains, leading to hydration and dissolution of P*n*PrOx below the LCST and a more hydrophilic contact angle of 39.9° at 16°C.

Since the drying process of this method provides a heterogenous coating, direct measurements to determine coating thickness have not been performed. However, with the assumption that the density of the applied polymer is comparable to the density of Poly(2-ethyl-2-oxazoline) (Sigma Aldrich, Munich, Germany) with 1.14g/cm³, the average thickness of coatings created with a 0.1 wt% aqueous solution per cm² can be approximated to 1 µm. Additionally, swelling capabilities of poly-(2-oxazoline)s have been shown in different studies with copolymer networks [191] and hydrogels [192]. Although not tested in this study, I therefore suggest that swelling behavior of the deposited P*n*PrOx-layer above the LCST might lead to an increase in its thickness.

Biocompatibility of the P*n*PrOx coating was confirmed by cultivating L929 on the P*n*PrOx coating for up to 72 hours. Proliferation and viability of the cells were comparable to standard PS-treated cell culture dishes, verifying the cytocompatibility of poly(2-alkyl-2-oxazoline)s [177]. To validate the technique, the cell sheet detachment was first tested using HMEC-1 cell line, because of strong intercellular junctions between endothelial cells in their confluent monolayer. After 60 minutes at 16 °C, cell monolayer detached spontaneously in every tested

well-size. Those cell sheets were able to be transferred to another culture dish for reattachment, enabling potential applications in creating multilayer tissue engineering constructs and regenerative medicine.

Also, for the other cell types tested, namely, primary MSCs, HUVECs and fibroblasts were seeded on the coated wells. Each of these cell types proliferated and spread on the P*n*PrOx coating and were able to detach as cell sheets. In detached endothelial monolayers, cells became rounded and showed a more contracted morphology, indicating an alteration of cytoskeletal stress fibers [174]. Therefore, attached and detached HUVEC-monolayers were stained with fluorescently labeled phalloidin to visualize the differences in F-actin cytoskeleton. In the detached, contracted cell sheets, cells were rounded with F-actin accumulation at the cortical region of the cell. The cells in the control monolayers in uncoated culture dishes exhibited a spread morphology with larger surface areaand a more uniform distribution of F-actin fibers in the cytoplasm.

These findings imply that dynamic changes and rapid rearrangement of cytoskeleton towards cell-cell adhesions can effectively hold the cells within monolayers together, even upon the detachment. This is clearly visible in endothelial cells which, typically for barrier cells, form very strong cell-cell contacts [193].

Compared to the in the introduction mentioned studies of Nash et al, this approach is based on an aqueous solution of P*n*PrOx and applied in standard well plates. The thermoresponsive coating with approximately 1 µm thickness is not uniformly distributed from aqueous solution compared to the approximately 100 nm thick PNIPAM-layer on spin-coated coverslips. Furthermore, this leads to an increased amount of dissolved polymer in the medium. Lowering the thickness of the polymer might be possible by using spin-coating technique but would impair the application in standard well-plates. Additionally, comparing the cell adhesion results, after 48h of culture the proliferation in case of PNIPAM and P*n*PrOx was at nearly 100%, indicating excellent biocompatibility in both cases. Also, the detachment times for hMSCs and fibroblasts are with less than 30 minutes comparable. However, because of smaller polymer-layer and the temperature-dependence of cell sheet detachments, a faster detachment rate can be assumed with the PNIPAM layer created by Nash et al.[186].

Taken together, I created a cheap and simple method that allows the generation of cell sheets in culture dishes, independent of their size or form. P*n*PrOx is commercially available and easy to obtain. Thus, scientists in every laboratory, even without specialized chemical equipment,

can coat cell culture dishes and produce cell sheets following this simple and fast procedure. Although poly(2-oxazoline)s have been proven to be highly biocompatible[7,177], there is still a risk of polymer contamination, especially from a clinical point of view. Nevertheless, this method is an interesting alternative in terms of proof-of-concept studies, which enables the development of new strategies and applications for cell sheet engineering. The amount of 1g P*n*PrOx dissolved in water produces an amount of 1000 ml of 0.1 wt% aqueous solution of P*n*PrOx, which permits the user to coat around 2,000 wells of a standard 12-well plate, equaling more than 160 well plates. In conclusion, coating dishes with a 0.1 wt% aqueous solution of P*n*PrOx is not only easy for the end-user, but it also proves to be a low-cost alternative to create cell sheets for tissue engineering and regenerative purposes.

Chapter 4

Melt Electrofibrillation: Biomimetic Hierarchically Structured Fibril-Scaffolds Enable Highly Efficient 3D Topography-Mediated Immunomodulation of Human Macrophages

Chapter 3 is based on the work of the author of this thesis Matthias Ryma, who developed and characterized the method of scaffold generation and introduced the concept to use them for topography-induction of macrophage differentiation. A publication that will be supplemented by other collaborators is in preparation at the time of handing in this thesis.

4.1 Abstract

Topography-mediated influence of cells has recently attracted increased interest because it enables a supplement-free method to induce differentiation and polarization for different cell types, which has been shown with 2-dimensional (2D) approaches like micropatterning and electrospinning. However, the creation of 3-dimensional (3D) scaffolds with micro- and nanotopography that influences cell differentiation remains a challenge to this day. Especially the differentiation of human macrophages based on topography-mediated elongation has yet to be shown in both 2d and 3d scaffolds.

In this study, a method is presented to create fibrous scaffolds based on aligned micro- and nanofibrils of polyblends. For this, poly(2-*n*propyl-2-oxazoline) (P*n*PrOx) and Poly(2-*cyclo*propyl-2-oxazoline) (P*cyclo*PrOx) were blended and printed via Melt Electrowriting (MEW). After subsequent bulk crystallization of P*n*PrOx the amorphous P*cyclo*PrOx was dissolved in water, exposing the maintained P*n*PrOx fibril bundles. Furthermore, I adapted this method to the clinically relevant polymer polycaprolactone (PCL) by blending it with polyvinylacetate (PVAc). Based on the formation/origin and composition of these fibrils, I conclude that this behavior seems to be caused by a ratio-dependent directed phase separation of the blend induced by pressure and the electrical field applied during the process of MEW. In addition, the fabricated fibrils showed biomimetic properties by reaching diameters close to those of natural collagen I.

Furthermore, an immunomodulatory application of the scaffolds to support regenerative processes is provided. The fibrillar structure induced a significant elongation of human monocyte-derived macrophages leading to a pro-healing M2-like polarization similar to those of IL-4 induced macrophages. Moreover, by comparison of synthetic- and natural-derived fibrils, hints of the biological importance of macrophage elongation were given. These results imply a potential application of fibrillar scaffolds created via Melt Electrowriting in the field of tissue engineering and regenerative medicine.

4.2 Introduction

The field of biofabrication and biomaterials is continuously growing and already consists of a considerable portfolio of different materials and fabrication methods. Naturally, this does not only lead to an even higher amount of possible material combinations but also to even more combinations with versatile fabrication methods. Amongst the variety of materials, Poly(2-oxazoline)s (POx) are an outstanding group of polymers due to their known biocompatibility and broad application range.[7,177] POx have been applied for preserving the activity of peptides and small molecules due to their functionalization potential[179], for the formulation of micelles as drug delivery carrier[180], for the creation of different hydrogel formulations[194,195], and as basis for cell sheet engineering.[181,196]

The biocompatibility of materials is either an intrinsic effect of the material itself, as for Polyethylenglycol[197,198] and Poly(2-oxazolines)[179], or can be adjusted by modification. Moreover, even biocompatible biomaterials can be enhanced by chemical functionalization like thiol-ene click reaction[199,200], surface treatment with plasma activation[201], or coating with other biocompatible materials.[202] A recent approach to modify biocompatibility is the introduction of topography on biomaterials. It was proven, that certain topographies have an influence on cell geometry and therefore cell adhesion[203] and even cell differentiation[77], leading to an overall improvement of biocompatibility.[204]

As a material allowing for the formation of topographies, POx have recently been applied as bioinks, as shown by Luxenhofer and coworkers[152], as well as for the production of Poly(2-ethyl-2-oxazoline) scaffolds created via Melt Electrowriting (MEW) as described by my group.[166] Thereby, MEW is an emerging technique that enables the user to deposit ultrafine polymer fibers in a directed manner directly. In principle, a polymer melt is pneumatically pressed through a nozzle and, by applying an electrical field, the resulting polymer jet is stabilized and collected on a moving collector plate.[205] Most research regarding MEW has been conducted with PCL, a polymer, which is clinically approved and is therefore already applied in different medical applications.[85]

A particularly interesting effect of topography as it can be generated by MEW is its influence on cell shape and, therefore, its potential application for cell differentiation.[206] One example is the immunomodulation of macrophages based on topography-mediated elongation. This is especially useful since macrophages are one of the key mediators between an implant and the body.[207] In general, macrophages are highly plastic cells, which are roughly classified into two

main subgroups, the “classically activated” pro-inflammatory M1 type and the “alternatively activated” M2 type. Nevertheless, they still have the ability to switch their polarization state depending on the environment and additional stimuli.[208] The M1 type is mainly involved in the initiation of the immune response and is characterized by the release of proinflammatory cytokines, like IL-1β or TNF-α, increased phagocytic activity, and the production of nitric oxide and reactive oxygen species.[209] In contrast, M2 macrophages are involved in tissue remodeling, regeneration, and immunoregulatory processes and can be divided into several further subtypes: M2a, M2b, M2c. While M2a macrophages (induced by IL-4) are considered to be involved in tissue regeneration and repair processes and are characterized by the expression of CD206, IL10, IL-6, and downregulation of IL-1β, M2c macrophages (activated by dexamethasone) are described as “deactivated type” and, characterized by inhibition of M1 markers and upregulation of CD163.[10] For proper wound healing both M1 and M2 macrophages are crucial. However, the timeline of their appearance is decisive. While the absence of M1 macrophages in early stages can impair healing, a prolonged appearance can lead to chronic inflammation or fibrosis. Moreover, a too early appearance of M2 macrophages was correlated with an increased fibrotic reaction.[210]

M1 and M2 macrophages also differ in their morphology depending on their stimulation and polarization.[13] Accordingly, murine macrophages differentiated into a regenerative type with an increased expression of anti-inflammatory M2 markers when topographical cues, i.e., nano- and micropatterned grooves on materials, drove their morphology into an elongated shape.[211] Electrospun aligned nanofibers were also proven to trigger the development of the healing macrophage M2 phenotype compared to randomly distributed nanofibers, which induced the inflammatory M1 polarization instead.[212] Thus, inducing macrophage polarization by the material’s topography into the anti-inflammatory, regenerative M2 phenotype provides a valuable strategy for the design of biomaterials and implants. However, the underlying mechanism and the biological importance of elongation still need to be clarified.

In this study, I have developed novel polyblend formulations, which, in combination with MEW, enables the fabrication of fibrillar thread-like structures for biocompatible scaffolds. In detail, Poly(2-*cyclo*propyl-2-oxazoline) (P*cyclo*PrOx) was blended with Poly(2-*n*propyl-2-oxazoline) (P*n*PrOx) in a defined ratio by dissolution in water and lyophilization. The blend was then used to create scaffolds via MEW. Following the dissolution of P*cyclo*PrOx by temperature decrease, bundles of aligned fibrils of P*n*PrOx within each single fiber thread

were visible. This effect likely arose from the directed phase separation of the polymer melt because of the pressure and the electrical field and provided the bioactive nanoscale topography that was further investigated within this study. I was further able to apply this system to the miscible blend system PCL/PVAc, which led to the creation of even smaller fibrils with better stability resembling natural collagen bundles even stronger. Also, dissolution of PVAc was executed in 70% Ethanol, which sterilizes the scaffolds directly in the same step.

In the next step, primary human macrophages were cultured on the fibrillar scaffolds derived from the blend. The comparison of fibrillar and fiber scaffolds led to differences in morphology and polarization correlated to chemical induction into M2 macrophages by IL-4 and DEX, respectively. In particular, fibrillar scaffolds showed the potential to be an optimal biomaterial for wound-healing applications by inducing a phenotypical switch from M1-M2 related-macrophages.

Taken together, a new technique based on polymer blends is presented, which allows for the formation of fibrillar, thread-like scaffold structures after being processed via Melt Electrowriting. Furthermore, these structured fibril bundles based on POx and PCL exerted a topographical stimulus that induced regenerative M2 marker expression in human macrophages. Besides its immunomodulatory effect, this combination of polymer blends and MEW has the potential to deliver a platform for topography-guided differentiation of several cell types and will also meet the urgent demand for nanofibrous scaffolds in a 3D setup[213], which structurally resembles the natural environment of several tissue environments for tissue engineering and regenerative purposes.

4.3 Materials and Methods

4.3.1 Chemicals

Synthesized and characterized P*n*PrOx has been kindly provided by Julia Blöhbaum.

4.3.2 Instrumentation for characterization

Differential scanning calorimetry (DSC) measurements were performed on a NETZSCH DSC 204F1 Phoenix 240-12-0083-L (Selb, Germany). The polymers were measured from -50 °C to 200°C with a heating rate of 10 K/min with three heating and two cooling cycles. The third heating cycle is shown in the results.

Stereomicroscopic images were taken with the Discovery V20 and SEM imaging was performed with a Crossbeam 340 SEM equipped with a Zeiss Gemini column (all Zeiss

Microscopy, Göttingen, Germany). The determination of diameters was performed by randomly measuring 30 fibril diameters in three repetitions. The Axio Observer Z1 (Zeiss Microscopy, Göttingen, Germany) was used for fluorescence and brightfield imaging.

4.3.3 Production of MEW fibers/scaffolds fabricated with P*n*PrOx, P*cyclo*PrOx, and their blend

To create blends with different ratios of P*n*PrOx and P*cyclo*PrOx, 1 g of each of the polymers was dissolved in 50 ml deionized water and lyophilized.

For the process of Melt Electrowriting, I used a custom-built device already described elsewhere.[214] In order to produce homogenous fibers, the MEW device was equipped with one heating zone at the syringe and another one at the nozzle. The process parameters for MEW of P*n*PrOx are described in Table 3.

Table 3: Process parameters for MEW with PnPrOx

Process parameters				
Voltage [kV]	5.0			
Collector distance [mm]	4.0			
Pressure [bar]	1.0	2.0	3.0	4.0
Temperature (Nozzle) [°C]	155	160	165	170
Temperature (Syringe) [°C]	140			

The same process parameters were used for P*cyclo*PrOx as well as for the polymer blend, except for the temperature of the syringe, which was increased to 210°C while the temperature of the nozzle was 225°C. Besides the standard collector plate, a heated collector plate connected to the temperature control device C 448 by Hotset (Lüdenscheid, Germany) was used. The G code used for fiber deposition via MEW is available in the SI (Code SI). P*n*PrOx and the P*n*PrOx + P*cyclo*PrOx blend scaffolds were finally crystallized by prolonged heating at 60°C for 24 hours. Before applied in cell culture, scaffolds were sterilized by UV-treatment (254 nm) with a UV-lamp (VL-4.LC, Vilber Lourmat, Essen, Germany).

2D controls were created by dissolving 0.1 wt% P*n*PrOx in water. 200 µl were added in each well of a 24 well plate, dried and heated at 60°C for 24h to create crystalline P*n*PrOx-coatings.

4.3.4 Production of PCL-fibrils based on PCL/PVAc blends

70% PVAc (Kremer Pigmente GmbH & Co. KG, Aichstetten, Germany) and 30% PCL (Corbion Purac, USA) were dissolved in dichlormethane (DCM) for 1 hour under stirring conditions. Films of the blend were casted, and DCM evaporated overnight. Afterwards, residual DCM was removed via ultra-high vacuum. Furthermore, the blends were also created in the compounder Xplore (Xplore Instruments BV) at 120°C, 100 rpm for 60 minutes.

For MEW, the polymer was heated in the syringe to 150°C, with the nozzle being heated to 165°C. The scaffolds were created with the same G code used for the POx blends. Before application in cell culture, the PCL fibrils were exposed by washing the scaffolds 3x for 30 minutes in 70% ethanol. This led to the dissolution of PVAc, while sterilizing the scaffolds at the same time. Afterward, the scaffolds were washed 3x in sterile PBS for 5 minutes each.

4.3.5 Creation of collagen-fibril scaffolds

Until used, the rat tails were stored at -80 °C. Rat tails were thawed at RT for 3 hours before the isolation of collagen fibrils. Collagen fibrils were retrieved as described elsewhere[215] and washed in PBS. Then, single fibrils were bundled, fixed in a clamp and subsequently, the endotenon was opened or removed by scalpel scrapping. Afterward, collagen was decellularized by 1h rotated incubation in 0.05% Trypsin-EDTA (Thermo Fisher Scientific, Waltham (USA)) in PBS, followed by 1h rotated incubation in 1% Trypsin-100 (Merck, Darmstadt (D)) in PBS at RT. Then, fibrils were washed 3-times in deionized water, incubated with 5 µg/ml RNase (Merck, Darmstadt (D)) and 10 µg/ml DNase (Merck, Darmstadt (D)) in PBS for 3 h at RT and washed again for 5-times with deionized water. Afterward, the collagen fibrils were straightened by scalpel scraping and clamped in 24-well cell crowns (scaffdex oy, Tampere (FIN)) and used as collagen fibril scaffolds.

4.3.6 Determination of the fiber diameters

Fiber diameters were determined using the straight-line selection tool of FIJI software. For this, 50 randomly selected fibers were measured from SEM images, and mean values were calculated.

4.3.7 Cell culture

All experiments were approved by the Local Ethics Committee of the University of Wuerzburg.

All cell culture experiments with following staining, gene expression analysis and cytokine release analysis were carried out by my colleague Tina Tylek.

4.3.8 SEM sample preparation

For SEM preparation, after seven days of cultivation, samples were fixed with 6% glutaraldehyde for 15 min on ice. Since P*n*PrOx dissolves in both acetone and ethanol, the samples were washed with deionized water and frozen in liquid nitrogen. After lyophilization, the samples were fixed on stubs and coated with a 2 nm platinum layer by a Leica EM ACE600 sputter coater (Leica Microsystems, Wetzlar, Germany).

PCL and collagen samples were incubated two times with PBS on ice prior to their dehydration by a graded ethanol series (2 times 70%, 2 times 90%, 2 times 100% (v/v)). After drying via hexamethyldisilazane, the samples were fixed and coated as described above.

4.3.9 Statistics

The determination of the statistical significance was performed by the two-way analysis of variance (Anova) using the Statstica 13 software (Statsoft, Hamburg, Germany). Results were considered to be significantly different at a p-value below 0.05.

4.4 Results

4.4.1 Melt Electrowriting of polyblends of P*n*PrOx + P*cyclo*PrOx and PCL + PVAc

Via Melt Electrowriting, I was able to deposit homogenous fibers of P*n*PrOx as scaffolds. The most important processing parameter for the diameter control was the pressure, which resulted in the need of temperature adaptation. By controlling and adjusting these two parameters, the homogenous deposition of fibers was possible, leading to the fabrication of uniform scaffolds (**Figure 13**).

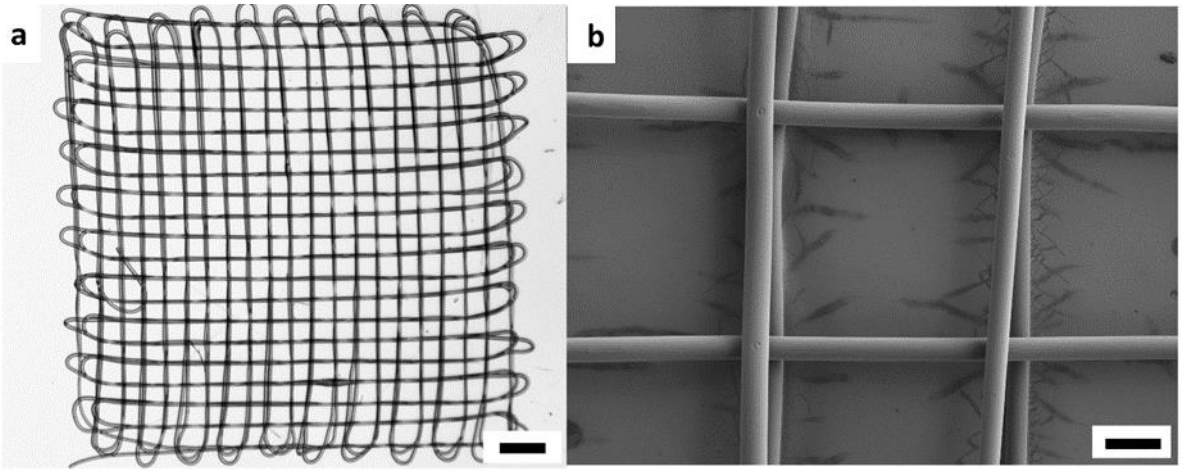

Figure 13: Establishment of the printing process of PnPrOx via MEW. *a, b: Example of scaffold made from PnPrOx with 1 bar pressure and 160°C nozzle temperature (Scale bar: C: 1000 µm, D: 500 µm).*

To counteract the expected swelling of scaffolds in aqueous solutions (**Figure 14**), longer heating periods were applied and increased the amount of non-dissolvable material (**Figure 15**). As optimized conditions to crystallize P*n*PrOx and prevent its dissolution in an aqueous solution, heating at 60°C for 24 hours was chosen for further experiments.

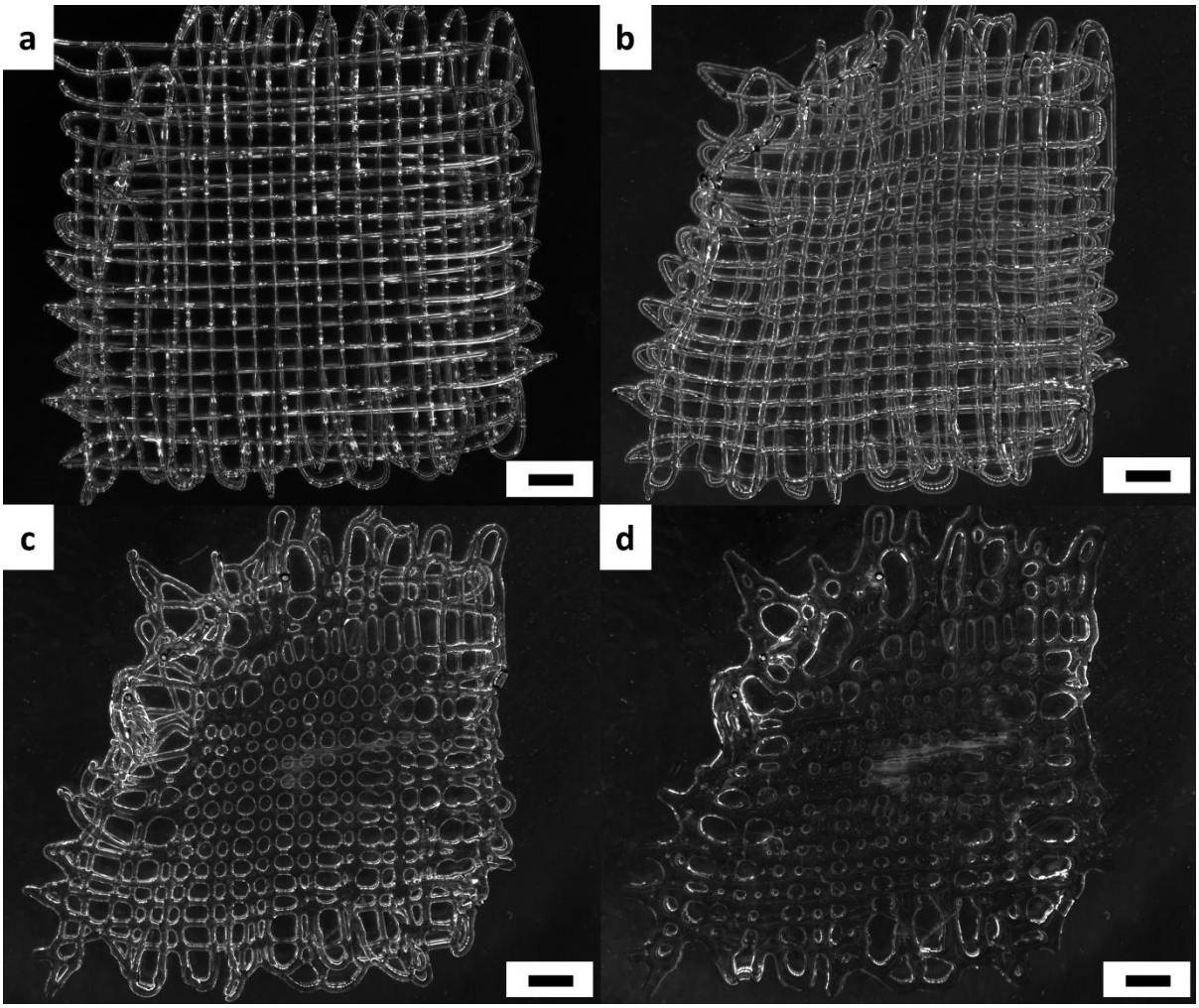

Figure 14: Swelling behaviour of amorphous PnPrOx scaffolds in aqueous solution. *a: PnPrOx scaffold created via MEW; b-d: Swelling-behaviour of a PnPrOx scaffold in water at 37°C after 1, 3, and 5 minutes. Scale bar: 1 mm.*

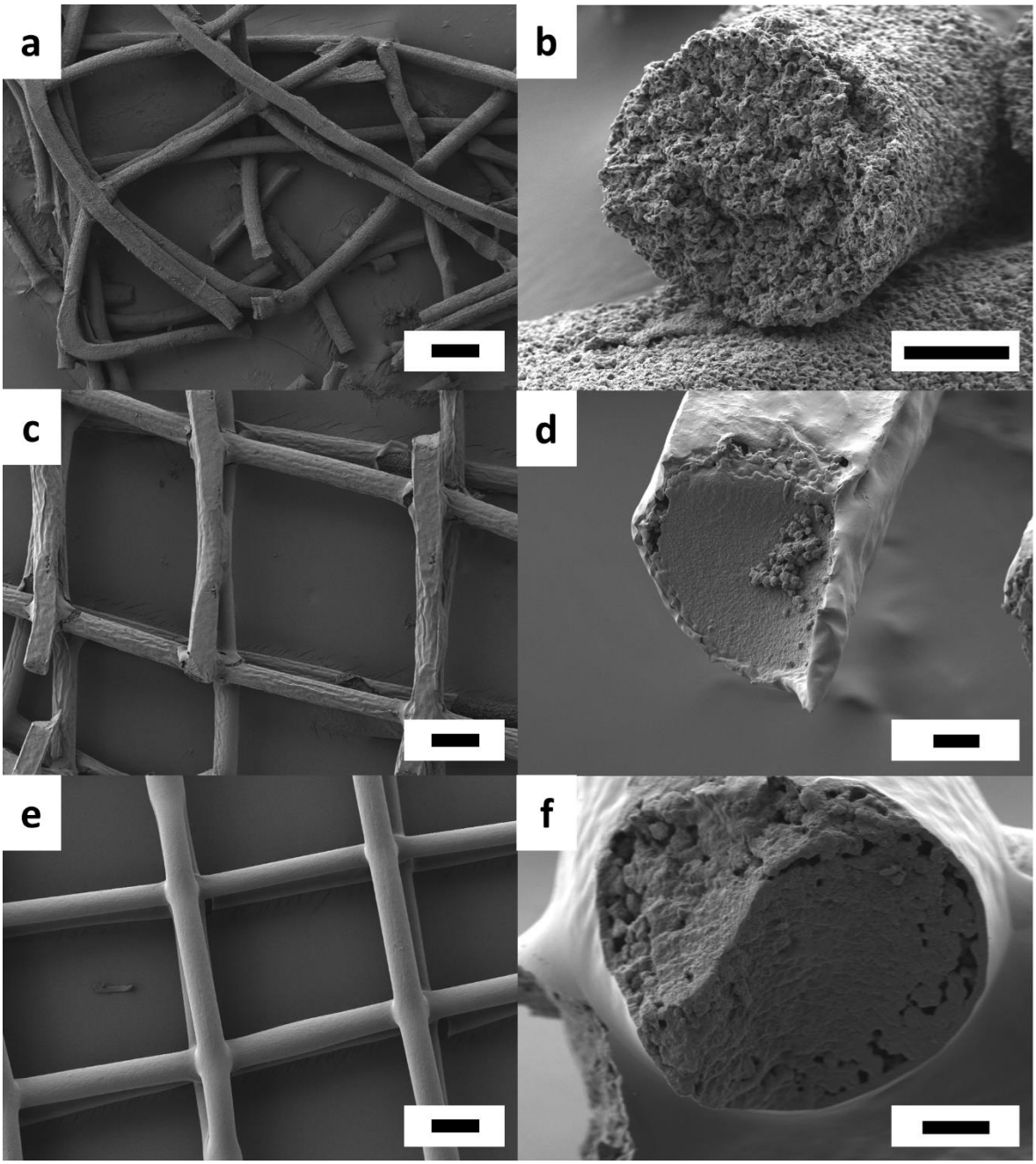

Figure 15: Crystallization of PnPrOx-Scaffolds at 60 °C for 2, 4 and 6 hours. *Afterwards, scaffolds were kept in ultrapure water at 4°C for 1 hour to dissolve the amorphous part. Leftovers were mounted for SEM-images. a, b: Crystallization for 2 hours; c, d: Crystallization for 4 hours; e, f: Crystallization for 6 hours; Scale bar: a, c, d: 100 µm; Scale bar: b, d, f: 10 µm*

To produce fibers from the P*cyclo*PrOx melt, higher processing temperatures of the syringe (210°C) and the nozzle (225 °C) were necessary. Similar to P*n*PrOx, the fiber diameter was mainly dependent on the applied pressure during the process of MEW. However, I was not able to create homogenously deposited fibers using the conventional collector plate of the MEW-device. By using a heated collector plate and increasing its temperature, the homogeneity of the P*cyclo*PrOx scaffolds was improved. A minimum temperature of 90°C on

the collector plate led to a uniform deposition of fibers, which resulted in the formation of homogenous scaffolds (**Figure 16**). Therefore a heated collector was used in further experiments.

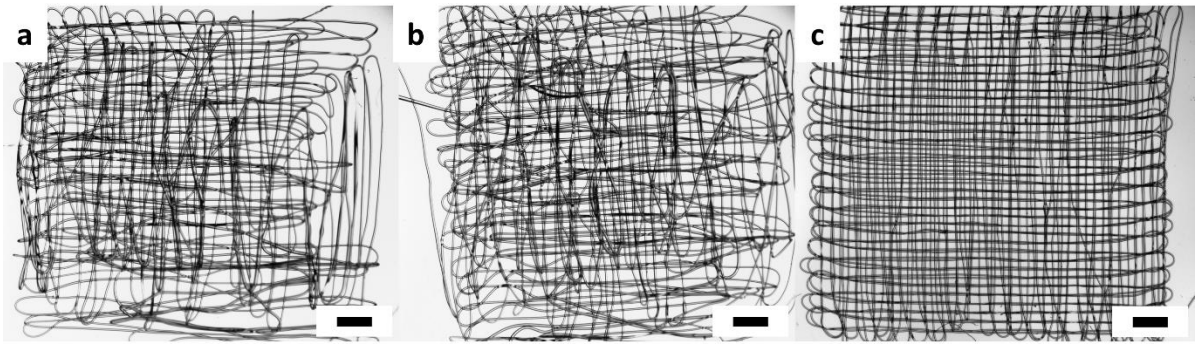

Figure 16: Deposition of PcycloPrOx fibers via MEW at different collector plate temperatures. *a: 20 °C; b: 50 °C; c: 90 °C (Scale bar: 1 mm)*

The printability of P*n*PrOx + P*cyclo*PrOx blends via MEW was initially tested with the parameters for the printing of P*cyclo*PrOx and different blend ratios, namely 80% P*n*PrOx + 20% P*cyclo*PrOx, 60% P*n*PrOx + 40% P*cyclo*PrOx, 40% P*n*PrOx + 60% P*cyclo*PrOx, and 20% P*n*PrOx + 80% P*cyclo*PrOx. The homogeneity of the deposited fibers improved with a decreasing ratio of P*n*PrOx in the blend. Interestingly, the blend with 20% P*n*PrOx and 80% P*cyclo*PrOx revealed a thread like structure composed of crystalline P*n*PrOx fibrils (**Figure 17**, Figure 19 e, h).

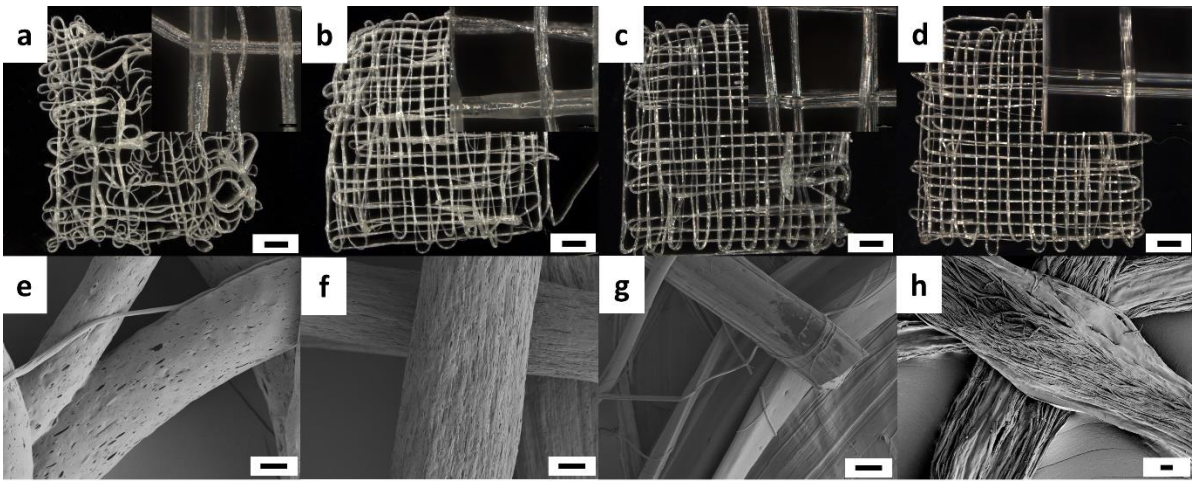

Figure 17: Scaffolds derived from varying blend compositions. *Stereomicroscopic images of scaffolds derived from a: 80% PnPrOx + 20% PcycloPrOx; b: 60% PnPrOx + 40% PcycloPrOx; c: 40% PnPrOx + 60% PcycloPrOx; d: 20% PnPrOx + 80% PcycloPrOx; SEM image of crystalline PnPrOx leftover scaffolds after washing derived from e: 80% PnPrOx + 20% PcycloPrOx; f: 60% PnPrOx + 40% PcycloPrOx g: 40% PnPrOx + 60% PcycloPrOx; h: 20% PnPrOx + 80% PcycloPrOx; (Scale bar: a-d: 1 mm, e-f: 20 µm)*

However, the scaffolds produced from these fibrillar structures were brittle and hard to handle. Additional blend ratios with 30% P*n*PrOx + 70% P*cyclo*PrOx and 10% P*n*PrOx + 90% P*cyclo*PrOx preserved the fibrillar structures whereas the stability of the fibrils was only enhanced with the higher amount of 30% PnPrOx in the blend (**Figure 18**).

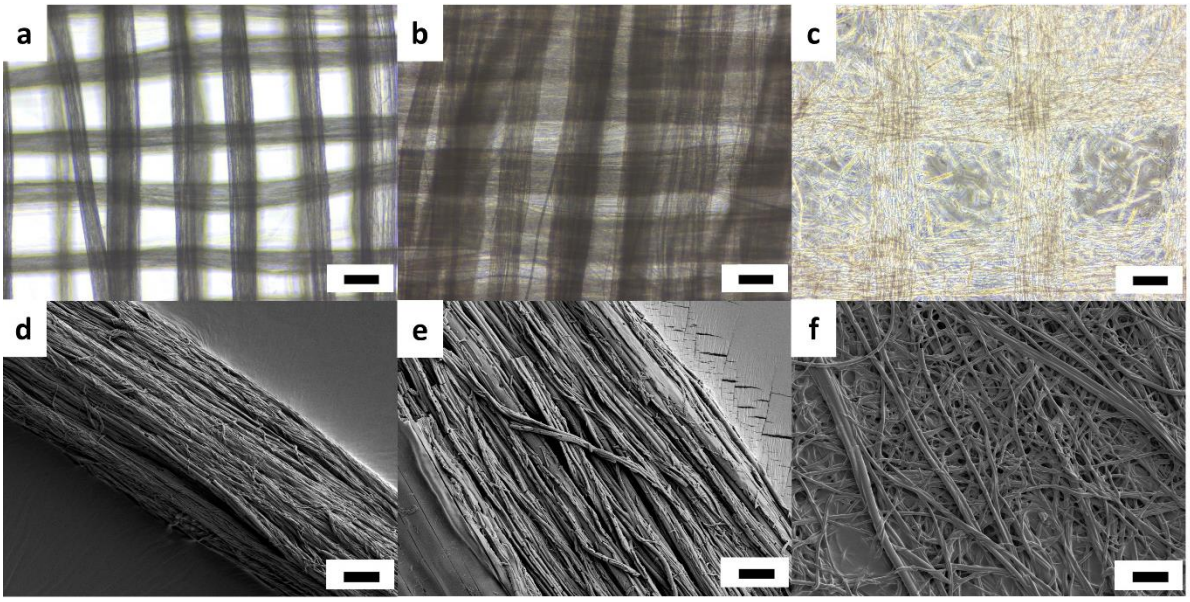

Figure 18: Stability of fibrillar scaffold derived from 10-30% PnPrOx content in water. *a: Brightfield microscopy image of fibrils derived from 30% PnPrOx + 70% PcycloPrOx; b: Brightfield microscopy image of fibrils derived from 20% PnPrOx + 80% PcycloPrOx; c: Brightfield microscopy image of fibrils derived from 10% PnPrOx + 90% PcycloPrOx; d: SEM image of fibrils derived from 30% PnPrOx + 70% PcycloPrOx; e: SEM image of fibrils derived from 20% PnPrOx + 80% PcycloPrOx; f: SEM image of fibrils derived from 10% PnPrOx + 90% PcycloPrOx. (Scale bar a, b, c: 100 µm; d, e, f: 20 µm)*

Consequently, using scaffolds based on 30% P*n*PrOx + 70% P*cyclo*PrOx led to an improved handling during cell culture and has therefore been used in the following biological experiments.

4.4.3 Characterization of fibrillar structures

The aligned fibrils created from one continuous fiber based on the 70% P*cyclo*PrOx + 30% P*n*PrOx blend were fabricated in reproducible quality by the method described above (**Figure 19** a). Optically, the fibril bundles are similar to silky wool, when submerged in water and also after lyophilization. SEM imaging revealed aligned fibers, which differ in diameter size but are still normally distributed at around 1.5 µm (**Figure 19** d, g, j).

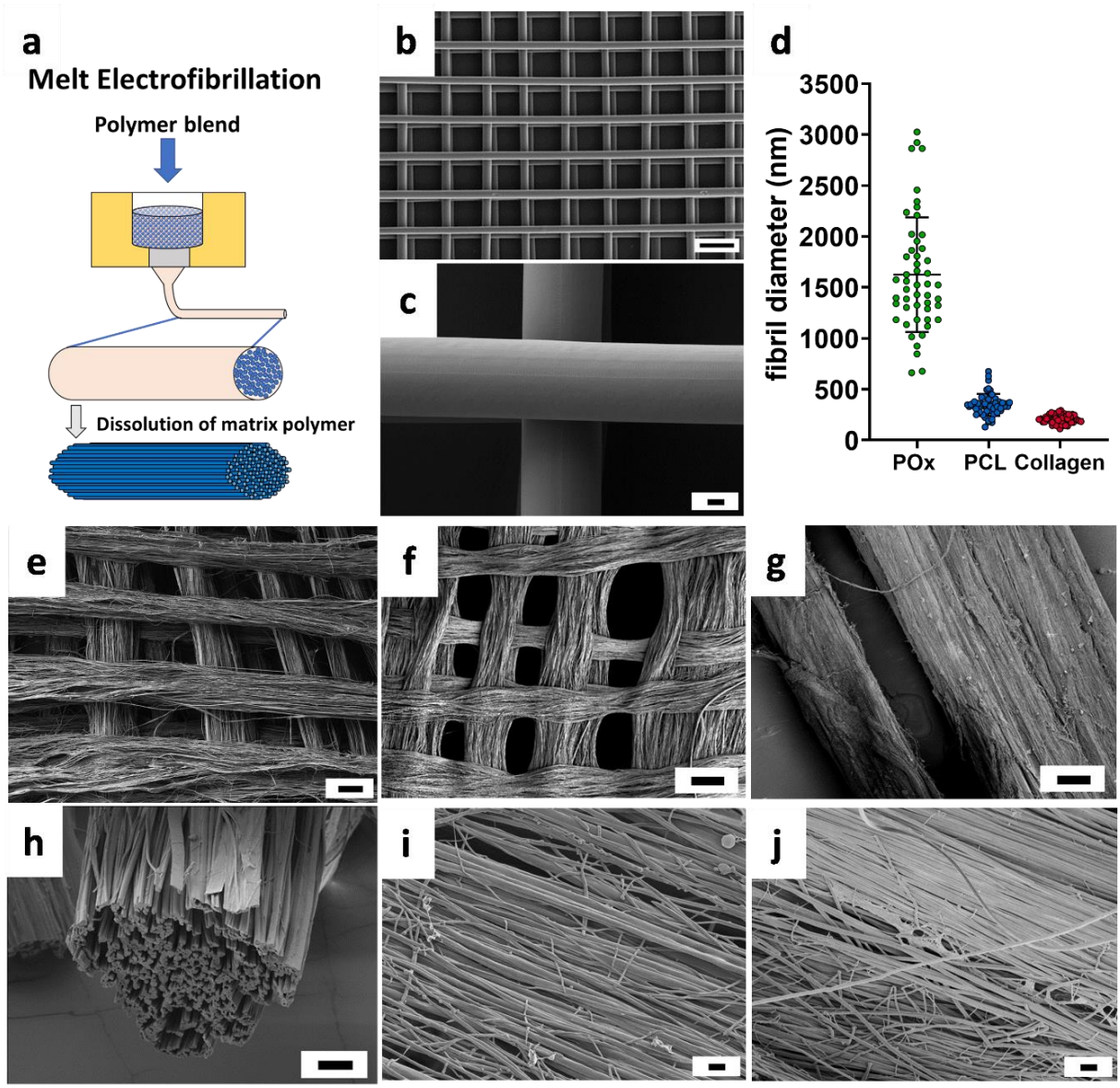

Figure 19: Melt Electrofibrillation. *a: Manufacturing scheme of fibrillar scaffolds. A polymer blend was processed via MEW. After dissolution of the matrix polymer, aligned nanofiber microbundles emerge; b, c: SEM image of blend scaffold before dissolution of the sacrificial polymer; d: fibril diameter measurements of POx-, PCL- and Collagen-fibrils (50 values each). e, h: SEM-images of PnPrOx fibril scaffold after dissolution of PcycloPrOx; f, i: SEM-images of PCL fibril scaffold after dissolution of PVAc; g, j: SEM-images of rat tail collagen fibrils (scale bar b:200 µm; e, f,g: 100 µm; c, h: 10 µm; i, j: 1 µm)*

To identify the reasons for the formation of this fibril morphology, I investigated the polymer blend behaviour in the melt. While after one hour at the specific processing temperature, the pure melts are transparent, but the melt of the blend has an opaque appearance without any macroscopically detectable phase separation. Next, the miscibility of P*n*PrOx and P*cyclo*PrOx was analyzed by the comparison of the respective glass transition temperatures (Tg) of the homopolymers with that of the blend via DSC. P*n*PrOx shows a Tg at 38°C, while the Tg of P*cyclo*PrOx is at 85°C. Since the DSC-measurement of the blend exhibits two peaks at the same temperature as the homopolymers, it indicates phase separation of P*n*PrOx and

P*cyclo*PrOx.[216,217] Furthermore, stereo-microscopical analysis revealed a uniform spherical phase separation of both polymers in the blend (**Figure 20**).

Moreover, the electrical field conventionally applied with MEW had an impact on fiber morphology. When the voltage was switched off, the pressure itself led to an initial fibril formation from the blend (**Figure 20** c), however, a uniform fibril morphology was only achieved by introducing the charge.

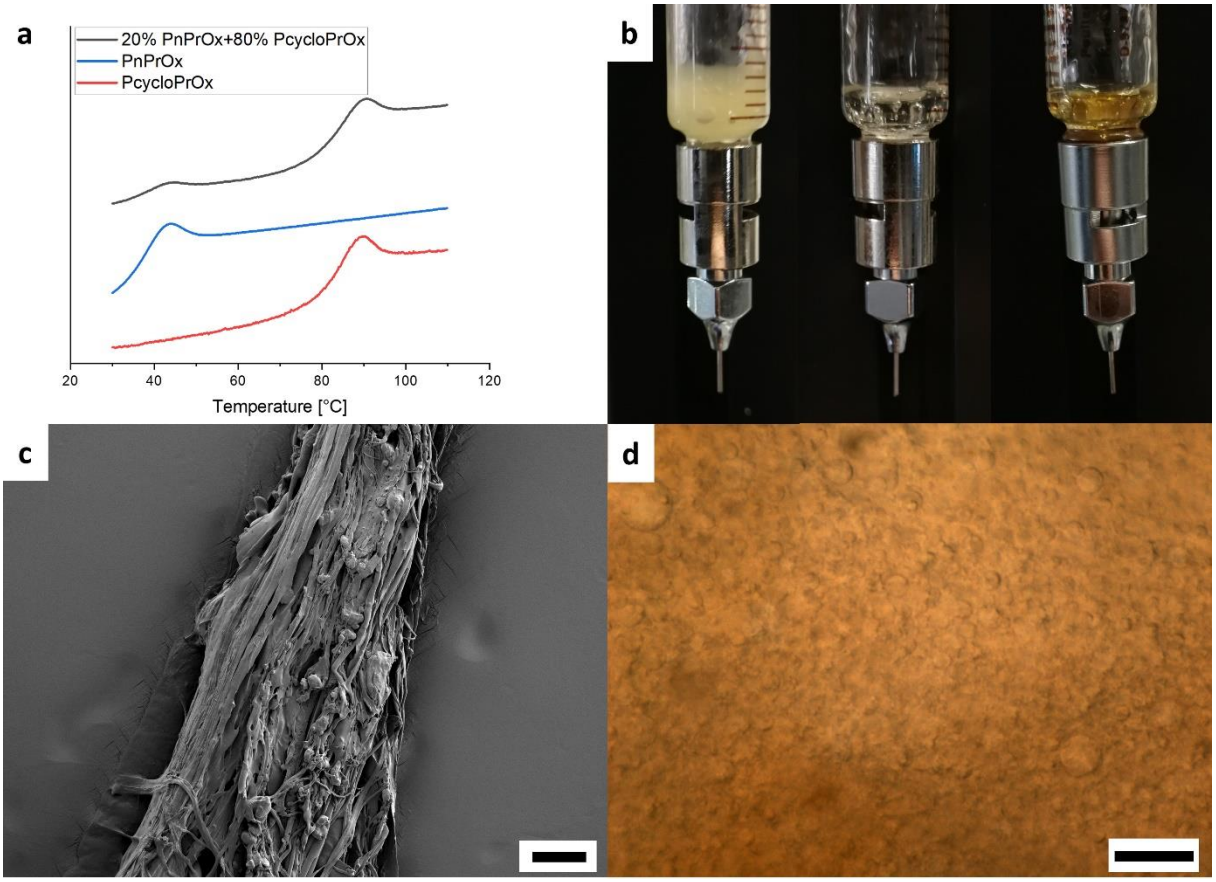

Figure 20: Investigation of PnPrOX + PcPrOx blend characteristics. *a: DSC-Measurement of PnPrOx, PcycloPrOx and 20% PnPrOx + 80% PcycloPrOx blend ranging from 30 to 110°C with a heating rate of 10K/min; b: Images of the melts from left to right: 20% PnPrOx + 80% PcycloPrOx, PnPrOx, PcycloPrOx; c: Fibrils created from fibers printed via MEW without electrical field. Scale bar: 100 µm; d: Phase separation behavior in the melt of 20% PnPrOx + 80% PcycloPrOx. Scale bar: 50 µm*

Additionally, I was not able to reproduce this effect by creating a blend of 80% P*cyclo*PrOx and 20% Poly(2-*iso*propyl-2-oxazoline) (P*iso*PrOx) instead of P*n*PrOx. Crystalline structures were formed, but their appearance was spherical, and no fibril shape was obtained after processing. Furthermore, by observing the melt after 1 h at 210 °C, a higher degree of phase separation could be observed (**Figure 21**).

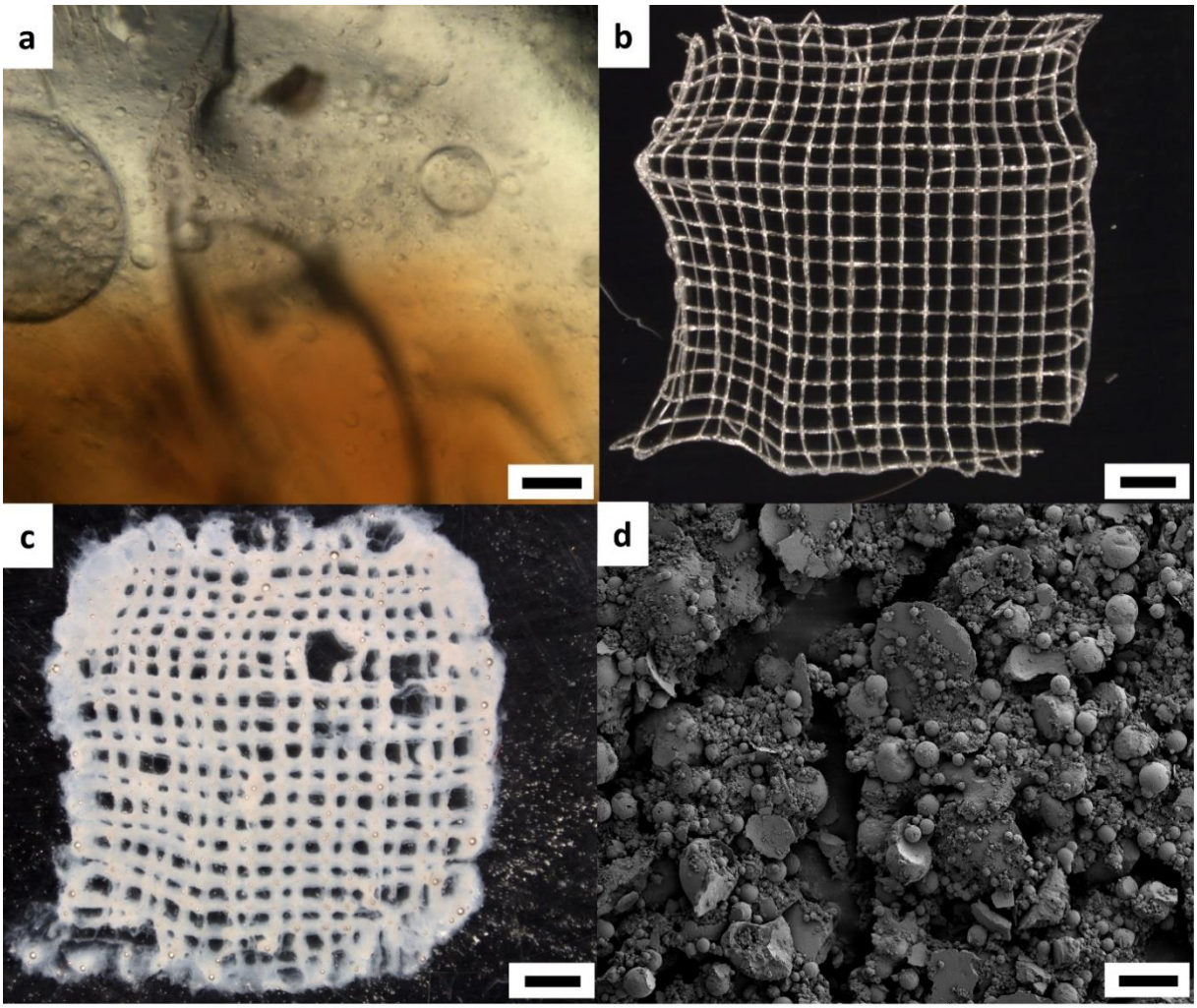

Figure 21: Behaviour of 20% PiPrOx + 80% PcycloPrOx scaffolds in water after crystallization. *a: Melt of blend 20% PiPrOx + 80% PcycloPrOx after 1 hour at 210 °C (Scale bar: 50 µm); b: 20% PiPrOx + 80% PcycloPrOx scaffold created via MEW and crystallized for 24 hours at 60 °C (Scale: 1000 µm); c: Crystalline leftovers of PiPrOx after dissolving PcycloPrOx in water at 20 °C (Scale bar: 1000 µm); d: SEM-images of crystalline leftovers of PiPrOx (Scale bar: 100 µm)*

4.4.4 Adaption of Melt Electrofibrillation on the miscible blend 70% PVAc + 30% PCL

One disadvantage of the fibrils based on P*n*PrOx is their stability and brittleness. Scaffolds must be handled very carefully; even simple shaking leads to breaking of the scaffolds. Contrarily, scaffolds based on PCL are known to exhibit good mechanical stability. Therefore, PCL was blended with certain sacrificial polymers, which can be dissolved in either water or 70% ethanol: Pluronic, PEG 4000 and PVAc.

Accordingly, I conducted MEW with 70% PEG + 30% PCL and 70% Pluronic + 30% PCL. Although the creation of scaffolds was feasible, the jet could not be stabilized properly, and fibril-like phase separation occurred in an unordered manner (**Figure 22**).

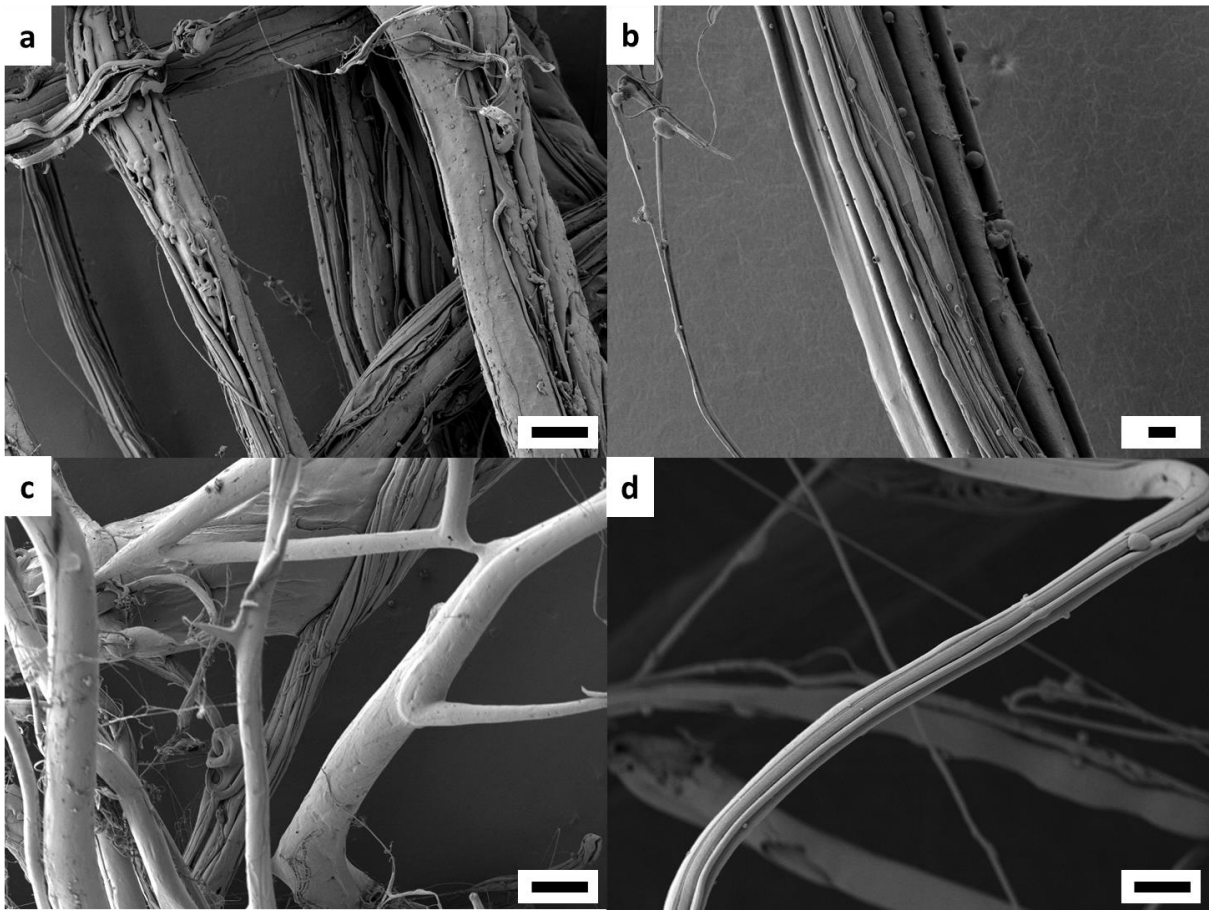

Figure 22: Melt electrowritten scaffolds after dissolution in water. *a, b: PCL + Pluronic; c,d: PCL + PEG 4000. Scale bar a, c: 100 µm; b, d: 10 µm*

MEW of 70% PVAc + 30% PCL led to the creation of ordered scaffolds. After dissolution of PVAc in 70% ethanol, highly ordered aligned PCL fibers were exposed, with smaller diameters (~300 nm) compared to fibrils based on P*n*PrOx. Based on the smaller diameter, the PCL fibrils showed higher morphological similarities to natural collagen fibrils prepared from decellularized rat tail collagen I (**Figure 19**d, g, j, **Figure 23**) than fibrils made of P*n*PrOx.

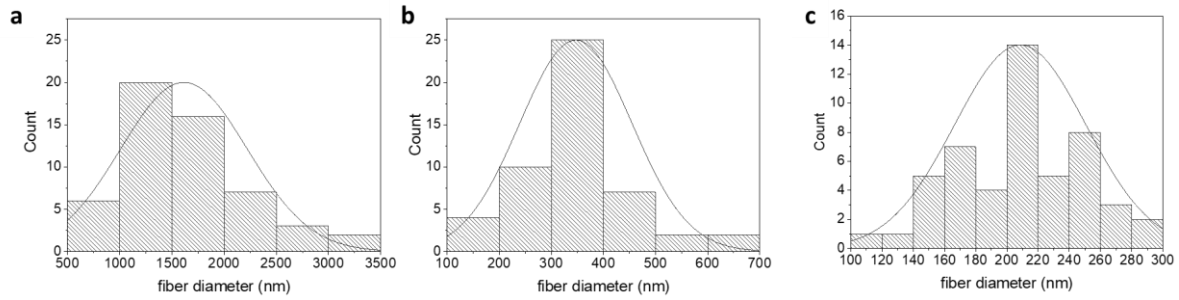

Figure 23: Normal distribution of fibril diameters. *a: PnPrOx; b: PCL; c: Rat tail collagen fibrils*

To avoid the use of DCM or other solvents, I further used a compounder to create the solvent-free blend. MEW, as well as fibril formation after dissolution of PVAc, was successful and the proof-of-concept was given (**Figure 24**).

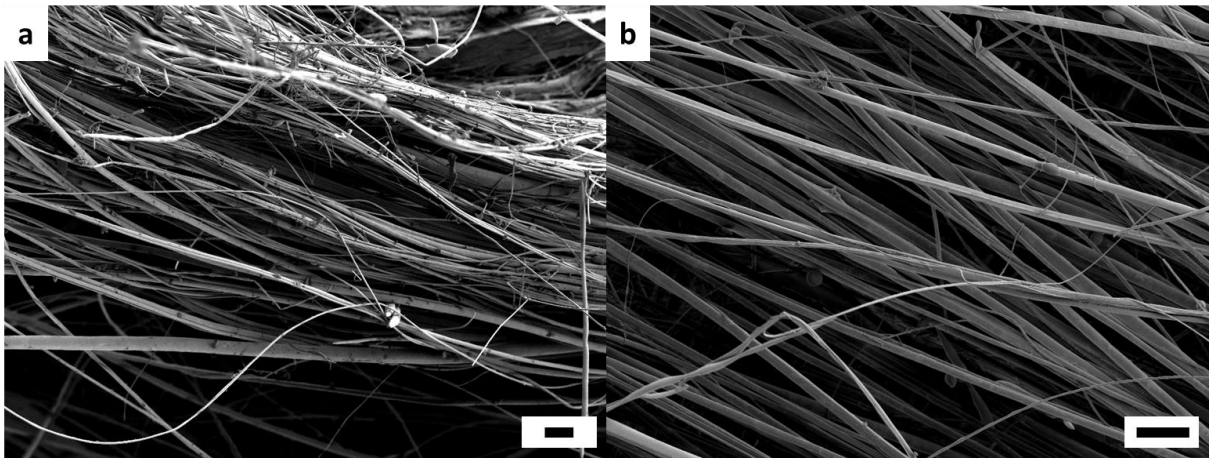

Figure 24: a, b: PCL fibrils made from PCL + PVAc blends created solvent-free in a compounder. *Scale bar: 20 µm*

4.5 Discussion

The combination of biocompatible polymers with the sophisticated 3D printing technique MEW has already been shown as a potential candidate for biofabrication. Here this approach is expanded by adding the possibility to create bundles of aligned fibrils together with a direct biological application as an immunomodulatory 3D scaffold.

In detail, I developed a method to create bundles of aligned polymer fibrils by combining a blend based on polyblends, namely P*n*PrOx + P*cyclo*PrOx or PCL + PVAc, with the fabrication technique of MEW. Furthermore, the successful application of these constructs as 3D biocompatible scaffolds was provided and has proven an immunomodulatory effect on human macrophages mediated solely by their nanoscale topography, as shown by my colleague Tina Tylek (**Figure 25**).

First, I established MEW for P*n*PrOx, P*cyclo*PrOx and their respective blends. Furthermore, a heated collector plate was introduced as an assisting tool to create homogenous scaffolds with P*cyclo*PrOx. The high Tg of this polymer[216] and the rapid cooling of the fiber when reaching a non-heated collector-plate leads to fast vitrification preventing the homogenous deposition of the fiber. The additional heat source in the collector plate kept the temperature between the plate and the nozzle at the same level and therefore enabled the directed printing of P*cyclo*PrOx. Secondly, I printed the blends of P*n*PrOx and P*cyclo*PrOx at higher temperatures suitable for P*cyclo*PrOx to ensure that both polymers were in their processable

molten state. Thereby, the printability was improved with a decreasing ratio of P*n*PrOx in the blends leading to the creation of more homogenous scaffolds.

After the scaffolds were printed, the bulk crystallization of P*n*PrOx was effectively induced by prolonged heating at 60°C for 24 hours, as shown by the loss of its lower critical solution temperature (LCST). The extended heating period/duration applied in the study seems to overcome the issues Hoogenboom and coworkers encountered, when they did not succeed in the crystallization of P*n*PrOx after heating the polymer only for 2 hours.[218] Apart from crystallizing pure P*n*PrOx scaffolds according to the prolonged heating protocol, I was able to specifically crystallize only the P*n*PrOx in the blended scaffolds. Meanwhile, P*cyclo*PrOx was still amorphous after temperature treatment, indicating that its LCST behavior (30°C)[219] remained. Therefore, by exposing these blended scaffolds to water at temperatures below the LCST of P*cyclo*PrOx, I was able to dissolve and separate the amorphous P*cyclo*PrOx from the crystalline P*n*PrOx.

When the ratio of P*n*PrOx in the blend was 30% and lower, fibril bundle-like structures with the fibril diameter in the nano- to micrometer range were exposed after dissolution. Subsequent DSC experiments suggested that the P*n*PrOx + P*cyclo*PrOx blend exhibited a phase separation and was therefore not miscible.[220] However, after one hour at 210°C, the blend did not fully separate into two separate phases macroscopically, although spherical separation could be observed microscopically. By additionally inducing pressure during the process of MEW, the phases seemed to obtain a certain orientation, which initially led to a directed phase separation. Nevertheless, the electrical field applied during MEW finally led to the creation of smooth fibrils by stretching and elongating the fiber and its included separated phases. After crystallization, these fibrillar scaffolds exhibited morphological similarities to woven nanofiber yarn scaffolds designed for tendon[221] and cardiac[222] tissue engineering.

Since POx-based scaffolds are very brittle, the handling and the maintenance of the original structure is quite complicated because of easily breaking fibrils and delamination. Therefore, I have investigated the possibility of transferring this system to other materials. Since PCL is the most extensively studied material for MEW and is furthermore clinically approved, I tested several blends with other sacrificial polymers. The combination of PCL with PVAc was successful. Here, I was able to create nicely shaped scaffolds with improved stability that are much easier to be handled during cell culture. Furthermore, a decreased average fibril diameter down to 300 nm compared to 1500 nm of P*n*PrOx fibrils was observed. One

explanation might be that the brittleness of very thin P*n*PrOx fibrils causes them to break and disperse in water so that they cannot be imaged anymore. Additionally, compared to the non-miscible POx blend, PVAc + PCL is already known to be a miscible blend.[223] By that, the blend morphology does not exhibit the same spherical structures, as shown for the POx blend, leading to the generation of fibrils with small diameters. As collagen fibrils have a diameter of about 150-200 nm, the fabricated PCL fibrils seem to be highly comparable to them and, therefore, can be described as biomimetic.

Since aligned fibers are known to have a certain influence in biological systems because of topographical cues[13,224,225], the 3D fibrillar scaffolds were further tested for their immunomodulatory effect on human monocyte-derived macrophages. As a 3D control, scaffolds derived solely from P*n*PrOx or PCL were printed via MEW. Since the fibrillar scaffolds that were made from PCL, were morphologically comparable to collagen fibrils, macrophage polarization was further determined on decellularized collagen I fibrils.

The influence of aligned surface topography on the elongation of macrophage morphology and a consequently improved polarization towards a healing-phenotype has already been described in studies with 2D samples[13,211], however, so far only for murine macrophages. Moreover, in a recent study of my colleagues, box-shaped scaffolds with 40 µm pores could be related to an increased elongation of human macrophages leading to an upregulation of M2 markers compared to scaffolds with bigger pores[90]. Nonetheless, the elongation behavior of human macrophages in 3D is almost unexplored, and so far, biological explanations for the elongation of human macrophages are missing. In this study, the phenomenon of topography mediated elongation and polarization towards the M2-type was proven for the first time in a directly written 3D approach for human monocyte-derived macrophages (Figure 25 a, b).

Changes in cell morphology were revealed after cultivation of human monocyte-derived macrophages on the different scaffold topographies. While on fiber scaffolds, macrophages adopted a roundish, flat morphology, macrophages on fibrillar scaffolds elongated partly extremely. In particular, macrophages on PCL fibrils had a cell length of up to 190 µm. The lower elongation length on POx and collagen fibrils may be explained by the bigger fibril diameter or by a denser scaffold structure, respectively.

Further biological experiments by Tina Tylek provided evidence that macrophages cultivated on fibril bundles show strong similarity to those cultivated on collagen I bundles in regard to

gene expression and protein secretion (**Figure 25** c). After 7 days, pro-healing and anti-inflammatory factors were upregulated, while pro-inflammatory factors were downregulated. Furthermore, the upregulation of pro-healing factors is nearly as strong as the induction via soluble factors (IL-4). This extent has not been shown by any other topography-polarization study before. The non-topographic control samples also showed a downregulation of inflammatory markers, however, no increase in anti-inflammatory/pro-healing factors have been observed, indicating the transition into the “deactivated” macrophage state that can be chemically induced, e.g., by dexamethasone[10].

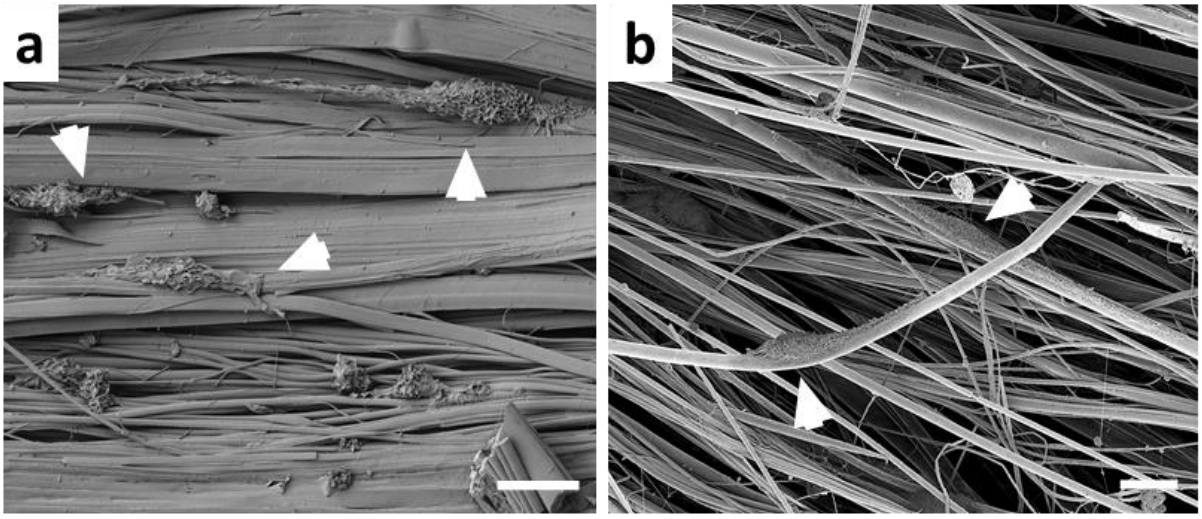

c

		PCL fiber		PCL fibril		Collagen I fibril	
Cell morphology		roundish, flat		elongated		elongated	
Gene Expression (e) /Release (r)		**d1/d3**	**d7**	**d1/d3**	**d7**	**d1/d3**	**d7**
Anti-inflammatory/ Pro-healing	CD163 (e)	1	14 (± 6.7)	1,6 (± 0.7)	0,7 (± 0.4)	4.6 (± 2.1)	5.8 (± 3.2)
	CD206 (e)	1	1.5 (± 0.6)	1.7 (± 0.9)	78 (± 13.2)	12.2 (± 5.1)	41 (± 11.2)
	IL-10 (r)	0.06 (± 0.02)	0.5 (± 0.15)	0.6 (± 0.22)	4.1 (± 0.4)	1.5 (± 0.34)	7.6 (± 0.96)
Pro-fibrotic	TGF-β (r)	280 (± 77)	160 (± 43)	183 (± 25)	92 (± 8.6)	76 (± 8.9)	42 (± 6)
Pro-inflammatory	IL-1β (r)	4.6 (± 2.6)	2.9 (± 1.3)	76 (± 26)	24 (± 1.5)	76 (± 8.9)	16 (± 3.4)
	TNF-α (r)	0.13 (± 0.11)	0.19 (± 0.05)	4.6 (± 2.1)	0.5 (± 0.13)	0.5 (± 0.9)	0.14 (± 0.03)
Pro-angiogenic	IL-8 (r)	1336.5(± 109.1)	1050 (± 189)	6672 (± 277)	5561 (± 883)	1653 (± 516)	1059 (± 263)
Similarities to macrophage-type (function, stimuli)		M2c (deactiviated, DEX-induced		M2a (tissue regeneration, IL-4-induced)		M2a (tissue regeneration, IL-4-induced)	

Figure 25: Overview of macrophage response to 3D-surfaces*. a: SEM-image of elongated and aligned macrophages (white arrows) seeded on PnPrOx fibril bundles. b: SEM-image of elongated and aligned macrophages (white arrows) seeded on PCL fibril bundles. c: Alterations in macrophage morphology, gene/protein expression, and cytokine release dependent on topographical cues over seven days compared to the first day considering changes on day three. +: higher expression/ release; –: lower expression/ release; 0: no change*

Proper wound healing after injuries or implantations of biomaterials requires the involvement of both M1 and M2 macrophages, however, in an ordered timeline. While the absence of M1 macrophages in the early stages of regeneration impairs healing, a prolonged occurrence can lead to chronic inflammation or fibrosis[210]. Therefore, a biomaterial should not inhibit the early M1 polarization but induce a punctual phenotypical switch. With the creation of fibrillar

scaffolds, a significant M1-to-M2 switch could be achieved that should fulfill the needed requirements for normal wound healing. Additionally, macrophages induced by fibrillar 3D topography showed a lower expression of the myofibroblast activating, profibrotic marker TGF-b1[226,227], compared to fiber scaffolds and may, thus, have the potential to reduce the risk of later fibrotic encapsulation of the biomaterial.

Based on previous studies demonstrating that *in vitro* elongation and M2 polarization of rodent macrophages could be transferred to *in vivo* models[228-230], I am confident that the fibrillar scaffolds would lead to similar results. Nevertheless, human and mouse data cannot be fully correlated, and therefore, experiments with human macrophages are important to reveal clinical relevance, which in this study could even be increased by the fabrication of an immunomodulatory scaffold using the clinically approved material PCL.

4.6 Conclusion

In this project, I describe a method to create biomimetic bundles of aligned P*n*PrOx fibrils by printing single fibers via Melt Electrowriting of a P*n*PrOx + P*cyclo*PrOx and a PCL + PVAc blend, which is based on directed phase separation of both polymers during the fabrication process. It was proven that these fibrillar structures lead to an elongated human macrophage phenotype concomitant with polarization towards the pro-healing M2 type. To the best of my knowledge, this project introduced immunomodulatory topographies for the first time in a directly written 3D scaffold fabrication approach, which provides a platform for further in-depth studies of topography dependent macrophage processes or mediated differentiation of other cell types. However, this project does not simply provide another topography-design but can rather be described as the mimicry of ECM ultrastructure. Therefore, this approach leads to a new insight that ultrastructural ECM elements are influencing and guiding the immunomodulation of macrophages. In summary, the fibrillar bundle structure of collagen I and its translation to biomaterials and biofabrication techniques is a promising potent design criterion for biomaterial induced immunomodulation.

Chapter 5

Sacrificial Poly(2-oxazoline) Scaffolds for Biocompatible Microchannel Creation and Prevascularization

This chapter is based on the work of the author of this theses Matthias Ryma, who performed all experiments and data evaluation. A publication that will be supplemented by other collaborators is in preparation at the time of handing in this thesis.

5.1 Abstract

Vascularization of 3D tissue-engineered constructs exceeding the thickness of 1 mm requires a perfusable channel network to enable uniform distribution of oxygen and nutrition. In tissues, the walls of these channels are covered uniformly with endothelial cells, which build up the endothelial barrier. This barrier regulates the uptake of nutrients, particles and even cells into the surrounding tissue. The standard method for endothelialization of channels in tissue constructs is post-process perfusion with cells. However, this method has the disadvantage of requiring many cells, as adequate attachment and proliferation is inhibited. Furthermore, proliferation is time-consuming and especially the endothelialization of small structures with channel diameters below 500 µm is problematic.

Here, these disadvantages were overcome by introducing a new method called “inverse biofabrication”.Two polymers from the poly-oxazoline polymer family have been used for the fabrication of scaffolds via Melt Electrowriting (MEW), namely poly(2-*n*propyl-2-oxazoline) (P*n*PrOx) and poly(2-*cyclo*propyl-2-oxazoline) (P*cyclo*PrOx). Different scaffold-shapes with varying fiber sizes were printed and tested for cell culture. Endothelial cells were seeded and grown to confluency on the scaffolds before embedding into a gelatin methacrylate (GelMA) hydrogel, followed by dissolution and flushing of the sacrificial polymer. It was shown that the endothelial cells attached to channel walls and cell viability was maintained. With this, the first proof-of-principle of inverse biofabrication was successfully given.

5.2 Introduction

The most crucial bottleneck in biofabrication and tissue engineering is the need for an abundant microvascular network in tissue analogues that exceed thicknesses of 1 mm.[14] In tissues with bigger sizes there is no guarantee of an equal distribution of nutrition and oxygen, as well as the removal of waste products. Creating a supporting microvascular network is also a highly complex procedure, since it requires channel diameters of below 100 µm, bifurcations and a tight layer of endothelial cells surrounding the channel walls.[231]

Several different approaches aim for the creation of perfusable hydrogels. One commonly used method is 3D-printing of cross-linkable bioinks combined with another sacrificial ink, e.g., thermoreversible gelatin.[232] By removing the sacrificial ink, perfusable channels are created. As another example, 3D-printed polylactide constructs were immersed in a hydrogel and removed afterward.[233] However, because of the large diameter of the printed strands, traditional 3D printing is strongly limited in creating perfusable channels for microvasculature.[42]

A high-resolution technique, which was adapted to cell containing hydrogels is stereolithography and digital light processing (DLP). Here, photopolymerizable biopolymer encapsulated with cells can be patterned by light enabling the creation of high-resolution 3D hydrogels.[16] Although it is theoretically possible to achieve resolutions below 100 µm, only a few studies managed to create channels below 200 µm, because the softness of hydrogels compared to resins leads to the loss of resolution.[15]

Another approach for vascularization is the core-shell method. Here, tubular constructs are created via specialized coaxial nozzle devices: the crosslinkable bioink is extruded on the outside of the nozzle, while the crosslinking solution is extruded on the inside (e.g., the combination of alginate as hydrogel with a calcium-solution for crosslinking). This finally leads to the generation of a tube, which can be extruded precisely, stacked and even perfused.[234] Since this described method is a 3D printing method, the size is also limited to diameters above 500 µm. Furthermore, a single long tube does not mimic the natural vasculature with its interconnected branches and bifurcations.

Another method to create perfusable channels with small diameters is micro-molding of hydrogels.[235,236] This method allows for generating tiny channel networks, however, only on flat surfaces. 3D-approaches based on this method were also developed by casting hydrogel around 3D-printed sacrificial carbohydrate glass fibers.[237] Simple dissolution of the fibers leads

to the creation of interconnected perfusable microchannels in the casted hydrogel. Recently, even freeform 3D-printing was achieved with carbohydrate glass, allowing for the creation of more complex sacrificial structures.[238] However, the disadvantages of these carbohydrate glasses are their direct and fast dissolution in water and their osmotic pressure, leading ultimately to cell death.

In conclusion, the prerequisite for a successful microchannel creation is a method with very high resolution combined with a material, which allows a controlled and biocompatible dissolution.

The most known additive manufacturing methods for thermoplastics are Fused Deposition Modelling (FDM) and Solution Electrospinning (SES). FDM allows for the directed deposition of the molten thermoplastics yet does not exhibit a high resolution (>200µm X/Y). Instead, for SES, a polymer solution is used as a basis. By applying an electrical force, a fiber is drawn from the polymer solution with diameters at the nanometer scale. However, the method itself does not allow a directed deposition of these fibers.[239]

A method, which combines the directed deposition of FDM with the high resolution of SES is Melt Electrowriting (MEW). Here, a polymer melt is used instead of a polymer solution. The high viscosity and the subsequent cooling of the polymer melt lead to the ability to deposit micron diameter fibers directly.[84] Furthermore, the absence of a solvent benefits biological applications, where solvent toxicity is a concern. Since the materials are melted during processing, it is only possible to use thermoplastics that do not degrade during heating.

Poly(2-oxazoline)s (POx) are an emerging polymer class with thermal stability, high biocompatibility and a broad application range.[7,177] They have recently been applied for bioprinting as bioinks,[152] as coatings for the creation of cell sheets,[9] as hydrogels[200], and even as thermoplastic for MEW.[166] Here, poly(2-ethyl-2-oxazoline) was established for MEW.

Interestingly, POx with longer sidechains exhibit a Lower Critical Solution Temperature (LCST) in water.[178] The polymer can be dissolved by temperature reduction, representing a simple, controllable, and biocompatible stimulus. Especially poly(2-*n*propyl-2-oxazoline) (P*n*PrOx) and poly(2-*cyclo*propyl-2-oxazoline) (P*cyclo*PrOx) exhibit their respective LCST in the physiological range between 20° C and 37° C.[216]

The common property of current vascularization methods is the way of endothelialization. Here, the endothelial cells are seeded after the formation of the tube, meaning cells need to adhere and proliferate.[240] For a proper cell adhesion and confluency, a high number of

endothelial cells is needed, and a full endothelialization is only achieved after a delay of several days[16], using even higher cell numbers could not overcome this delay.[16,17]

To directly generate a full endothelialization of tissue-engineered constructs from the beginning of the cultivation period, a new strategy for vascularization was investigated in this project, namely inverse biofabrication. For this, the endothelial cells are seeded on a fibrous sacrificial scaffold and cultivated until confluency. After embedding the cell-laden scaffolds into a hydrogel, the scaffold is dissolved, resulting in an endothelialized channel network.

In detail, P*n*PrOx and P*cyclo*PrOx were established for MEW and different natural branching scaffolds with varying diameters were printed. By embedding these scaffolds into a hydrogel, the scaffolds swelled due to water adsorption, leading to fiber fusion and the generation of an interconnected channel network after polymer dissolution by temperature decrease. Since both polymers do not retain their shape in aqueous solutions, the following measures were taken: First, P*n*PrOx was partially crystallized to increase stability for the cost of dissolution potential.[218] Secondly, the amorphous P*cyclo*PrOx was coated with a poly(lactid-*co*-glycolid) (PLGA) (50:50) layer to increase stability and allow cell adhesion. Afterwards, endothelial cells were seeded on the scaffolds, grown to confluency, and embedded into Gelatin-methacryloyl (GelMA) hydrogels. Finally, after dissolution and flushing of the polymer, the cells attached to the channel walls and stayed viable.

5.3 Materials & Methods

5.3.1 Chemicals and synthesis of P*n*PrOx and P*cyclo*PrOx

The same chemicals and synthesis were utilized as described in Chapter 3 of the thesis.

5.3.2 Production of MEW fibers/scaffolds fabricated with P*n*PrOx and P*cyclo*PrOx

For the process of MEW, I used a custom-built device already described elsewhere.[214] In order to produce homogenous fibers, the MEW device was equipped with one heating zone at the syringe and another one at the nozzle. The process parameters for MEW of P*n*PrOx and P*cyclo*PrOx with 0.5 to 2.0 bar pressure are described in Table 4.

Table 4: MEW parameters for PnPrOx and PcycloPrOx

Material	**T Syringe (°C)**	**T Nozzle(°C)**	**T Collector plate (°C)**	**Distance (mm)**
P*n*PrOx	160	175	Not used	2,2
P*cyclo*PrOx	200	215	50°C	2,2

Besides the standard collector plate, a heated collector plate connected to the temperature control device C 448 by Hotset (Lüdenscheid, Germany) was used. The G code used for fiber deposition via MEW is available in the SI (Code SI).
To enable easier handling of the scaffolds, simple box-shaped polycaprolactone (PCL) scaffolds with 5 µm fiber diameter and 200 µm fiber spacing were attached to the POx-scaffolds via heat gun treatment (50 °C, 10 seconds) to simplify the handling during cell culture.

5.3.3 Dipcoating and air plasma treatment of P*cyclo*PrOx

PLGA (Resomer 405, Evonik) was dissolved in 10 ml acetone to create solutions with the final concentrations of 5, 10, and 15%. First, the P*cyclo*PrOx scaffolds were kept above a 37°C warm waterbath to introduce pre-swelling. Then, the scaffolds were dipped by hand with forceps into the PLGA solutions for less than 3 seconds, as P*n*PrOx and P*cyclo*PrOx are dissolvable in acetone. The scaffolds were then dried on a Polytetrafluoroethylene film for 60 min, followed by a 15 min incubation in water below the LCST of P*cyclo*PrOx, ensuring a tight coating.
To improve cell adhesion, the scaffolds were treated with air plasma in a Pico low-pressure plasma system (Diener electronic, Ebhausen, Germany). The scaffolds were placed in a petri dish (Thermo Fisher Scientific) and treated with air plasma at 100% output for 5 minutes on each side.

5.3.4 Cell culture

L929 cells were cultivated in DMEM media with 10% FCS and 1% PenStrep (Thermo Fisher Scientific). Primary dermal microvascular endothelial cells (HDMVECn) (ATCC) were cultivated in Vascular Cell Basal Medium with the Microvascular Endothelial Cell Growth Kit-VEGF. The endothelial cell line HMEC-1 (ATCC) was cultivated in MCDB 131 (Thermo Fisher Scientific) medium with 10% fetal calf serum (FCS), 1% Penicillin/Streptomycin, 10 ng/ml endothelial growth factor (EGF), 1 µg/ml hydrocortisone and 10 mM glutamine (Thermo Fisher Scientific).

After reaching confluency, cells were incubated with PBS/EDTA (0.45 M EDTA) for 5 minutes and afterward trypsinization with 0.05% Trypsin-EDTA 1X (Thermo Fischer Scientific). Cells were cultivated in 75 cm^2 and 175 cm^2 cell culture flasks with an initial seeding density of 8.000 cells/cm^2 (Greiner Bio-One, Kremsmuenster, Germany).

5.3.5 Cell seeding on scaffolds

Scaffolds were sterilized for 30 minutes by UV-treatment (254 nm) with a UV-lamp (VL-4.LC, Vilber Lourmat, Essen, Germany). 12-well plates were filled with 1% sterile agarose (in PBS) until the bottom of the wells were covered. After cooling, the wells were prefilled with medium and the scaffolds were incubated overnight at 37° C. Afterwards, 500.000 cells/scaffold were seeded in the wells and cultivated for 24h. The scaffolds were then transferred into new agarose coated wells with fresh medium for the proliferation period of seven days.

5.3.6 Embedding of cell laden scaffolds in GelMA hydrogel

The cell laden scaffolds were embedded in GelMA, bloom 300 (Thermo Fisher Scientific). The precursor solution for the GelMA hydrogel was created by dissolving GelMA in PBS to a final concentration of 10 wt% with 0.05 wt% Irgacure 2959 (BASF). The cell laden scaffolds were placed in a 12-well plate and 100 µl of the GelMA solution was added on top of the scaffolds, leading to their immersion. Next, GelMA was crosslinked via UV-treatment (365 nm) with a UV-lamp (VL-4.LC, Vilber Lourmat, Essen, Germany) for 10 minutes.

5.3.7 Live/Dead and CellTracker staining

Live/Dead assay was conducted with the LIVE/DEAD® Viability/Cytotoxicity Kit for mammalian cells (Molecular Probes) as described in the manual. CellTracker™ Green CMFDA Dye (Invitrogen) was also applied as described.

5.3.8 Immunofluorescence staining

Immunofluorescence staining was performed as described in Chapter 2.

5.3.9 SEM-Preparation

SEM preparation was performed as described in Chapter 3.

5.4 Results

5.4.1 Melt Electrowriting of P*n*PrOx and P*cyclo*PrOx

Based on previous results of the thesis, Melt Electrowriting with P*n*PrOx and P*cyclo*PrOx was established. The fiber deposition was programmed to resemble natural bifurcating structures. By mainly changing the pressure between 0.5 to 2 bar during printing, these structures were printed with different fiber diameters (**Figure 26** A). Furthermore, it was possible to increase the complexity of the structures by adapting the G-code. However, this also led to a higher susceptibility for inaccuracies (**Figure 26** B).

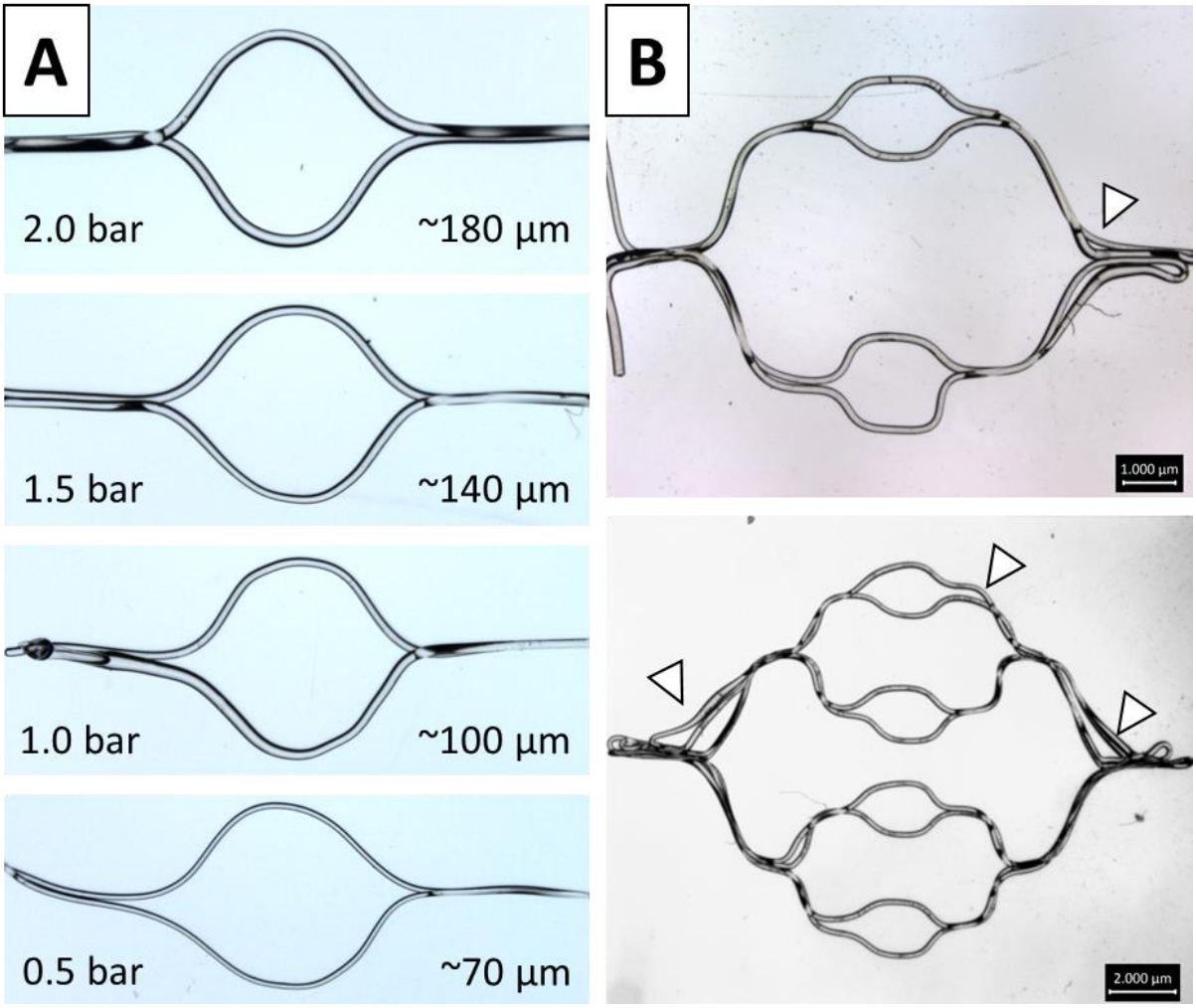

Figure 26: Melt Electrowriting of scaffolds based on POx. *A: Simple bifurcation structures with different fiber diameters. The pressure and the corresponding fiber diameter are noted in the image. B: Complex structures with successive bifurcations. Arrows indicate the inaccuracies of the fabrication process.*

5.4.2 Behavior of P*n*PrOx and P*cyclo*PrOx scaffolds in hydrogels

An important issue to address of scaffolds created for biological purposes is their behavior in aqueous buffers or media. Here, the scaffolds were embedded in GelMA. After immersion, the scaffolds swelled, resulting in the fusion of adjacent fibers. Due to this process, natural bifurcation structures appeared, where one bigger fiber branched into 2 smaller ones (**Figure 27**).

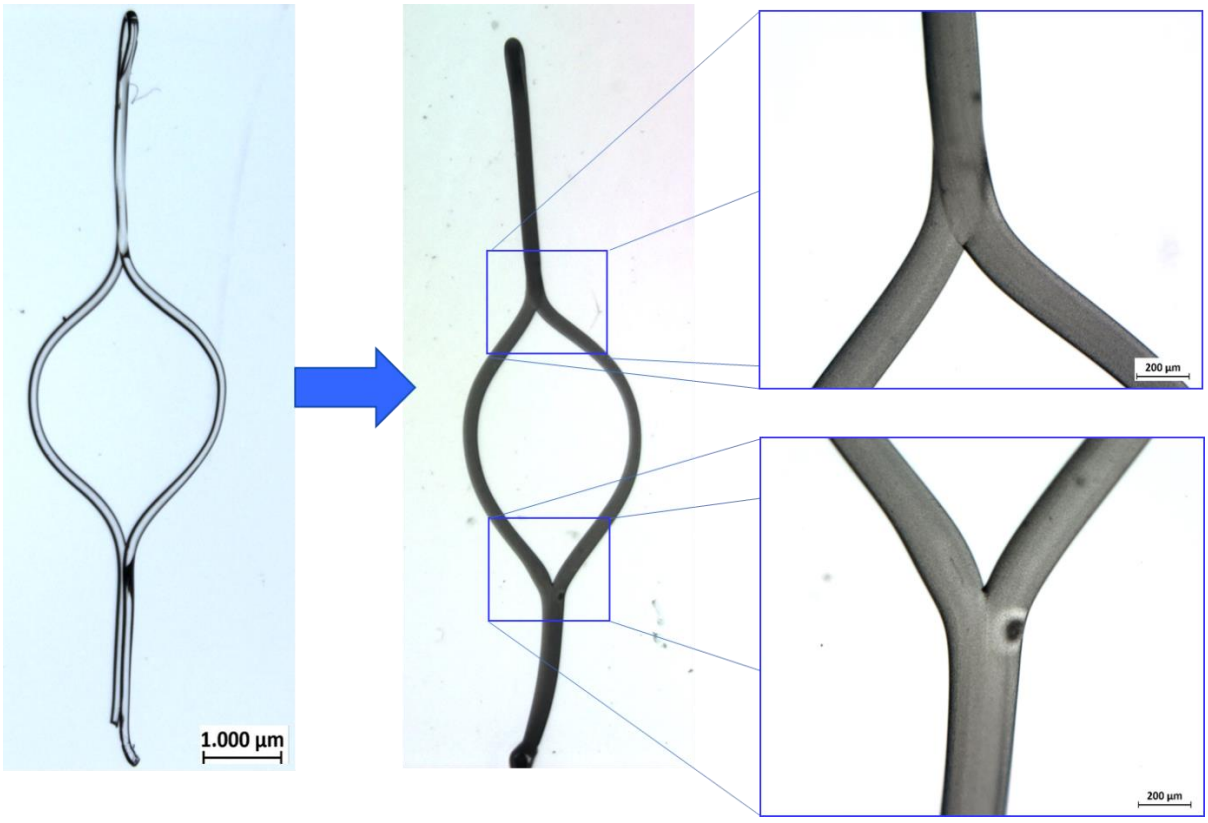

Figure 27: Behavior of POx-Scaffolds in water . *When immersed in a hydrogel, the fibers swell, leading to the fusion of adjacent fibers resulting in natural bifurcation structures. Scale bar left: 1000 µm; right: 200 µm.*

Next, the temperature was reduced to below 20°C for P*n*PrOx and below 25°C for P*cyclo*PrOx, which led to the dissolution of the scaffold. Dissolution of the scaffolds into the hydrogel took at least 2 hours, but the timeframe could be significantly reduced to 2 minutes by having direct connections of the inlet and the outlet of the scaffold to the surrounding buffer/medium (**Figure 28** A). Perfusion with Coomassie blue revealed, that the channels and bifurcations are interconnected (**Figure 28** B), even in more complex structures (**Figure 28** C, D).

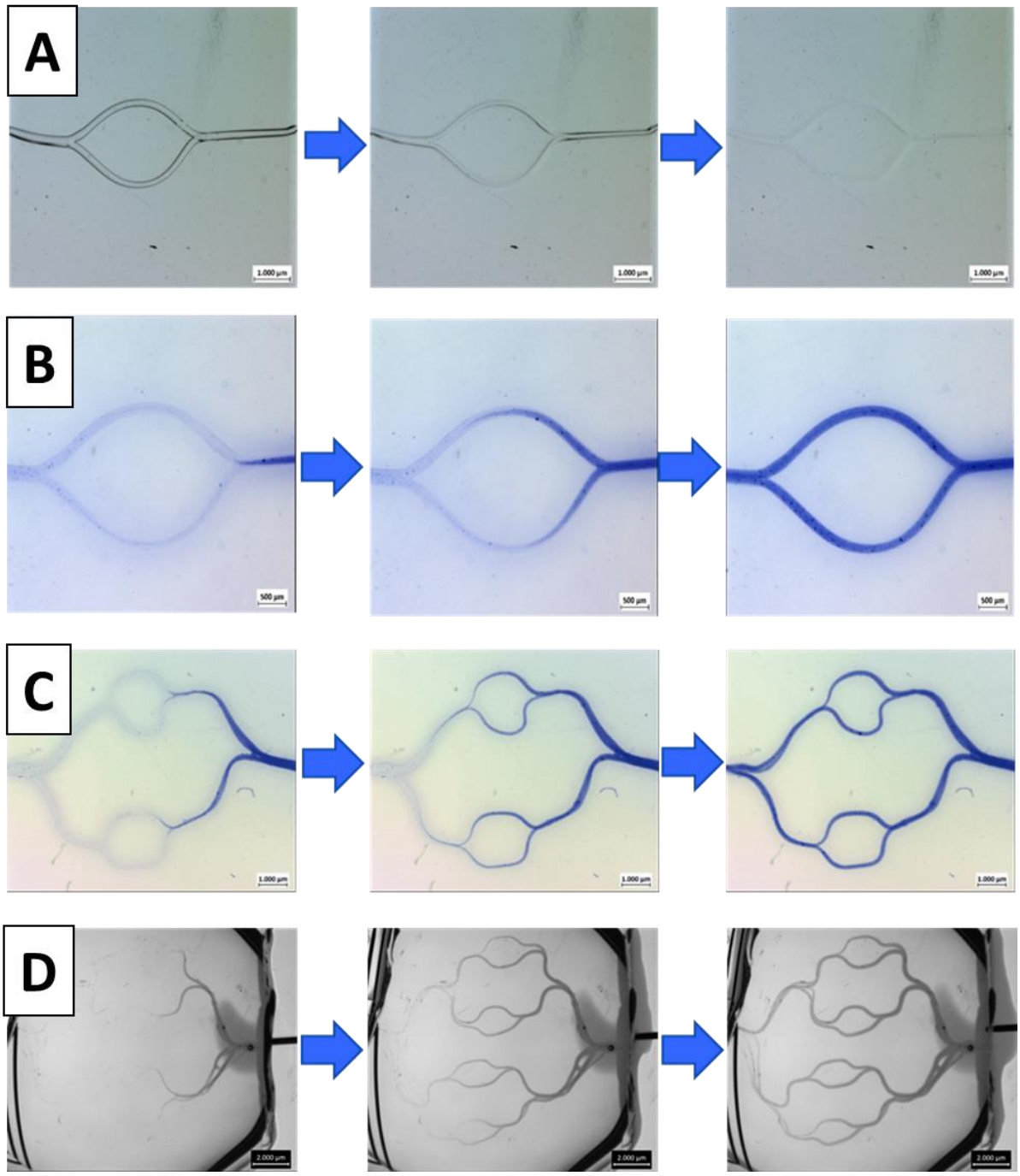

Figure 28: Channel generation with sacrificial POx-scaffolds. *A: Dissolution of POx after temperature reduction below the LCST. B: Perfusion of interconnected channel system with 2 bifurcations. C: Perfusion of interconnected channel system with 6 bifurcations. D: Perfusion of interconnected channel system with 14 bifurcations. Scale bar a, c, d: 1000 µm; b: 500 µm.*

5.4.3 Cytocompatibility of P*n*PrOx and P*cyclo*PrOx

To test for the cytocompatibility of the material before and after dissolution, cells of the L929 cell line were cultivated in 10% GelMA hydrogel (1.000.000 cells/ml) with the embedded scaffolds for 72h. Live/Dead staining revealed that before and after dissolution no increased cell death occurred in the vicinity of the scaffolds (Figure 29).

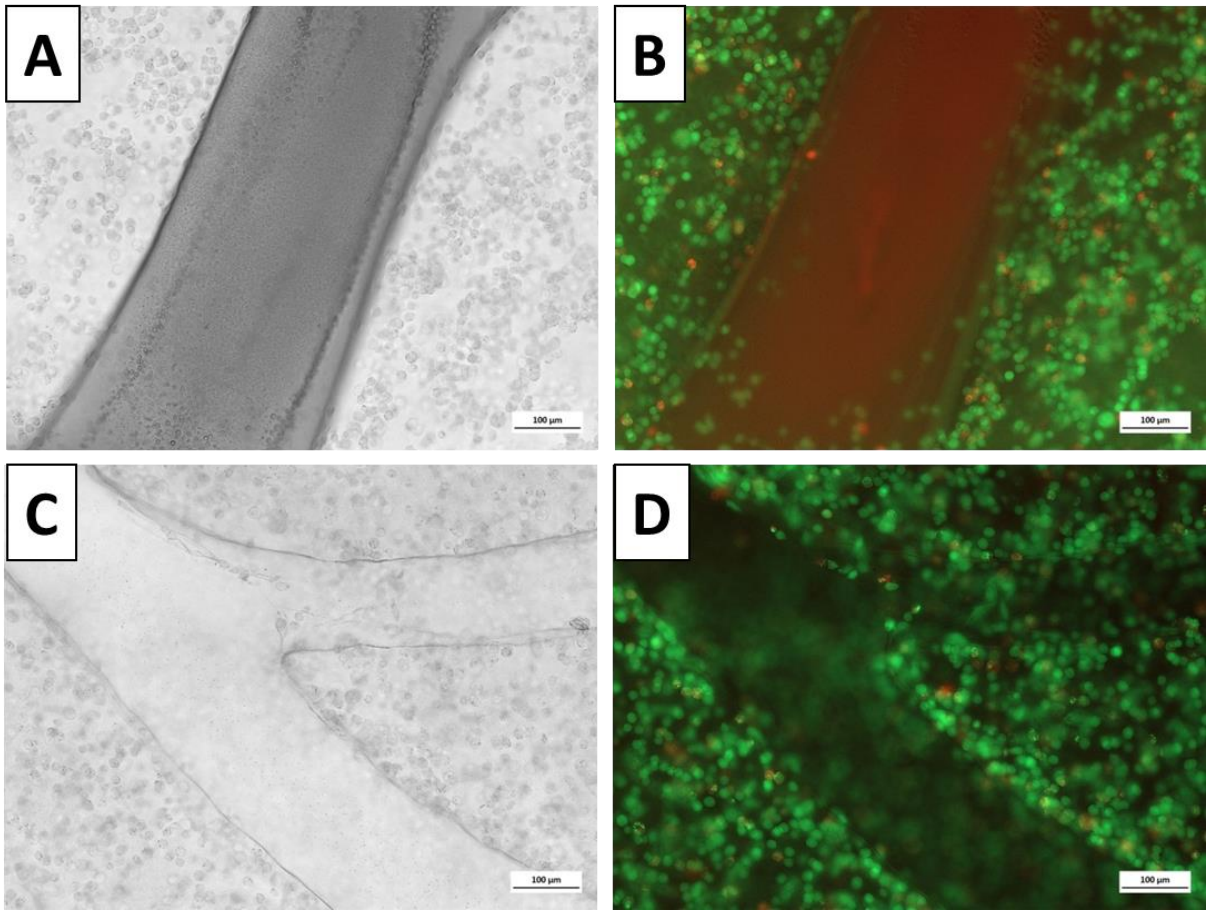

Figure 29: Viability analysis of L929 cells in GelMA . *A: Brightfield image of POx scaffold in GelMA with embedded L929 cells, before dissolution. B: Corresponding Live/Dead staining image of POx scaffold in GelMA with embedded L929 cells, before dissolution. C: Brightfield image of POx scaffold in GelMA with embedded L929 cells, after dissolution. B: Corresponding Live/Dead staining image of POx scaffold in GelMA with embedded L929 cells, after dissolution. Green: Live cells; Red: Dead Cells. Scale bar: 100 µm.*

5.4.4 Behaviour of scaffolds in water

Cultivation of cells on culture surfaces until confluency can take up to several days, depending on the cell type and seeding density. However, the POx scaffolds do not retain their structure for longer than 10 minutes in an aqueous environment, because of their swelling and eventual softening (Figure 30). This leads to the loss of stability and shape, while also becoming sticky.

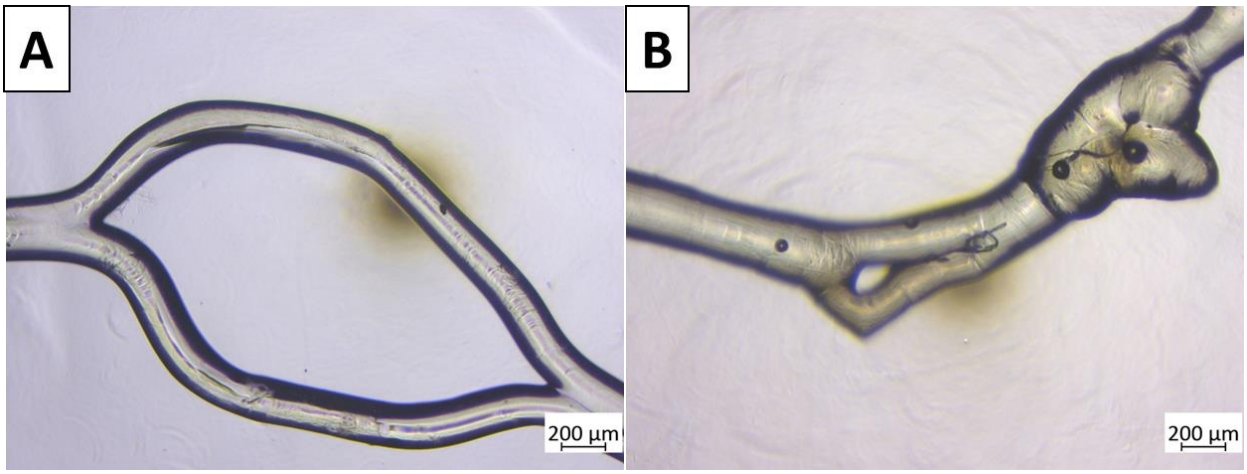

Figure 30: Swelling behavior of POx-scaffolds in aqueous solution. *A: Swollen POx-scaffold after 1 minute in PBS. B: Swollen POx-scaffolds after 10 minutes, losing its stability and shape. Scale bar: 200 µm.*

5.4.5 Stabilization of PnPrOx by crystallization

POx exhibit their thermoresponsive behavior only in their amorphous state. Some POx are known for their loss of LCST behavior upon crystallization[241], with PnPrOx exhibiting this behavior. Therefore, to increase the stability of P*n*PrOx-scaffolds, I crystallized the P*n*PrOx partially by inducing heat treatment for 90, 120 or 150 minutes at 60, 70 or 80° C. Longer incubation times and higher temperatures led to increased stability(**Figure 31** A), while more material remained after dissolving the polymer (**Figure 31** B). Based on these results, I used scaffolds crystallized at 60° C for 150 minutes because of the maintained stability and less leftover materials. As seen in **Figure 31** A, another problem was the stickiness of the scaffolds, which led to the entrapment of bubbles after immersion of the scaffolds in media, destroying the initial structure.

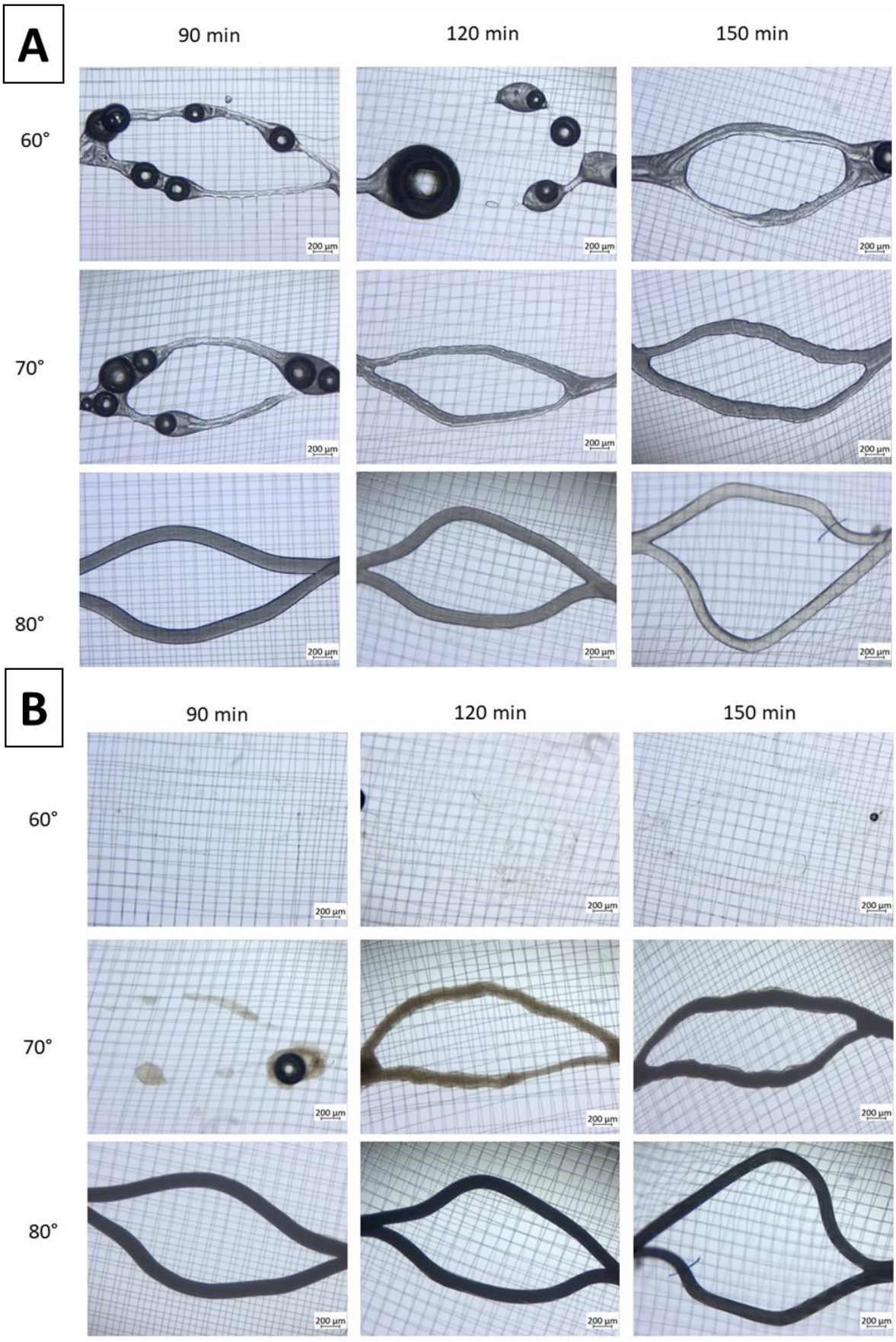

Figure 31: Stability of PnPrOx scaffolds in an aqueous environment during heat treatment *for 90, 120 and 150 minutes at 60, 70 or 90° C. A: Scaffolds at T > LCST. B: Scaffolds after dissolving PnPrOx at T < LCST. Scale bar: 200 µm.*

5.4.6 Endothelial cell seeding

In the next step, the human endothelial cell line HMEC-1 (100.000 cells/ml) was seeded in 1 ml media on the partially crystallized P*n*PrOx scaffolds. After 7 days of cultivation, the endothelial cells created a dense layer. To test for negative effects of the materials, the viability of cells seeded directly on the scaffolds was analyzed. Live/Dead staining revealed only a low number of dead cells in this layer (**Figure 32**). In accordance with the previous viability results of L929 cells, directly attached endothelial cells did not show a decreased viability.

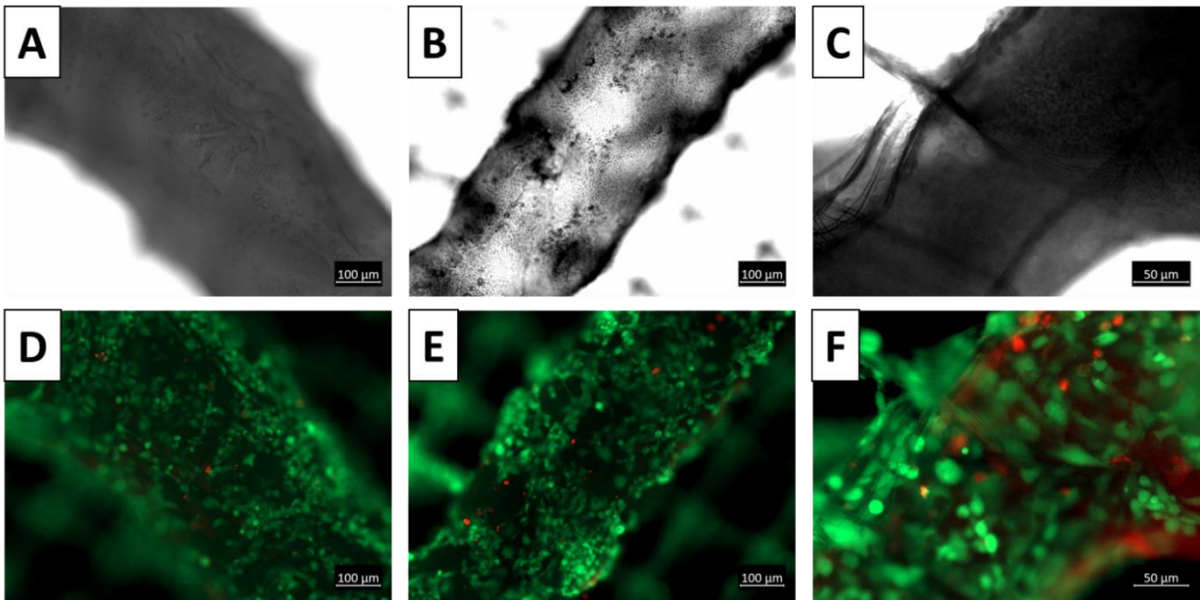

Figure 32: Live-Dead Staining of HMEC-1 cultivated for 7 days on pre-crystallized PnPrOx scaffolds *. A-C: Brightfield images of three different representative scaffolds. D-F: Live-Dead staining of three different representative scaffolds. Green: live cells; Red: dead cells. Scale bar: 100 µm.*

Next, the density of the layer was investigated via SEM-imaging (Figure 33). The endothelial cells created a mostly dense layer, which was wrapping around the whole structure. The uniform cell layer at the bifurcation shows that the fibers fused fully before cell seeding.

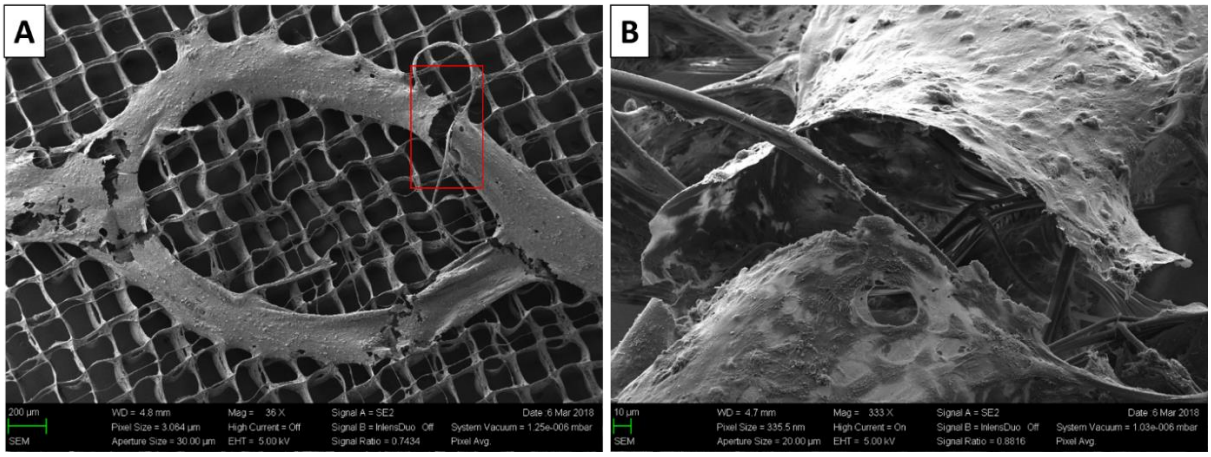

Figure 33: SEM-images of PnPrOx scaffolds cultivated with HMEC-1 for 7 days . *A: Overview of the bifurcation part. B: Closer look into a break.*

5.4.7 Embedding into GelMA

After 7 days of cultivation, the cell-laden scaffolds were embedded into a GelMA hydrogel. The temperature was decreased below 20°C to induce dissolution of the amorphous part of P*n*PrOx. By flushing the channels with a PBS-filled syringe, the crystalline leftovers were partially removed. It was possible to flush out the entry of the channels from both sides (**Figure 34** A) (black arrows). However, an increasing number of bifurcations and therefore complexity hindered the full removal of the crystalline leftovers (**Figure 34** B-D) (white arrows).

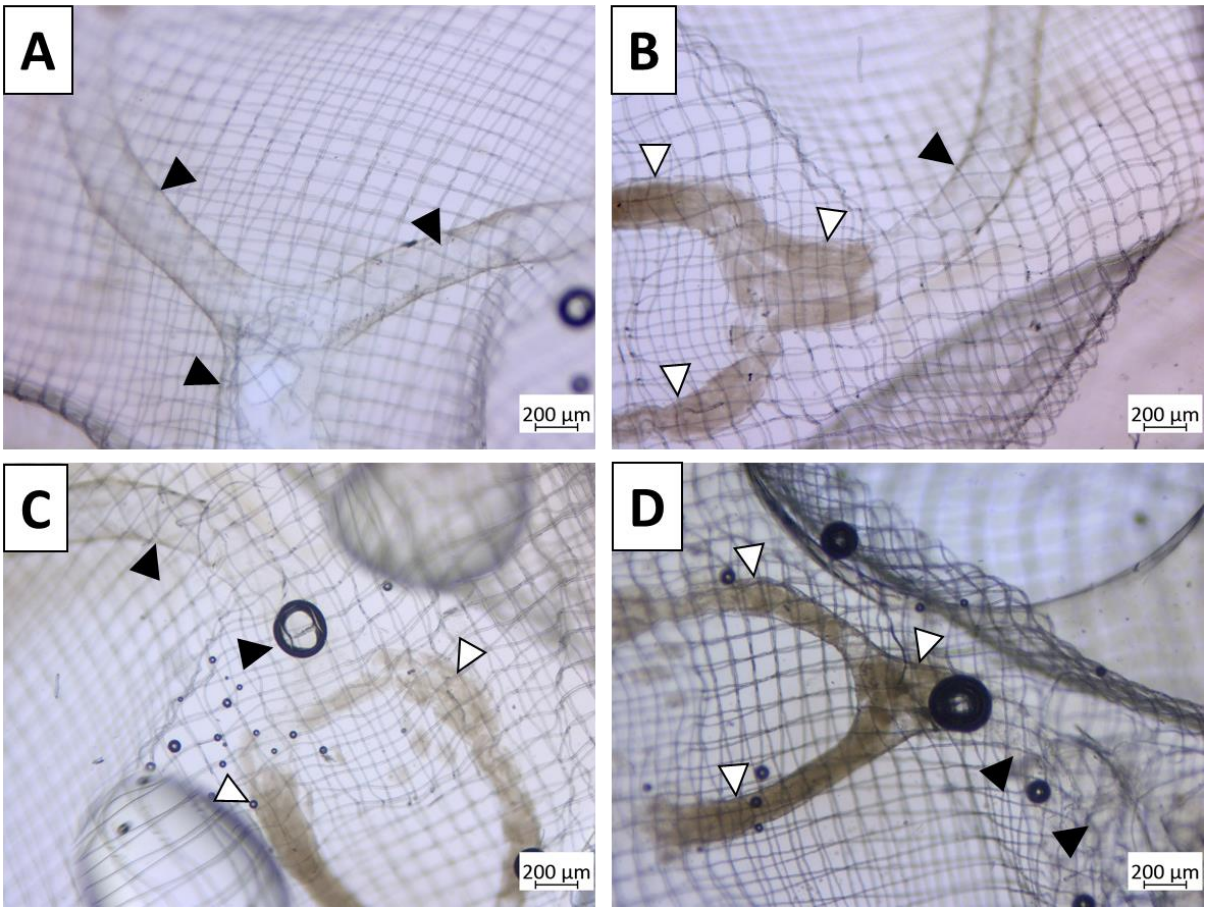

Figure 34: Brightfield images of cell-laden PnPrOx scaffolds after dissolving and flushing . *A: Entry of the channels. First bifurcation is empty after being flushed. B, C, D: Second bifurcations. Flushing does not remove all the leftover crystalline PnPrOx. Black arrows indicate empty channels, white arrows indicate crystalline leftovers. Scale bar: 200 µm.*

These hydrogels were then stained with Cell Tracker (**Figure 35** A, B) to visualize cell attachment to the walls of the channels. After flushing and removing the amorphous P*n*PrOx and the crystalline leftovers, endothelial cells could be visualized at the wall via CellTracker staining. Live/Dead-staining revealed that most of the cells survived the procedure (**Figure 35** C, D).

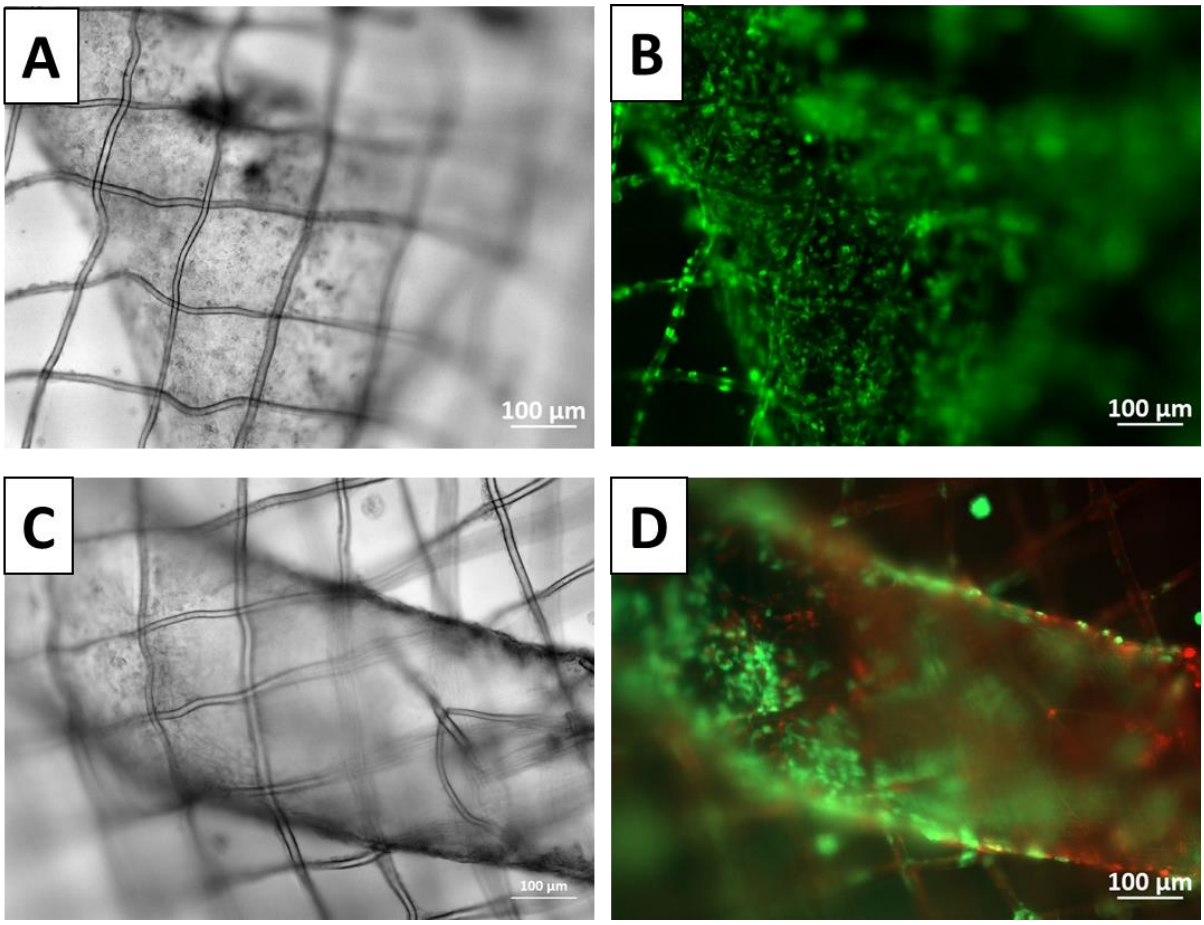

Figure 35: Fluorescence images of endothelial cells attached to the channel wall after removal of the PnPrOx residues. *A: Brightfield image of a bifurcation after flushing cell-laden PnPrOx constructs. B: Fluorescence image of A stained with cell tracker. Cells attached to the walls of the channel. C: Brightfield image of a channel after flushing cell-laden PnPrOx constructs. D: Fluorescence image of C stained with Live/Dead staining. Cells attached to the walls of the channel. Green: live cells; Red: dead cells. Scale bar: 100 µm.*

Further analysis of endothelial features was impossible because of differences between the cell line and primary cells. In detail, the cell line did not show the typical cobblestone morphology like primary endothelial cells. Furthermore, the cells are smaller and do not express intercellular junctions correctly, as shown by VE-Cadherin staining. Also, they do not grow in typical monolayers and partially grow on top of each other (Figure 36). Therefore, I used primary microvascular endothelial cells instead. However, the cells did not attach onto the scaffolds.

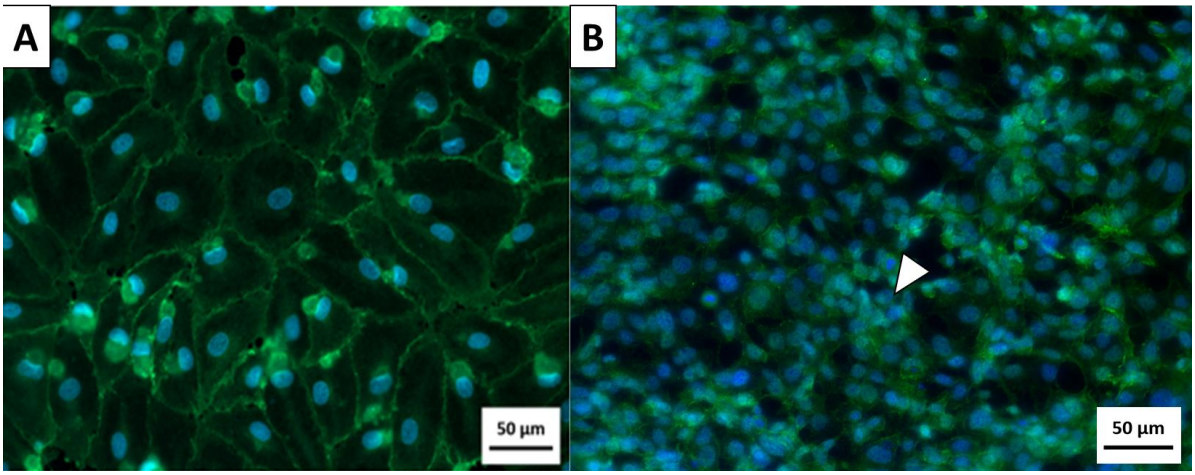

Figure 36: VE-Cadherin staining of monolayers of (A) primary human dermal endothelial cells and(B) the cell line HMEC-1. *The arrow indicates cells not growing in a monolayer, but on top of each other. Scale bar: 50 µm.*

5.4.8 Stabilization by dip-coating with PLGA

Since coatings with proteins did not increase stability nor improved primary cell adhesion, PLGA dip-coating was used to create a thin layer of PLGA around the scaffolds. PLGA solutions with different concentrations (5%, 10% and 15% PLGA in acetone) were tested to determine the best concentration for a complete coating (**Figure 37** A-C). However, for this approach, P*n*PrOx scaffolds could not be used because of crystallization in the presence of acetone or other organic solvents (**Figure 37** D, E). After testing several concentrations, a 15% PLGA in Acetone solution was used to dip-coat the scaffolds, which led to increased stability during longer incubation in aqueous solution at 37° C (**Figure 37** F, G).

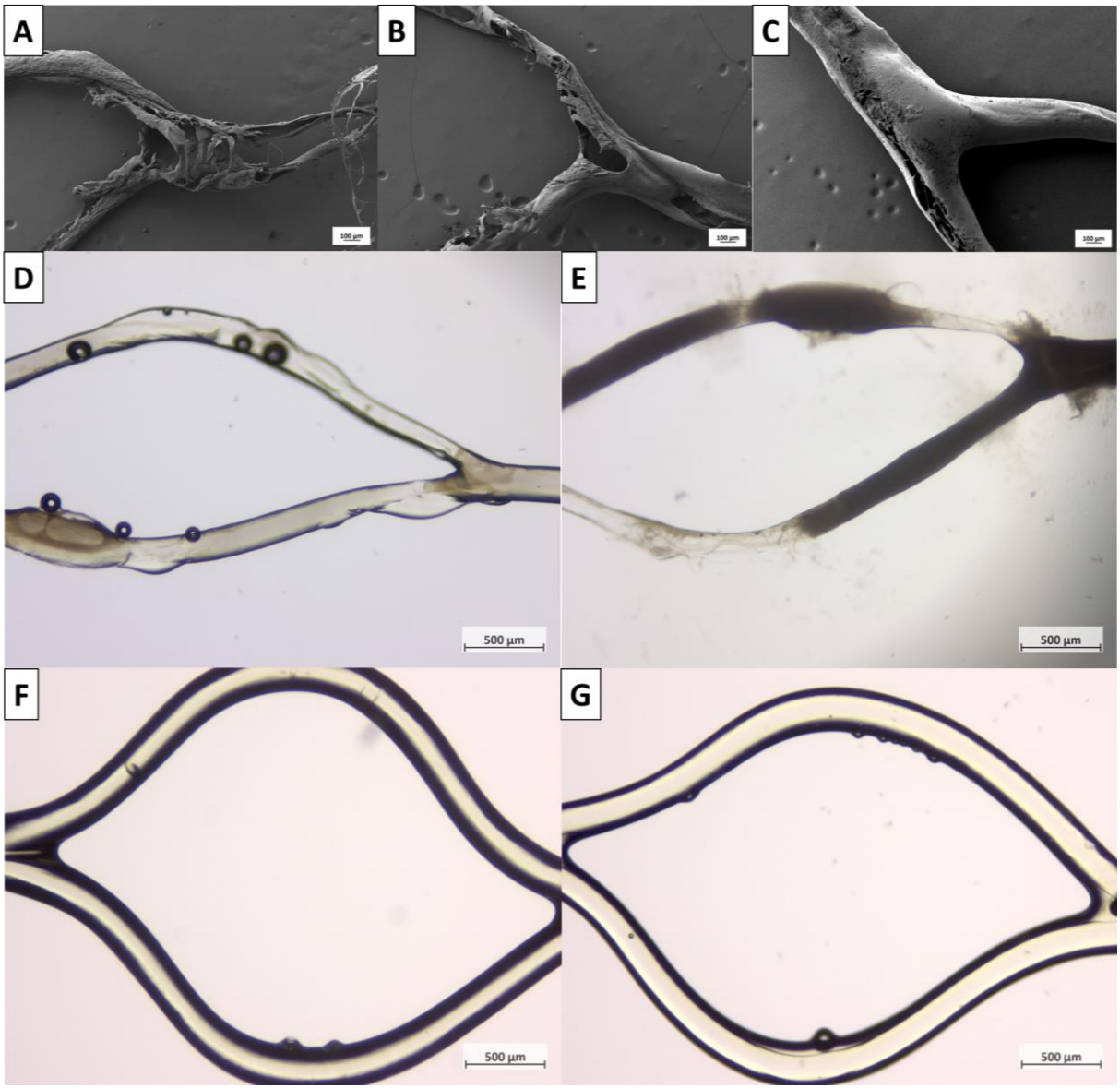

Figure 37: PLGA-coating of PcycloPrOx-scaffolds . *A: 5% PLGA-coating after PcycloPrOx dissolution. B: 10% PLGA-coating after PcycloPrOx dissolution. C: 15% PLGA-coating after PcycloPrOx dissolution. D: PLGA-coated PnPrOx scaffold in aqueous solution at 37°C. E: PLGA-coated PnPrOx-scaffold in aqueous solution after dissolution by temperature decrease. Non-dissolvable crystalline parts are visible as dark spots. F: Dry scaffolds coated with 15% PLGA-acetone solution. G: Scaffolds coated with 15% PLGA-acetone solution are stable in aqueous solution after 24h. Scale bar: 500 µm.*

Next, primary microvascular endothelial cells were seeded onto the PLGA-coated scaffolds. However, initially, only a few cells adhered (**Figure 38** A, B). Therefore, I also used pretreatment with air plasma to increase cell adhesion. Here, more cells adhered and grew evenly to a monolayer. These cells expressed a flattened, roundish cobblestone morphology, which resembles the natural state of endothelial cells shown by VE-Cadherin staining (**Figure 38** C, D, E).

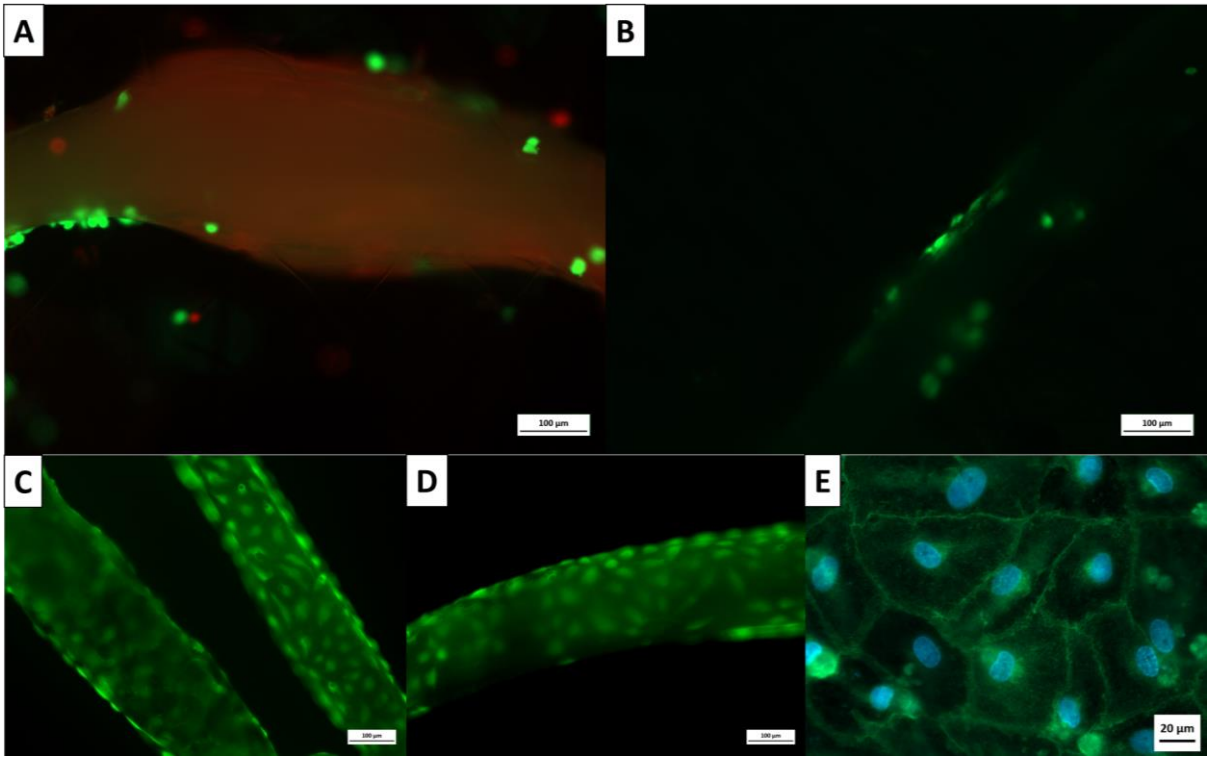

Figure 38: PcycloPrOx-scaffolds dip coated with 15% PLGA-acetone solution were seeded with primary microvascular human endothelial cells . *A, B: PLGA-coated PcycloPrOx scaffolds without plasma-treatment. C, D: Cell Tracker staining of primary microvascular endothelial cells on scaffolds pretreated with air plasma. E: Immunofluorescence staining of VE-Cadherin of primary microvascular endothelial cells on scaffolds pretreated with air plasma. Green: VE-Cadherin, Blue: cell nuclei. Scale bar A-D: 100 µm; E: 20 µm.*

5.5 Discussion

This thesis successfully provides a proof of principle for the new biofabrication method called inverse biofabrication: a new way to vascularize tissue constructs by embedding cell-laden sacrificial scaffolds in hydrogels followed by dissolution of the scaffolds. After dissolution, endothelial cells still attached to the walls of the created channels, resulting in an endothelialized channel network.

First, different scaffold designs with increasing complexity and varying fiber diameter were fabricated via MEW. The designs were chosen to resemble natural bifurcating structures with an inlet and outlet. These interconnected bifurcations were created by stacking fibers on top of each other. Naturally, the higher complexity of the structures leads to a higher number of stacked fibers, especially at the inlet and the outlet.

5.5.1 Establishment of hydrogel microchannel networks via sacrificial POx-scaffolds

Next, the scaffolds were embedded into GelMA. Interestingly, the scaffolds swelled, which led to the fusion of fibers in the vicinity to each other. With this, the former stacked fibers were

not separated anymore and generated bifurcations. After crosslinking, the gels were cooled down either below 25°C (P*cyclo*PrOx) or 20°C (P*n*PrOx) to induce dissolution of the thermoresponsive scaffolds. When the sacrificial scaffold had a direct connection to the aqueous solution, it dissolved after 2 minutes after temperature decrease. This led to the creation of a channel network with branches and an in- and outlet, which resembles the natural morphology of vascularization. Perfusion tests showed that the perfused dye could reach every subchannel and the divided flows reunited towards the end of the channel system and leaked out of the outlet. This proves the interconnectivity based on the successful fiber fusion created by the water induced swelling of the polymer.

In accordance with previous studies[177,242], the biocompatibility of the P*n*PrOx and P*cyclo*PrOx scaffolds was proven via Live/Dead-staining with L929 cells. The polymer itself before and after dissolving did not show any negative influence on the surrounding embedded cells as expected.[8]

Compared to other channel creation methods, the hereby established sacrificial scaffolds provide several advantages. First, the diameter of the channels can be influenced by simply varying the pressure during the process of MEW. Although MEW can produce fibers with diameter up to submicron size, it is not reasonable because handling difficulty increases below 80 µm. However, the resolution is still better than that of current methods. Furthermore, design adaption, like multimodal scaffolds[89] can reduce handling problems by introducing small diameter fibers between bigger ones.

Besides the high resolution, this method further allows the creation of sequential bifurcations because of the swelling and fusion behavior of POx. Therefore, an improved mimicking of the branching structure of natural blood vessels is possible. Furthermore, since the design is adaptable, even separate inlets and outlets for perfusion systems can be created.

5.5.2 Establishment of the inverse engineering approach

The next step was the seeding of endothelial cells before embedding the scaffolds into a hydrogel. The emerging problem was that the scaffolds did not exhibit long-term stability in aqueous solutions like water, buffer, or media even above their respective LCST because the swelling and eventual softening of the scaffolds lead to the loss of the structure and stability. One distinct property of P*n*PrOx is the crystallization induced by prolonged heat treatment.[241] When P*n*PrOx crystallizes, it loses its thermoresponsive capabilities, meaning temperature

decrease does not lead to dissolution in aqueous solutions anymore.[243] However, swelling is also prevented, and the overall stability in water is increased. Therefore, a compromise between stability and dissolution capabilities was found to retain the shape of the scaffolds during cell culture, while being able to dissolve most of it after temperature decrease. For this, different temperatures and incubation times were tested during heat treatment. Thereby, it was observed that only scaffolds incubated at 60°C for 150 minutes kept their structure while still being dissolvable. Scaffolds heated for either longer and/or higher temperature showed too much crystallinity and could not be dissolved. On the other hand, scaffolds with less crystallinity were not able to keep their structure during cultivation in media.

Therefore, these scaffolds were used for seeding with the endothelial cell line HMEC-1, and adherence and viability was analyzed via Live/Dead-staining. The results demonstrate that cells covered the whole fiber, which was also confirmed by SEM-analysis. Next, the scaffolds were embedded into GelMA hydrogels, and the temperature was decreased to dissolve P*n*PrOx. As expected, crystalline leftovers remained in the channels. However, it was possible to flush out the remains from the inlet to the second bifurcation, but the secondary branches blocked the flushing of the remains. Further tests with simplified structures need to be conducted next. However, this will impair the usefulness regarding the creation of real channel networks and their usability for tissue engineering.

It was then investigated whether the endothelial cells attached to the channel wall by microscopy. Via CellTracker and Live/Dead staining I was able to find HMEC-1 cells that attached from the P*n*PrOx scaffold onto the inner surface of the hydrogel. However, the dissolution and flushing led to increased dead cells. The reason might be since flushing of crystalline leftovers could lead to cell damage, as the remnants could scrape parts of the cell layer.

Besides non-dissolvable remains, another problem was the missing attachment of primary endothelial cells onto the scaffolds, even with coating of gelatin, collagen, or fibronectin. To overcome this problem, I tested PLGA-coating for cell adhesion and stabilization, because of its biocompatibility and biodegradability.[244] For this, scaffolds were dip coated in 15% PLGA in acetone solution to create a stabilizing coating. However, P*n*PrOx scaffolds showed partial crystallization upon contact with the solvent acetone, as already reported for poly(2-*iso*propyl-2-oxazoline).[243] Therefore, I decided to use P*cyclo*PrOx, which also has its LCST in

the physiological range. In contrast to P*n*PrOx, P*cyclo*PrOx does not crystallize upon heat treatment and remains amorphous.[216]

The scaffolds retained their shape in aqueous solutions for at least 1 week. However, primary cells did not attach to the PLGA-coated samples. Therefore, to increase cell attachment and proliferation, the samples were plasma treated with air plasma to activate the surface and, therefore, allow cell adhesion, as reported previously.[245] The endothelial cells attached, proliferated, and exhibited their typical cobblestone morphology with intact adherens junctions.

Hence, in this project, sacrificial scaffolds based on thermoresponsive P*n*PrOx and P*cyclo*PrOx were established. These scaffolds can be designed to recreate natural branching vasculature with interconnected bifurcations. Since MEW is used as fabrication method, the resolution is in the range of microvasculature. The thermoresponsive dissolution by cooling is a biocompatible and simple stimulus, making this an ideal platform for channel creation in hydrogels.

Furthermore, I investigated the potential of melt electrowritten P*n*PrOx and P*cyclo*PrOx scaffolds as a basis for inverse engineering. P*n*PrOx scaffolds can be stabilized by crystallization induced by heat treatment. However, primary cells do not attach, and flushing is only possible to a certain complexity. Therefore, this method will only be usable for structures with low complexity and hence, will miss the first and important aim to create channel networks.

To enable primary cell adhesion, P*cyclo*PrOx scaffolds were dip-coated with PLGA and afterward, plasma treated. In the following experiments to this thesis, less complex P*n*PrOx scaffolds should be tested with the endothelial cell line. In doing so, the P*cyclo*PrOx scaffolds should be implemented into hydrogels, where adhesion to the hydrogel, the degradation of the PLGA, and the upcoming biological function can be tested.

Chapter 6

General Discussion

Within this thesis, three different applications based on the thermoresponsive behavior of poly(2-oxazoline)s (POx) have been developed. For this, basic polymers, namely poly(2-*n*propyl-2-oxazoline) (P*n*PrOx) and poly(2-*cyclo*propyl-2-oxazoline) (P*cyclo*PrOx), have been provided by my colleague Julia Blöhbaum and used without further chemical modification. These polymers are especially interesting for biological applications, since their LCST is in the physiological range near room temperature. Compared to poly(2-*iso*propyl-2-oxazoline), which provides a LCST at 36°C, the usability is increased because these polymers do not quickly dissolve at room temperature. P*n*PrOx has been used as sacrificial material for the creation of cell sheets and channel creation in hydrogels, as well as remaining material for fibril creation. P*cyclo*PrOx was used as a sacrificial material for fibril and channel creation.

6.1 Thermoresponsive Coating for Cell Sheet Engineering

The cell sheet approach provides a way to easily coat surfaces with a layer of P*n*PrOx without chemical binding to surfaces (**Figure 39** A). By dissolving the polymer in water and drying it on top of the surface, a thermoresponsive layer is created. Different cell types, here tested with fibroblasts and endothelial cells, can be seeded on top of the created layer. After cultivation, the cell layer can be harvested via temperature reduction. Compared to common cell sheet engineering approaches[125], no complex grafting procedure with specialized equipment and qualified personnel is needed to create thermoresponsive coatings for cell sheet engineering. Since the polymer can be acquired commercially, this technique can be used by every common biological lab. In terms of simplicity, another approach was previously reported. Here, thermoresponsive poly(glycidyl ether) brushes, dissolved in water, were physically adsorbed to the surface of standard cell culture polystyrene surfaces used for cell culture and immobilized by UV-radiation.[246] Compared to the here developed “quick-and-dirty” method, their method created a more precise coating, which can even be immobilized in a simple way. However, the chemicals cannot be acquired commercially and therefore it needs the involvement of a chemical lab.

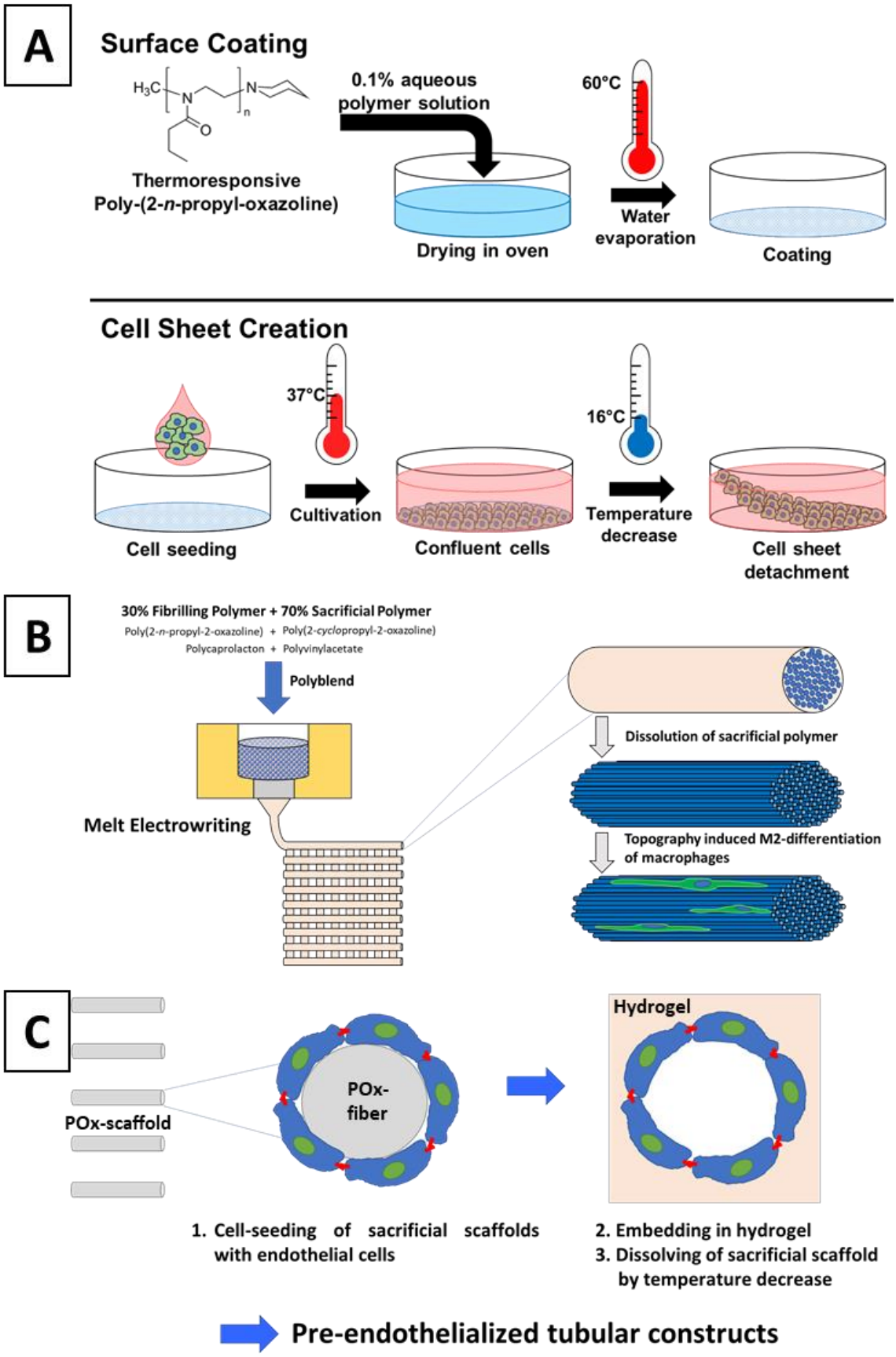

Figure 39: Schemes of the three projects of the thesis. *A: Easy-to-apply coating with PnPrOx for cell sheet engineering and cell sheet creation. B: Generation of fibrillar scaffolds for topography-induced M2-differentiation of macrophages. C: Prevascularization approach.*

Furthermore, the method presented in this thesis leads to polymer contamination because the polymer is not covalently bound to the surface and dissolves into the solution. Since POx provide an intrinsic biocompatibility, this should not affect cell culture without clinical relevance. Most importantly, comparable to other established methods, functional cell sheets can be obtained with this method, that can be used for subsequent processing.[9]

6.2 Biomimetic Hierarchically Structured Fiber-Scaffolds

The next method developed during this thesis is the combination of two-component polyblends with the MEW technique: Melt Electrofibrillation (**Figure 39** B). Here, one part of the polyblend is sacrificial, while the other one remains after dissolution of the prior. The application of pressure and the induced shear stress during MEW leads to a directed phase separation and alignment of the polyblend. In this work, two different blends were used to create aligned fibril bundles: 30% P*n*PrOx + 70% P*cyclo*PrOx and 30% PCL + 70% PVAc. In these blends, the sacrificial parts were P*cyclo*PrOx and PVAc, which can be dissolved in aqueous solution and 70% ethanol, respectively. In the case of the poly(2-oxazoline)s, the blend is not miscible and leads to the creation of fibril bundles with the diameter of single fibrils ranging around 1500 nm, while the miscible blend of PCL and PVAc leads to fibril diameters of 300 nm. Comparing both fibrillary scaffods, the fibrils based on crystalline P*n*PrOx were brittle and thus hard to handle, while the PCL scaffolds were more stable and kept their stability during cell culture handling. Besides the novel combination of MEW with partially sacrificial polyblends to introduce microfibrillation, the effect of the hereby introduced topography on the differentiation potential of cells was examined. Studies have already shown that certain topographies introduce or at least improve the differentiation of cells. [77,211,224] Within this thesis, this effect has also been shown for the fibril scaffolds on human macrophages, that elongated on and inside the fibrillar bundle. Moreover, macrophages differentiated solely by the topographical cues without the addition of reagents, proven via RNA- and protein analysis. Furthermore, the smaller PCL fibrils had a similar diameter to collagen fibrils, which might explain their increased differentiation potential compared to the P*n*PrOx fibrils. The developed method to directly deposit fibrillar bundles provides a new way to create biomimetic scaffolds. The basic box-shaped scaffold already led to a strong differentiation induction comparable to molecule-based differentiation, which is normally conducted via proteins or small molecules.[247]

Since MEW allows direct writing of fibers, different designs can be used for the generation of scaffolds for different tissue. Especially tissues like muscle and tendon can be easily mimicked by adapting the G-code for the scaffold design. For example, scaffolds can be designed in an aligned way without fiber crossing. These flat scaffolds can then be used for cell seeding, which can later be rolled into thicker constructs to ensure homogenous cell distribution.
In summary, the developed system can be considered as a platform technology with potential applications for different tissues by creating collagen fiber mimicry with PCL.

6.3 Sacrificial Poly(2-oxazoline) Scaffolds for Biocompatible Microchannel Creation and Prevascularization

The third project in this dissertation is the establishment of a prevascularization approach (**Figure 39** C). For this, MEW processed sacrificial P*n*PrOx and P*cyclo*PrOx scaffolds were seeded with endothelial cells, cultivated until a confluent monolayer is formed and then embedded into a hydrogel. After embedment, the scaffolds were sacrificed by temperature reduction, a biocompatible stimulus.
First, the scaffolds were designed with natural branching structures and embedded into a hydrogel. During embedment, the fibers in the scaffolds swelled and led to the fusion of adjacent fibers, resulting in interconnected microchannel networks. This property, combined with the directed deposition via MEW, led to the establishment of natural branching structures. After crosslinking of the hydrogel, the embedded scaffolds were dissolved by temperature reduction, leaving perfusable, branching and interconnected networks with separate in- and outlet behind. Compared to sugar-based sacrificial scaffolds, these POx scaffolds dissolve without osmotic pressure-induced cell death. Furthermore, the dissolution can be triggered by a stimulus, and the scaffolds do not dissolve directly, increasing the timeframe for hydrogels to harden. Thus, the hereby developed scaffolds have the potential to become an easy-to-use tool for microchannel creation in hydrogels. Furthermore, depending on the desired 3D tissue analog, e.g., skin or muscle, the microchannel morphology can easily be adapted to its requirements.
In order to achieve prevascularization, the scaffolds need to be seeded with endothelial cells. For this, they were immersed in the media for the cultivation period. However, the scaffolds are not stable for long-term immersion in an aqueous solution, as their water uptake leads to swelling and, consequently, to a loss of stability. Therefore, the next aim was to increase the

stability during cell culture. For P*n*PrOx scaffolds, partial crystallization led to an increase in stability and endothelial cells were able to adhere. However, crystallization of POx also leads to the loss of the thermoresponsive behavior, and, therefore, crystalline leftovers had to be flushed out. Thus, a crystallization ratio was found, which had enough crystalline parts to keep the stability, but is still amorphous enough for removal. This only worked partially for simple structures and additionally, primary cells were not able to adhere. The reason could be that primary cells are more sensitive to their environment than cell lines, which can be cultivated for hundreds of passages in standard cell culture conditions, leading to the adaption to this environment and, therefore, to changes in morphology and gene expression.[248]

Another possible solution to increase short-term stability during cell culture was dip-coating with a polymer. For this, the biocompatible and biodegradable PLGA[244] was dissolved in Acetone and used as dip-coating solution, resulting in solvent-induced crystallization of P*n*PrOx.[243] Therefore, P*cyclo*PrOx, which is not able to crystallize, was used as an alternative. After plasma treatment, primary endothelial cells were able to attach and proliferate after seeding, because of increased hydrophilicity and roughness of the surface.[245] The following experiments to this thesis should focus on the embedment of preseeded scaffolds into different hydrogels. Here, a big challenge will be the finetuning between degradation and stabilization of the PLGA-layer after dissolution of POx. This will be important for the functionality of the endothelial layer to act as a mediator and barrier between the perfused nutritions and the tissue.

6.4 Conclusion of the Thesis

In conclusion, within this thesis three different biofabrication approaches were, which are based on two thermoresponsive polymers, that exhibit their LCST in physiological range: P*n*PrOx and P*cyclo*PrOx. Without further modification, the polymers were combined with existing fabrication methods to create new applications for tissue engineering and regenerative medicine.

The thermoresponsive behavior was exploited to generate these approaches as biofabrication methods. The cell sheet engineering approach does not contribute much novelty to the community because this technique is already 20 years old[249] and has been investigated thoroughly. However, it is an easy-to-apply approach that is not dependent on chemical equipment and knowledge.

Compared to this, Melt Electrofibrillation is a novel technique for MEW that increases the biomimetic capabilities of this direct writing approach and can be used as a platform technology for topography-mediated cell differentiation. Since the POx-based approach is hard to handle, this technique was adapted to PCL, a clinically approved polymer. This increased the stability, as well as the biological mimicry of collagen fibrils and the effect of the scaffolds on cell differentiation.

The third approach tackles the greatest bottleneck of tissue engineering: vascularization. Here, scaffolds with an intrinsic swelling and fusion behavior provide a successful biocompatible way to create interconnected channel networks in the size of microvascularization. In upcoming projects, this will be developed into an easy-to-use vascularization product, providing a simple way to create perfusable tissues. Furthermore, it will be applied to bioreactors to further prove their potential in the field of tissue engineering and regenerative medicine. However, the prevascularization approach could not be established as a useful tool yet, as the instability of the scaffolds in aqueous solutions proved to be a challenge that is hard to overcome. Therefore, a sufficient and satisfying solution still must be developed.

Chapter 7

Summary/Zusammenfassung

7.1 Summary

In this thesis, non-modified POx, namely P*n*PrOx and P*cyclo*PrOx, with an LCST in the physiological range between 20 and 37°C have been utilized as materials for three different biofabrication approaches. Their thermoresponsive behavior and processability were exploited to establish an easy-to-apply coating for cell sheet engineering, a novel method to create biomimetic scaffolds based on aligned fibrils via Melt Electrowriting (MEW) and the application of melt electrowritten sacrificial scaffolds for microchannel creation for hydrogels.

Chapter 3 describes the establishment of a thermoresponsive coating for tissue culture plates. Here, P*n*PrOx was simply dissolved in water and dried in well plates and petri dishes in an oven. P*n*PrOx adsorbed to the surface, and the addition of warm media generated a cell culture compatible coating. It was shown that different cell types were able to attach and proliferate. After confluency, temperature reduction led to the detachment of cell sheets. Compared to standard procedures for surface coating, the thermoresponsive polymer is not bound covalently to the surface and therefore does not require specialized equipment and chemical knowledge. However, it should be noted that the detachment of the cell layer requires the dissolution of the P*n*PrOx-coating, leading to possible polymer contamination. Although it is only a small amount of polymer dissolved in the media, the detached cell sheets need to be washed by media exchange for further processing if required.

Chapter 4 shows the establishment of a novel method for the direct deposition of bundles of aligned fibrils via MEW. For processing, polyblends with 70% sacrificial polymer and 30% remaining polymers were used. The poly(2-oxazoline) blend consisted of 70% P*cyclo*PrOx and 30% P*n*PrOx, where the latter was crystallized via heat treatment after fabrication to decrease solubility, and thermoresponsiveness. By dissolving P*cyclo*PrOx in a cold aqueous solution, bundles of aligned P*n*PrOx fibrils with diameters in the range of 1500 nm emerged. However, these fibrils were very brittle because of the crystallinity of P*n*PrOx. Thus, this method was further adapted to PCL by blending with PVAc, which can be dissolved in 70% ethanol. The dissolution of PVAc led to the creation of bundles of PCL fibrils with a mean diameter of ~300

nm. The size of these fibrils is comparable to natural collagen fibrils, which exhibit a diameter of ~200 nm after drying. Both systems were proven to have a topography-mediated influence on macrophage polarization into the pro-healing M2-phenotype, compared to non-fibrillar fibers of the same material. Interestingly, the PCL fibrils showed a stronger capability for differentiation, which might be based on the biomimetic similarity to collagen fibrils (**Figure 40**).

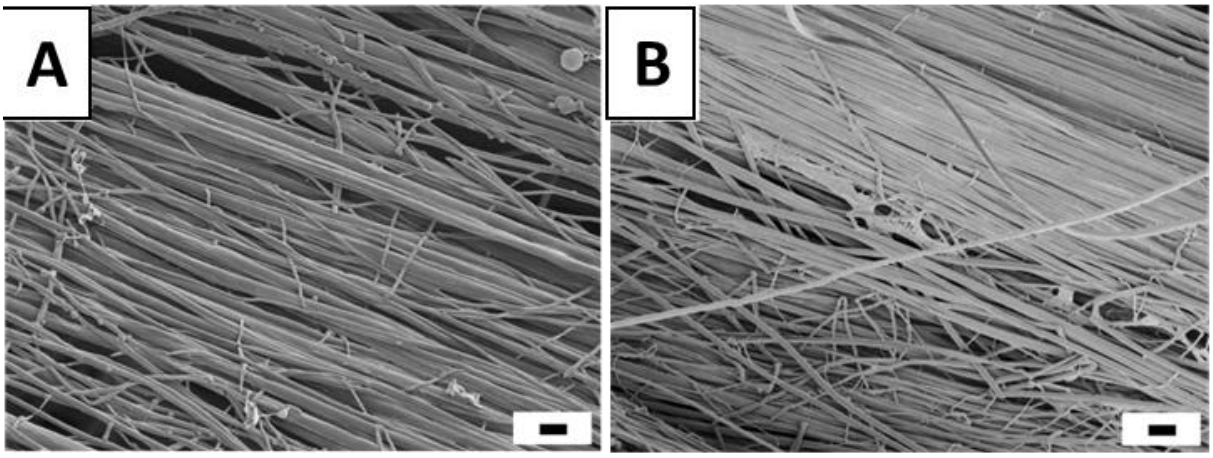

Figure 40: Morphological comparison of (A) PCL-based fibril bundles with (B) collagen I fibril bundles from rat tails. *Size and form of both fibrils are similar, leading to a strong immunomodulatory effect. (scale bar: 1 µm)*

Furthermore, the increase of M2-differentiation markers via topography was comparable to differentiation via IL-4, a strong molecule-based differentiation reagent. Compared to common 2D topography differentiation studies, the cells have a more biomimetic 3D environment of aligned fibers, which allows for the migration of the cells between the aligned fibrils. The combination of MEW with partially sacrificial poly-blends provides a novel platform to create biomimetic scaffolds with cell differentiation potential based on 3D topography. For the first time, it is possible to mimic the ultrastructural features of an ECM component, namely collagen I. Its unprecedented immunomodulatory effect might lead to the recognition that collagen ultrastructure mimicry can be a potent design criterion for biomaterial induced immunomodulation.

The development of a microchannel generation method for hydrogels by combining POx and MEW and a prevascularization approach has been described in **Chapter 5**. Scaffolds based on P*n*PrOx and P*cyclo*PrOx were directly deposited to resemble natural branching structures with bifurcations. After embedding these scaffolds into hydrogels, the fibers swelled, leading to the fusion of adjacent fibers. After temperature decrease, the scaffolds dissolved and generated interconnected microchannels with a different inlet and outlet. To achieve preseeding of the scaffolds with endothelial cells, long-term exposition in an aqueous solution is required.

However, the POx scaffolds lose stability because of their swelling behavior. To counter this effect, P*n*PrOx scaffolds were partially crystallized, which led to increased stability for the cost of decreased solubility. After embedding into hydrogels, it was possible to dissolve and flush the remaining P*n*PrOx in simple structures. A first proof-of-principle could be shown with an endothelial cell line, but primary cells did not attach. Therefore, P*cyclo*PrOx scaffolds were stabilized with a PLGA coating, leading to possible attachment and proliferation of primary endothelial cells.

In conclusion, the combination of basic poly(2-oxazoline)s with established biofabrication methods led to the creation of applicable and useful approaches in the field of tissue engineering. Especially the fibril and the microchannel creation approach via MEW has the potential to become platform approaches that can help overcome current tissue engineering challenges like vascularization and differentiation.

7.2 Zusammenfassung

In dieser Dissertation wurden die unmodifizierten Poly(2-oxazoline) P*n*PrOx und P*cyclo*Prox, welche eine LCST im physiologischen Bereich zwischen 20 und 37°C aufweisen, für drei verschiedene Biofabrikationsansätze verwendet. Deren Thermoresponsivität und Prozessierbarkeit wurde genutzt, um ein simples Beschichten von Oberflächen für Cell Sheet Engineering, eine neue Methode zur Herstellung biomimetischer Gerüststrukturen basierend auf der Generierung von Fibrillenbündeln via Melt Electrowriting und die Anwendung als Opferstrukturen zur Generierung von Mikrokanälen in Hydrogelen zu etablieren.

Kapitel 3 beschreibt die Etablierung einer thermoresponsiven Oberfläche für Gewebekulturplatten. Dazu wurde P*n*PrOx in Wasser gelöst und in Well-Platten oder Petrischalen im Ofen getrocknet. Das P*n*PrOx adsorbierte an die Oberfläche und nach Zugabe von warmem Medium wurde die zellkulturkompatible Beschichtung generiert. Es konnte gezeigt werden, dass verschiedene Zellarten darauf adhärieren und proliferieren können. Nachdem die Zellen konfluent wurden, konnte sich durch Temperaturerniedrigung eine zusammenhängende Zellschicht ablösen. Verglichen mit den Standartprozeduren zur Generierung von Beschichtungen ist das thermoresponsive Polymer nicht kovalent an die Oberfläche gebunden. Daher setzt diese Methode keine spezielle Ausstattung und Vorwissen in der Chemie voraus. Zum Ablösen der Zellschicht wird jedoch das Auflösen von P*n*PrOx benötigt, was zu einer möglichen Polymerkontamination führt. Obwohl sich nur eine kleine

Menge an gelöstem Polymer im Medium befindet, sollten die Zellschichten gewaschen werden, falls es für weiteres Prozessieren notwendig sein sollte.

Kapitel 4 beschreibt die Etablierung einer neuen Methode zum direkten Ablegen von ausgerichteten Fibrillenbündeln mittels Melt Electrowriting. Für die Prozessierung wurden Blends aus 70% Opferpolymer und 30% zurückbleibenden Polymer benutzt. Der Poly(2-oxazoline)-Blend bestand hierbei aus 70% P*cyclo*PrOx und 30% P*n*PrOx. Letzteres wurde durch Hitzebehandlung kristallisiert, um Löslichkeit zusammen mit den thermoresponsiven Eigenschaften zu entfernen. Indem P*cyclo*PrOx in kalter wässriger Lösung gelöst wurde, kamen Bündel ausgerichteter P*n*PrOx-Fibrillen zum Vorschein. Die einzelnen Fibrillen wiesen Durchmesser um 1500 nm auf und waren aufgrund ihrer Kristallinität sehr brüchig. Diese Methode wurde deswegen an PCL adaptiert, indem dieses mit PVAc geblendet wurde, welches in 70% Ethanol gelöst werden kann. Das Auflösen von PVAc führe zur Generierung von PCL Fibrillenbündeln mit Einzeldurchmesser von 300 nm. Dieser Durchmesser ist vergleichbar mit dem von Kollagenfibrillen, welche einen Trockendurchmesser von 200 nm aufweisen. Für beide Systeme wurde gezeigt, dass diese alleine aufgrund der Topografie die Polarisierung von Makrophagen in den heilenden M2-Phänotyp fördern, im Gegensatz zu nicht-fibrillären Fasern aus dem gleichen Material. Interessanterweise zeigten die PCL-Fibrillen einen stärkeren Einfluss auf die Differenzierung, was möglicherweise an der biomimetischen Ähnlichkeit zu Kollagenfibrillen liegt (**Figure 41**).

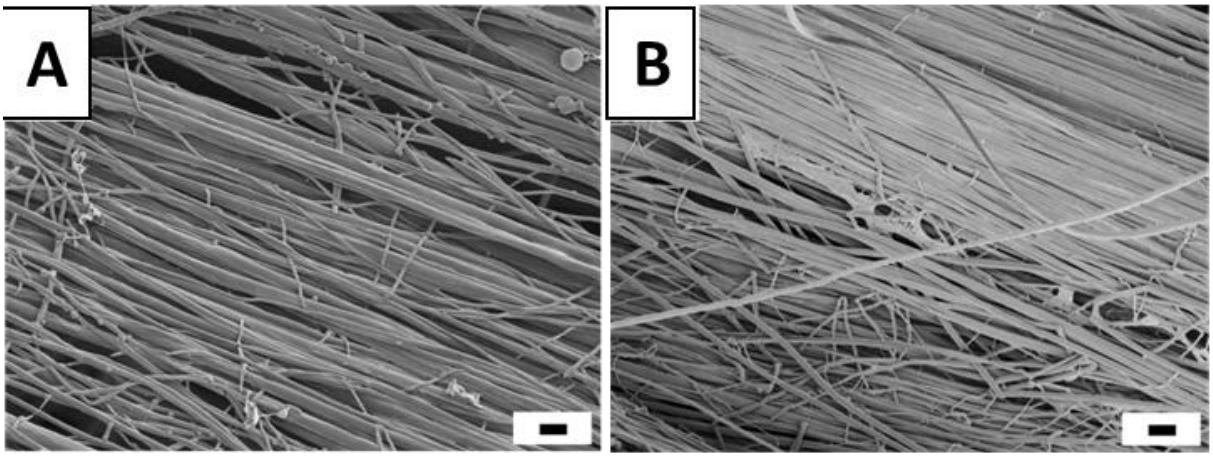

Figure 41: Morphologischer Vergleich von (A) PCL-basierten Fibrillen und (B) Collagen I Fibrillen aus Rattenschwänzen. *Größe und Form beider Fibrillen sind ähnlich, was zu einem starken immunmodulatorischen Effekt geführt hat. (Skalierung: 1 µm)*

Zudem war der Einfluss der Topografie auf die M2-Differenzierungsmarker vergleichbar mit Makrophagen welche mittels IL-4, einem Zytokin, welches zur in vitro Differenzierung in den M2 Typ genutzt wird, induziert wurden. Verglichen mit anderen Differenzierungsstudien

mittels 2D Topografie haben die Zellen aufgrund der ausgerichteten Fibrillenbündeln eine biomimetische 3D-Umgebung, welche die Migration der Zellen zwischen die Fibrillen erlaubt. Die Kombination aus MEW mit teilweise löslichen Polymerblends bietet eine neuartige Plattform für die Herstellung biomimetischer Gerüststrukturen mit Zelldifferenzierungspotential basierend auf 3-dimensionaler Topografie.

In dieser Arbeit konnte daher zum ersten Mal gezeigt werden, dass es möglich ist, mittels MEW die ultrastrukturellen Merkmale einer ECM Komponente, in diesem Fall Collagen I, nachzuahmen. Der beispiellose immunmodulatorische Effekt führte zur Erkenntnis, dass die Mimikry der Collagenstruktur ein starkes Designkriterium für biomaterialinduzierte Immunmodulation sein kann.

Die Entwicklung einer Methode zur Generierung von Mikrokanälen in Hydrogelen über die Kombination aus Poly(2-oxazoline) und Melt Electrowriting und einen Ansatz zur Prävaskularisierung wurde in **Kapitel 5** beschrieben. Auf P*n*PrOx und P*cyclo*PrOx basierende Gerüststrukturen wurden so abgelegt, dass diese natürlichen Aufzweigungen mit Bifurkationen ähneln. Nachdem diese Strukturen in Hydrogele eingebettet wurden, schwellten die Fasern an, was zur Fusion von angrenzenden Fasern führte. Nach Temperaturerniedrigung lösten sich die Gerüststrukturen auf und führten so zur Ausbildung von verbundenen Mikrokanälen mit getrenntem Ein- und Auslass. Um ein Vorbesiedeln der Gerüststrukturen mir Endothelzellen zu erreichen, ist eine längere Auslagerung in wässriger Lösung nötig. Jedoch verlieren die P*n*PrOx Gerüststrukturen ihre Stabilität durch ihr Schwellverhalten. Um diesen Effekt entgegenzuwirken, wurden P*n*PrOx Gerüststrukturen teilweise kristallisiert, was zu einer verbesserten Stabilität zu Kosten der Löslichkeit führt. Ein erster konzeptioneller Beweis konnte mit einer Endothelzelllinie erbracht werden, jedoch zeigten primäre Zellen keine Adhärenz. Daher wurden P*cyclo*PrOx Gerüststrukturen mit Hilfe einer PLGA Tauchbeschichtung stabilisiert, die eine Adhäsion und Proliferation von primären Endothelzellen ermöglichte.

Die in dieser Arbeit entwickelte Kombination einfacher Poly(2-oxazolin)e mit etablierten Methoden der Biofabrikation hat zu der Entwicklung anwendbarer und nützlicher Herangehensweisen im Tissue Engineering geführt. Besonders die Herstellung fibrillärer Gerüststrukturen und biomimetischer Mikrokanäle mittels Melt Electrowriting hat das Potential, eine Plattformtechnologie zur Bewältigung aktueller Herausforderungen des Tissue Engineering, wie Vaskularisierung und Differenzierung, zu werden.

References

1 Groll, J. *et al.* Biofabrication: reappraising the definition of an evolving field. *Biofabrication* **8**, 013001, doi:10.1088/1758-5090/8/1/013001 (2016).

2 Yang, F. *et al.* The effect of incorporating RGD adhesive peptide in polyethylene glycol diacrylate hydrogel on osteogenesis of bone marrow stromal cells. *Biomaterials* **26**, 5991-5998, doi:10.1016/j.biomaterials.2005.03.018 (2005).

3 Janmey, P. A., Winer, J. P. & Weisel, J. W. Fibrin gels and their clinical and bioengineering applications. *J R Soc Interface* **6**, 1-10, doi:10.1098/rsif.2008.0327 (2009).

4 Yung, C. W. *et al.* Transglutaminase crosslinked gelatin as a tissue engineering scaffold. *Journal of Biomedical Materials Research Part A* **83a**, 1039-1046, doi:10.1002/jbm.a.31431 (2007).

5 Nahm, D. *et al.* A versatile biomaterial ink platform for the melt electrowriting of chemically-crosslinked hydrogels. *Mater Horizons* **7**, 928-933, doi:10.1039/c9mh01654f (2020).

6 Shin, J. Y., Yeo, Y. H., Jeong, J. E., Park, S. A. & Park, W. H. Dual-crosslinked methylcellulose hydrogels for 3D bioprinting applications. *Carbohyd Polym* **238**, doi:ARTN 11619210.1016/j.carbpol.2020.116192 (2020).

7 Hoogenboom, R. Poly(2-oxazoline)s: a polymer class with numerous potential applications. *Angew Chem Int Ed Engl* **48**, 7978-7994, doi:10.1002/anie.200901607 (2009).

8 de la Rosa, V. R. Poly(2-oxazoline)s as materials for biomedical applications. *J Mater Sci-Mater M* **25**, 1211-1225, doi:10.1007/s10856-013-5034-y (2014).

9 Ryma, M. *et al.* Easy-to-Prepare Coating of Standard Cell Culture Dishes for Cell-Sheet Engineering Using Aqueous Solutions of Poly(2-n-propyl-oxazoline). *Acs Biomaterials Science & Engineering* **5**, 1509-1517, doi:10.1021/acsbiomaterials.8b01588 (2019).

10 Roszer, T. Understanding the Mysterious M2 Macrophage through Activation Markers and Effector Mechanisms. *Mediat Inflamm*, doi:10.1155/2015/816460 (2015).

11 Almonacid Suarez, A. M., Zhou, Q., van Rijn, P. & Harmsen, M. C. Directional topography gradients drive optimum alignment and differentiation of human myoblasts. *J Tissue Eng Regen Med* **13**, 2234-2245, doi:10.1002/term.2976 (2019).

12 Liguori, G. R. *et al.* Directional Topography Influences Adipose Mesenchymal Stromal Cell Plasticity: Prospects for Tissue Engineering and Fibrosis. *Stem Cells Int* **2019**, 5387850, doi:10.1155/2019/5387850 (2019).

13 McWhorter, F. Y., Wang, T., Nguyen, P., Chung, T. & Liu, W. F. Modulation of macrophage phenotype by cell shape. *Proc Natl Acad Sci U S A* **110**, 17253-17258, doi:10.1073/pnas.1308887110 (2013).

14 Chang, W. G. & Niklason, L. E. A short discourse on vascular tissue engineering. *NPJ Regen Med* **2**, doi:10.1038/s41536-017-0011-6 (2017).

15 Benjamin, A. D. *et al.* Light-based 3D printing of hydrogels with high-resolution channels. *Biomedical Physics & Engineering Express* **5**, 025035, doi:10.1088/2057-1976/aad667 (2019).

16 Zhu, W. *et al.* Direct 3D bioprinting of prevascularized tissue constructs with complex microarchitecture. *Biomaterials* **124**, 106-115, doi:10.1016/j.biomaterials.2017.01.042 (2017).

17 Jia, W. *et al.* Direct 3D bioprinting of perfusable vascular constructs using a blend bioink. *Biomaterials* **106**, 58-68, doi:10.1016/j.biomaterials.2016.07.038 (2016).
18 Kapałczyńska, M. *et al.* 2D and 3D cell cultures - a comparison of different types of cancer cell cultures. *Arch Med Sci* **14**, 910-919, doi:10.5114/aoms.2016.63743 (2018).
19 Baker, B. M. & Chen, C. S. Deconstructing the third dimension - how 3D culture microenvironments alter cellular cues. *J Cell Sci* **125**, 3015-3024, doi:10.1242/jcs.079509 (2012).
20 Duval, K. *et al.* Modeling Physiological Events in 2D vs. 3D Cell Culture. *Physiology* **32**, 266-277, doi:10.1152/physiol.00036.2016 (2017).
21 Langhans, S. A. Three-Dimensional in Vitro Cell Culture Models in Drug Discovery and Drug Repositioning. *Front Pharmacol* **9**, doi:ARTN 610.3389/fphar.2018.00006 (2018).
22 Mandrycky, C., Phong, K. & Zheng, Y. Tissue engineering toward organ-specific regeneration and disease modeling. *MRS Commun* **7**, 332-347, doi:10.1557/mrc.2017.58 (2017).
23 Dzobo, K. *et al.* Advances in Regenerative Medicine and Tissue Engineering: Innovation and Transformation of Medicine. *Stem Cells Int* **2018**, 2495848, doi:10.1155/2018/2495848 (2018).
24 Ottani, V., Martini, D., Franchi, M., Ruggeri, A. & Raspanti, M. Hierarchical structures in fibrillar collagens. *Micron* **33**, 587-596, doi:10.1016/s0968-4328(02)00033-1 (2002).
25 Tsang, H. H. & Raza, S. Impact energy absorption of bio-inspired tubular sections with structural hierarchy. *Compos Struct* **195**, 199-210, doi:10.1016/j.compstruct.2018.04.057 (2018).
26 Screen, H. R. C., Lee, D. A., Bader, D. L. & Shelton, J. C. An investigation into the effects of the hierarchical structure of tendon fascicles on micromechanical properties. *P I Mech Eng H* **218**, 109-119, doi:Doi 10.1243/095441104322984004 (2004).
27 Mansfield, J. C., Mandalia, V., Toms, A., Winlove, C. P. & Brasselet, S. Collagen reorganization in cartilage under strain probed by polarization sensitive second harmonic generation microscopy. *J R Soc Interface* **16**, doi:ARTN 2018061110.1098/rsif.2018.0611 (2019).
28 Kruger-Genge, A., Blocki, A., Franke, R. P. & Jung, F. Vascular Endothelial Cell Biology: An Update. *Int J Mol Sci* **20**, doi:10.3390/ijms20184411 (2019).
29 Farage, M. A., Miller, K. W., Elsner, P. & Maibach, H. I. Structural characteristics of the aging skin: a review. *Cutan Ocul Toxicol* **26**, 343-357, doi:10.1080/15569520701622951 (2007).
30 Yang, G., Mahadik, B., Choi, J. Y. & Fisher, J. P. Vascularization in tissue engineering: fundamentals and state-of-art. *Progress in Biomedical Engineering* **2**, 012002, doi:10.1088/2516-1091/ab5637 (2020).
31 Jain, R. K., Au, P., Tam, J., Duda, D. G. & Fukumura, D. Engineering vascularized tissue. *Nat Biotechnol* **23**, 821-823, doi:10.1038/nbt0705-821 (2005).
32 Noor, N. *et al.* 3D Printing of Personalized Thick and Perfusable Cardiac Patches and Hearts. *Adv Sci (Weinh)* **6**, 1900344, doi:10.1002/advs.201900344 (2019).
33 Reuter, C., Walles, H. & Groeber, F. Preparation of a Three-Dimensional Full Thickness Skin Equivalent. *Methods Mol Biol* **1612**, 191-198, doi:10.1007/978-1-4939-7021-6_14 (2017).
34 Griffith, C. K. *et al.* Diffusion limits of an in vitro thick prevascularized tissue. *Tissue Eng* **11**, 257-266, doi:10.1089/ten.2005.11.257 (2005).

35 Jungst, T. *et al.* Heterotypic Scaffold Design Orchestrates Primary Cell Organization and Phenotypes in Cocultured Small Diameter Vascular Grafts. *Adv Funct Mater* **29**, doi:ARTN 190598710.1002/adfm.201905987 (2019).
36 Schoneberg, J. *et al.* Engineering biofunctional in vitro vessel models using a multilayer bioprinting technique. *Sci Rep-Uk* **8**, doi:ARTN 1043010.1038/s41598-018-28715-0 (2018).
37 Sarker, M. D., Naghieh, S., Sharma, N. K. & Chen, X. B. 3D biofabrication of vascular networks for tissue regeneration: A report on recent advances. *Journal of Pharmaceutical Analysis* **8**, 277-296, doi:10.1016/j.jpha.2018.08.005 (2018).
38 Peters, E. B., Christoforou, N., Leong, K. W., Truskey, G. A. & West, J. L. Poly(Ethylene Glycol) Hydrogel Scaffolds Containing Cell-Adhesive and Protease-Sensitive Peptides Support Microvessel Formation by Endothelial Progenitor Cells. *Cellular and Molecular Bioengineering* **9**, 38-54, doi:10.1007/s12195-015-0423-6 (2016).
39 Kobayashi, J., Kikuchi, A., Aoyagi, T. & Okano, T. Cell sheet tissue engineering: Cell sheet preparation, harvesting/manipulation, and transplantation. *J Biomed Mater Res A* **107**, 955-967, doi:10.1002/jbm.a.36627 (2019).
40 Nishida, K. *et al.* Corneal reconstruction with tissue-engineered cell sheets composed of autologous oral mucosal epithelium. *N Engl J Med* **351**, 1187-1196, doi:10.1056/NEJMoa040455 (2004).
41 Saidy, N. T. *et al.* Biologically Inspired Scaffolds for Heart Valve Tissue Engineering via Melt Electrowriting. *Small* **15**, e1900873, doi:10.1002/smll.201900873 (2019).
42 Moroni, L. *et al.* Biofabrication strategies for 3D in vitro models and regenerative medicine. *Nat Rev Mater* **3**, 21-37, doi:10.1038/s41578-018-0006-y (2018).
43 Li, D. & Xia, Y. N. Electrospinning of nanofibers: Reinventing the wheel? *Advanced Materials* **16**, 1151-1170, doi:10.1002/adma.200400719 (2004).
44 Moxon, S. R. *et al.* Suspended Manufacture of Biological Structures. *Adv Mater* **29**, doi:10.1002/adma.201605594 (2017).
45 Groll, J. *et al.* A definition of bioinks and their distinction from biomaterial inks. *Biofabrication* **11**, 013001, doi:10.1088/1758-5090/aaec52 (2018).
46 Mironov, V. Printing technology to produce living tissue. *Expert Opin Biol Ther* **3**, 701-704, doi:10.1517/14712598.3.5.701 (2003).
47 Mota, C., Puppi, D., Chiellini, F. & Chiellini, E. Additive manufacturing techniques for the production of tissue engineering constructs. *J Tissue Eng Regen Med* **9**, 174-190, doi:10.1002/term.1635 (2015).
48 Choudhury, D., Anand, S. & Naing, M. W. The Arrival of Commercial Bioprinters - Towards 3D Bioprinting Revolution! *2018* **4**, doi:10.18063/ijb.v4i2.139 (2018).
49 Saunders, R. E., Gough, J. E. & Derby, B. Delivery of human fibroblast cells by piezoelectric drop-on-demand inkjet printing. *Biomaterials* **29**, 193-203, doi:10.1016/j.biomaterials.2007.09.032 (2008).
50 Ma, X. *et al.* Deterministically patterned biomimetic human iPSC-derived hepatic model via rapid 3D bioprinting. *Proc Natl Acad Sci U S A* **113**, 2206-2211, doi:10.1073/pnas.1524510113 (2016).
51 Xing, J. F., Zheng, M. L. & Duan, X. M. Two-photon polymerization microfabrication of hydrogels: an advanced 3D printing technology for tissue engineering and drug delivery. *Chem Soc Rev* **44**, 5031-5039, doi:10.1039/c5cs00278h (2015).
52 Bernal, P. N. *et al.* Volumetric Bioprinting of Complex Living-Tissue Constructs within Seconds. *Adv Mater* **31**, e1904209, doi:10.1002/adma.201904209 (2019).

53 Grigoryan, B. *et al.* Multivascular networks and functional intravascular topologies within biocompatible hydrogels. *Science* **364**, 458-464, doi:10.1126/science.aav9750 (2019).
54 Hinton, T. J. *et al.* Three-dimensional printing of complex biological structures by freeform reversible embedding of suspended hydrogels. *Sci Adv* **1**, e1500758, doi:10.1126/sciadv.1500758 (2015).
55 Highley, C. B., Song, K. H., Daly, A. C. & Burdick, J. A. Jammed Microgel Inks for 3D Printing Applications. *Adv Sci (Weinh)* **6**, 1801076, doi:10.1002/advs.201801076 (2019).
56 Zhao, P. *et al.* Fabrication of scaffolds in tissue engineering: A review. *Frontiers of Mechanical Engineering* **13**, 107-119, doi:10.1007/s11465-018-0496-8 (2018).
57 Aram, E. & Mehdipour-Ataei, S. A review on the micro- and nanoporous polymeric foams: Preparation and properties. *Int J Polym Mater Po* **65**, 358-375, doi:10.1080/00914037.2015.1129948 (2016).
58 Costeux, S., Bunker, S. P. & Jeon, H. K. Homogeneous nanocellular foams from styrenic-acrylic polymer blends. *J Mater Res* **28**, 2351-2365, doi:10.1557/jmr.2013.100 (2013).
59 Ganan-Calvo, A. M., Davila, J. & Barrero, A. Current and droplet size in the electrospraying of liquids. Scaling laws. *J Aerosol Sci* **28**, 249-275, doi:Doi 10.1016/S0021-8502(96)00433-8 (1997).
60 Jana, S., Bhagia, A. & Lerman, A. Optimization of polycaprolactone fibrous scaffold for heart valve tissue engineering. *Biomed Mater* **14**, 065014, doi:10.1088/1748-605X/ab3d24 (2019).
61 Teixeira, M. A., Amorim, M. T. P. & Felgueiras, H. P. Poly(Vinyl Alcohol)-Based Nanofibrous Electrospun Scaffolds for Tissue Engineering Applications. *Polymers (Basel)* **12**, doi:10.3390/polym12010007 (2019).
62 Russo, V. *et al.* Tendon Biomimetic Electrospun PLGA Fleeces Induce an Early Epithelial-Mesenchymal Transition and Tenogenic Differentiation on Amniotic Epithelial Stem Cells. *Cells* **9**, doi:10.3390/cells9020303 (2020).
63 Grkovic, M. *et al.* Improvement of mechanical properties and antibacterial activity of crosslinked electrospun chitosan/poly (ethylene oxide) nanofibers. *Compos Part B-Eng* **121**, 58-67, doi:10.1016/j.compositesb.2017.03.024 (2017).
64 Law, J. X., Liau, L. L., Saim, A., Yang, Y. & Idrus, R. Electrospun Collagen Nanofibers and Their Applications in Skin Tissue Engineering. *Tissue Eng Regen Med* **14**, 699-718, doi:10.1007/s13770-017-0075-9 (2017).
65 Choktaweesap, N., Arayanarakul, K., Aht-Ong, D., Meechaisue, C. & Supaphol, P. Electrospun gelatin fibers: Effect of solvent system on morphology and fiber diameters. *Polym J* **39**, 622-631, doi:10.1295/polymj.PJ2006190 (2007).
66 Snetkov, P., Morozkina, S., Uspenskaya, M. & Olekhnovich, R. Hyaluronan-Based Nanofibers: Fabrication, Characterization and Application. *Polymers-Basel* **11**, doi:ARTN 203610.3390/polym11122036 (2019).
67 Geng, X. Y., Kwon, O. H. & Jang, J. H. Electrospinning of chitosan dissolved in concentrated acetic acid solution. *Biomaterials* **26**, 5427-5432, doi:10.1016/j.biomaterials.2005.01.066 (2005).
68 Nemati, S., Kim, S. J., Shin, Y. M. & Shin, H. Current progress in application of polymeric nanofibers to tissue engineering. *Nano Converg* **6**, 36, doi:10.1186/s40580-019-0209-y (2019).

69 Aldana, A. A. & Abraham, G. A. Current advances in electrospun gelatin-based scaffolds for tissue engineering applications. *Int J Pharmaceut* **523**, 441-453, doi:10.1016/j.ijpharm.2016.09.044 (2017).
70 Zhang, Q., Lv, S., Lu, J. F., Jiang, S. T. & Lin, L. Characterization of polycaprolactone/collagen fibrous scaffolds by electrospinning and their bioactivity. *Int J Biol Macromol* **76**, 94-101, doi:10.1016/j.ijbiomac.2015.01.063 (2015).
71 Unalan, I., Colpankan, O., Albayrak, A. Z., Gorgun, C. & Urkmez, A. S. Biocompatibility of plasma-treated poly(3-hydroxybutyrate-co-3-hydroxyvalerate) nanofiber mats modified by silk fibroin for bone tissue regeneration. *Mater Sci Eng C Mater Biol Appl* **68**, 842-850, doi:10.1016/j.msec.2016.07.054 (2016).
72 Yin, Z. *et al.* The regulation of tendon stem cell differentiation by the alignment of nanofibers. *Biomaterials* **31**, 2163-2175, doi:10.1016/j.biomaterials.2009.11.083 (2010).
73 Wu, T. *et al.* Fabrication and preliminary study of a biomimetic tri-layer tubular graft based on fibers and fiber yarns for vascular tissue engineering. *Mat Sci Eng C-Mater* **82**, 121-129, doi:10.1016/j.msec.2017.08.072 (2018).
74 Prabhakaran, M. P. *et al.* Electrospun biocomposite nanofibrous scaffolds for neural tissue engineering. *Tissue Eng Part A* **14**, 1787-1797, doi:10.1089/ten.tea.2007.0393 (2008).
75 Moradi, S. L., Golchin, A., Hajishafieeha, Z., Khani, M. M. & Ardeshirylajimi, A. Bone tissue engineering: Adult stem cells in combination with electrospun nanofibrous scaffolds. *J Cell Physiol* **233**, 6509-6522, doi:10.1002/jcp.26606 (2018).
76 Li, W. J., Danielson, K. G., Alexander, P. G. & Tuan, R. S. Biological response of chondrocytes cultured in three-dimensional nanofibrous poly(epsilon-caprolactone) scaffolds. *J Biomed Mater Res A* **67**, 1105-1114, doi:10.1002/jbm.a.10101 (2003).
77 Laranjeira, M., Domingues, R. M. A., Costa-Almeida, R., Reis, R. L. & Gomes, M. E. 3D Mimicry of Native-Tissue-Fiber Architecture Guides Tendon-Derived Cells and Adipose Stem Cells into Artificial Tendon Constructs. *Small* **13**, doi:UNSP 1700689 10.1002/smll.201700689 (2017).
78 Ryan, C. N. M. *et al.* An academic, clinical and industrial update on electrospun, additive manufactured and imprinted medical devices. *Expert Rev Med Devic* **12**, 601-612, doi:Doi 10.1586/17434440.2015.1062364 (2015).
79 Persano, L., Camposeo, A., Tekmen, C. & Pisignano, D. Industrial Upscaling of Electrospinning and Applications of Polymer Nanofibers: A Review. *Macromol Mater Eng* **298**, 504-520, doi:10.1002/mame.201200290 (2013).
80 Shahriar, S. M. S. *et al.* Electrospinning Nanofibers for Therapeutics Delivery. *Nanomaterials (Basel)* **9**, doi:10.3390/nano9040532 (2019).
81 Stoddard, R. J., Steger, A. L., Blakney, A. K. & Woodrow, K. A. In pursuit of functional electrospun materials for clinical applications in humans. *Ther Deliv* **7**, 387-409, doi:10.4155/tde-2016-0017 (2016).
82 Afghah, F., Dikyol, C., Altunbek, M. & Koc, B. Biomimicry in Bio-Manufacturing: Developments in Melt Electrospinning Writing Technology Towards Hybrid Biomanufacturing. *Appl Sci-Basel* **9**, doi:ARTN 354010.3390/app9173540 (2019).
83 Han, J. J., Wu, Q. L., Xia, Y. N., Wagner, M. B. & Xu, C. H. Cell alignment induced by anisotropic electrospun fibrous scaffolds alone has limited effect on cardiomyocyte maturation. *Stem Cell Res* **16**, 740-750, doi:10.1016/j.scr.2016.04.014 (2016).
84 Brown, T. D., Dalton, P. D. & Hutmacher, D. W. Direct writing by way of melt electrospinning. *Adv Mater* **23**, 5651-5657, doi:10.1002/adma.201103482 (2011).

85 Robinson, T. M., Hutmacher, D. W. & Dalton, P. D. The Next Frontier in Melt Electrospinning: Taming the Jet. *Adv Funct Mater* **29**, doi:10.1002/adfm.201904664 (2019).
86 Youssef, A. *et al.* The Impact of Melt Electrowritten Scaffold Design on Porosity Determined by X-Ray Microtomography. *Tissue Eng Part C Methods* **25**, 367-379, doi:10.1089/ten.TEC.2018.0373 (2019).
87 Bas, O. *et al.* An Integrated Design, Material, and Fabrication Platform for Engineering Biomechanically and Biologically Functional Soft Tissues. *ACS Appl Mater Interfaces* **9**, 29430-29437, doi:10.1021/acsami.7b08617 (2017).
88 McColl, E., Groll, J., Jungst, T. & Dalton, P. D. Design and fabrication of melt electrowritten tubes using intuitive software. *Mater Design* **155**, 46-58, doi:10.1016/j.matdes.2018.05.036 (2018).
89 Hrynevich, A. *et al.* Dimension-Based Design of Melt Electrowritten Scaffolds. *Small* **14**, e1800232, doi:10.1002/smll.201800232 (2018).
90 Tylek, T. *et al.* Precisely defined fiber scaffolds with 40 mum porosity induce elongation driven M2-like polarization of human macrophages. *Biofabrication* **12**, 025007, doi:10.1088/1758-5090/ab5f4e (2020).
91 Hochleitner, G. *et al.* Melt Electrowriting of Thermoplastic Elastomers. *Macromol Rapid Comm* **39**, doi:ARTN 1800055 10.1002/marc.201800055 (2018).
92 Florczak, S. *et al.* Melt electrowriting of electroactive poly(vinylidene difluoride) fibers. *Polym Int* **68**, 735-745, doi:10.1002/pi.5759 (2019).
93 Haigh, J. N., Dargaville, T. R. & Dalton, P. D. Additive manufacturing with polypropylene microfibers. *Mat Sci Eng C-Mater* **77**, 883-887, doi:10.1016/j.msec.2017.03.286 (2017).
94 Delalat, B. *et al.* 3D printed lattices as an activation and expansion platform for T cell therapy. *Biomaterials* **140**, 58-68, doi:10.1016/j.biomaterials.2017.05.009 (2017).
95 Blum, C. *et al.* Extracellular Matrix-Modified Fiber Scaffolds as a Proadipogenic Mesenchymal Stromal Cell Delivery Platform. *Acs Biomaterials Science & Engineering* **5**, 6655-6666, doi:10.1021/acsbiomaterials.9b00894 (2019).
96 Hammerl, A., Cano, C. E. D., De-Juan-Pardo, E. M., van Griensven, M. & Poh, P. S. P. A Growth Factor-Free Co-Culture System of Osteoblasts and Peripheral Blood Mononuclear Cells for the Evaluation of the Osteogenesis Potential of Melt-Electrowritten Polycaprolactone Scaffolds. *Int J Mol Sci* **20**, doi:ARTN 106810.3390/ijms20051068 (2019).
97 Cao, K., Liu, Y., Olkhov, A. A., Siracusa, V. & Iordanskii, A. L. PLLA-PHB fiber membranes obtained by solvent-free electrospinning for short-time drug delivery. *Drug Deliv Transl Re* **8**, 291-302, doi:10.1007/s13346-017-0463-7 (2018).
98 Lian, H. & Meng, Z. X. Melt electrospinning of daunorubicin hydrochloride-loaded poly (epsilon-caprolactone) fibrous membrane for tumor therapy. *Bioact Mater* **2**, 96-100, doi:10.1016/j.bioactmat.2017.03.003 (2017).
99 He, F.-L. *et al.* Controlled release of antibiotics from poly-ε-caprolactone/polyethylene glycol wound dressing fabricated by direct-writing melt electrospinning. *Polymers for Advanced Technologies* **30**, 425-434, doi:10.1002/pat.4481 (2019).
100 Castilho, M. *et al.* Melt Electrowriting Allows Tailored Microstructural and Mechanical Design of Scaffolds to Advance Functional Human Myocardial Tissue Formation. *Adv Funct Mater* **28**, doi:ARTN 180315110.1002/adfm.201803151 (2018).
101 Saidy, N. T. *et al.* Biologically Inspired Scaffolds for Heart Valve Tissue Engineering via Melt Electrowriting. *Small* **15**, doi:ARTN 1900873 10.1002/smll.201900873 (2019).

102 Abbasi, N., Abdal-hay, A., Hamlet, S., Graham, E. & Ivanovski, S. Effects of Gradient and Offset Architectures on the Mechanical and Biological Properties of 3-D Melt Electrowritten (MEW) Scaffolds. *Acs Biomaterials Science & Engineering* **5**, 3448-3461, doi:10.1021/acsbiomaterials.8b01456 (2019).
103 Hochleitner, G. *et al.* Additive manufacturing of scaffolds with sub-micron filaments via melt electrospinning writing. *Biofabrication* **7**, doi:Artn 035002 10.1088/1758-5090/7/3/035002 (2015).
104 Wu, S. H. *et al.* Effect of scaffold morphology and cell co-culture on tenogenic differentiation of HADMSC on centrifugal melt electrospun poly (L-lactic acid) fibrous meshes. *Biofabrication* **9**, doi:ARTN 04410610.1088/1758-5090/aa8fb8 (2017).
105 Muerza-Cascante, M. L. *et al.* Endosteal-like extracellular matrix expression on melt electrospun written scaffolds. *Acta Biomaterialia* **52**, 145-158, doi:10.1016/j.actbio.2016.12.040 (2017).
106 McMaster, R. *et al.* Tailored Melt Electrowritten Scaffolds for the Generation of Sheet-Like Tissue Constructs from Multicellular Spheroids. *Adv Healthc Mater* **8**, e1801326, doi:10.1002/adhm.201801326 (2019).
107 Bock, N. *et al.* Engineering osteoblastic metastases to delineate the adaptive response of androgen-deprived prostate cancer in the bone metastatic microenvironment. *Bone Res* **7**, doi:ARTN 1310.1038/s41413-019-0049-8 (2019).
108 Haigh, J. N. *et al.* Hierarchically Structured Porous Poly(2-oxazoline) Hydrogels. *Macromol Rapid Commun* **37**, 93-99, doi:10.1002/marc.201500495 (2016).
109 Kotz, F. *et al.* Fabrication of arbitrary three-dimensional suspended hollow microstructures in transparent fused silica glass. *Nat Commun* **10**, 1439, doi:10.1038/s41467-019-09497-z (2019).
110 Kim, Y.-J. & Matsunaga, Y. T. Thermo-responsive polymers and their application as smart biomaterials. *Journal of Materials Chemistry B* **5**, 4307-4321, doi:10.1039/C7TB00157F (2017).
111 Yin, X., Hoffman, A. S. & Stayton, P. S. Poly(N-isopropylacrylamide-co-propylacrylic acid) copolymers that respond sharply to temperature and pH. *Biomacromolecules* **7**, 1381-1385, doi:10.1021/bm0507812 (2006).
112 Zhu, Y. C., Batchelor, R., Lowe, A. B. & Roth, P. J. Design of Thermoresponsive Polymers with Aqueous LCST, UCST, or Both: Modification of a Reactive Poly(2-vinyl-4,4-dimethylazlactone) Scaffold. *Macromolecules* **49**, 672-680, doi:10.1021/acs.macromol.5b02056 (2016).
113 Kohno, Y., Saita, S., Men, Y. J., Yuan, J. Y. & Ohno, H. Thermoresponsive polyelectrolytes derived from ionic liquids. *Polym Chem-Uk* **6**, 2163-2178, doi:10.1039/c4py01665c (2015).
114 Maeda, T., Akasaki, Y., Yamamoto, K. & Aoyagi, T. Stimuli-responsive coacervate induced in binary functionalized poly(N-isopropylacrylamide) aqueous system and novel method for preparing semi-ipn microgel using the coacervate. *Langmuir* **25**, 9510-9517, doi:10.1021/la9007735 (2009).
115 Soppimath, K. S., Aminabhavi, T. M., Dave, A. M., Kumbar, S. G. & Rudzinski, W. E. Stimulus-responsive "smart" hydrogels as novel drug delivery systems. *Drug Dev Ind Pharm* **28**, 957-974, doi:10.1081/Ddc-120006428 (2002).
116 Aoyagi, T., Ebara, M., Sakai, K., Sakurai, Y. & Okano, T. Novel bifunctional polymer with reactivity and temperature sensitivity. *J Biomat Sci-Polym E* **11**, 101-110, doi:Doi 10.1163/156856200743526 (2000).

117 Yoshida, T., Aoyagi, T., Kokufuta, E. & Okano, T. Newly designed hydrogel with both sensitive thermoresponse and biodegradability. *Journal of Polymer Science Part a-Polymer Chemistry* **41**, 779-787, doi:10.1002/pola.10595 (2003).
118 Gilcreest, V. P. *et al.* Thermoresponsive poly(N-isopropylacrylamide) copolymers: Contact angles and surface energies of polymer films. *Langmuir* **20**, 10138-10145, doi:10.1021/la0487996 (2004).
119 Jeong, B., Kim, S. W. & Bae, Y. H. Thermosensitive sol-gel reversible hydrogels. *Adv Drug Deliv Rev* **54**, 37-51, doi:10.1016/s0169-409x(01)00242-3 (2002).
120 Calejo, M. T. *et al.* Interactions between ethyl(hydroxyethyl) cellulose and lysine-based surfactants in aqueous media. *European Polymer Journal* **48**, 1622-1631, doi:10.1016/j.eurpolymj.2012.06.009 (2012).
121 Calejo, M. T. *et al.* In vitro cytotoxicity of a thermoresponsive gel system combining ethyl(hydroxyethyl) cellulose and lysine-based surfactants. *Colloids Surf B Biointerfaces* **102**, 682-686, doi:10.1016/j.colsurfb.2012.09.033 (2013).
122 André, X., Zhang, M. & Müller, A. H. E. Thermo- and pH-Responsive Micelles of Poly(acrylic acid)-block-Poly(N,N-diethylacrylamide). *Macromol Rapid Comm* **26**, 558-563, doi:10.1002/marc.200400510 (2005).
123 Arndt, K. F., Schmidt, T. & Reichelt, R. Thermo-sensitive poly(methyl vinyl ether) micro-gel formed by high energy radiation. *Polymer* **42**, 6785-6791, doi:Doi 10.1016/S0032-3861(01)00164-1 (2001).
124 Webster, M. *et al.* Tunable Thermo-Responsive Poly(N-vinylcaprolactam) Cellulose Nanofibers: Synthesis, Characterization, and Fabrication. *Macromol Mater Eng* **298**, 447-453, doi:10.1002/mame.201200081 (2013).
125 Okano, T., Yamada, N., Sakai, H. & Sakurai, Y. A novel recovery system for cultured cells using plasma-treated polystyrene dishes grafted with poly(N-isopropylacrylamide). *Journal of Biomedical Materials Research* **27**, 1243-1251, doi:10.1002/jbm.820271005 (1993).
126 Yang, J. *et al.* Cell delivery in regenerative medicine: The cell sheet engineering approach. *Journal of Controlled Release* **116**, 193-203, doi:10.1016/j.jconrel.2006.06.022 (2006).
127 Hasegawa, M., Yamato, M., Kikuchi, A., Okano, T. & Ishikawa, I. Human periodontal ligament cell sheets can regenerate periodontal ligament tissue in an athymic rat model. *Tissue Eng* **11**, 469-478, doi:DOI 10.1089/ten.2005.11.469 (2005).
128 Kanzaki, M. *et al.* Functional closure of visceral pleural defects by autologous tissue engineered cell sheets. *Eur J Cardio-Thorac* **34**, 864-869, doi:10.1016/j.ejcts.2008.05.048 (2008).
129 Tsumanuma, Y. *et al.* Comparison of different tissue-derived stem cell sheets for periodontal regeneration in a canine 1-wall defect model. *Biomaterials* **32**, 5819-5825, doi:10.1016/j.biomaterials.2011.04.071 (2011).
130 Kanzaki, M. *et al.* Dynamic sealing of lung air leaks by the transplantation of tissue engineered cell sheets. *Biomaterials* **28**, 4294-4302, doi:DOI 10.1016/j.biomaterials.2007.06.009 (2007).
131 Qi, Y. Y. *et al.* Combined Mesenchymal Stem Cell Sheets and rhBMP-2-Releasing Calcium Sulfate-rhBMP-2 Scaffolds for Segmental Bone Tissue Engineering. *Cell Transplant* **21**, 693-705, doi:10.3727/096368911x623844 (2012).
132 Chen, G. *et al.* Application of the cell sheet technique in tissue engineering. *Biomed Rep* **3**, 749-757, doi:10.3892/br.2015.522 (2015).

133 Okuzaki, H., Kobayashi, K., Hishiki, F., Su, S. J. & Yan, H. Thermo-responsive nanofiber mats fabricated by electrospinning of poly(N-isopropylacrylamide-co-stearyl acrylate). *J Nanosci Nanotechnol* **11**, 5193-5198, doi:10.1166/jnn.2011.4186 (2011).
134 Kim, Y. J., Takahashi, Y., Kato, N. & Matsunaga, Y. T. Fabrication of biomimetic bundled gel fibres using dynamic microfluidic gelation of phase-separated polymer solutions. *Journal of Materials Chemistry B* **3**, 8154-8161, doi:10.1039/c5tb01395j (2015).
135 Kim, Y. J., Tachibana, M., Umezu, M. & Matsunaga, Y. T. Bio-inspired smart hydrogel with temperature-dependent properties and enhanced cell attachment. *Journal of Materials Chemistry B* **4**, 1740-1746, doi:10.1039/c5tb02735g (2016).
136 Hoo, S. P., Sarvi, F., Li, W. H., Chan, P. P. Y. & Yue, Z. L. Thermoresponsive Cellulosic Hydrogels with Cell-Releasing Behavior. *Acs Appl Mater Inter* **5**, 5592-5600, doi:10.1021/am4009133 (2013).
137 Yu, L. & Ding, J. D. Injectable hydrogels as unique biomedical materials. *Chemical Society Reviews* **37**, 1473-1481, doi:10.1039/b713009k (2008).
138 Li, L. *et al.* Biodegradable and injectable in situ cross-linking chitosan-hyaluronic acid based hydrogels for postoperative adhesion prevention. *Biomaterials* **35**, 3903-3917, doi:10.1016/j.biomaterials.2014.01.050 (2014).
139 Jeong, B., Bae, Y. H. & Kim, S. W. Drug release from biodegradable injectable thermosensitive hydrogel of PEG-PLGA-PEG triblock copolymers. *J Control Release* **63**, 155-163, doi:10.1016/s0168-3659(99)00194-7 (2000).
140 Zhang, J., Chen, H., Xu, L. & Gu, Y. The targeted behavior of thermally responsive nanohydrogel evaluated by NIR system in mouse model. *J Control Release* **131**, 34-40, doi:10.1016/j.jconrel.2008.07.019 (2008).
141 Seeliger, W. *et al.* Recent syntheses and reactions of cyclic imidic esters. *Angew Chem Int Ed Engl* **5**, 875-888, doi:10.1002/anie.196608751 (1966).
142 Tomalia, D. A. & Sheetz, D. P. Homopolymerization of 2-Alkyl- and 2-Aryl-2-Oxazolines. *J Polym Sci A1* **4**, 2253-&, doi:DOI 10.1002/pol.1966.150040919 (1966).
143 Lorson, T. *et al.* Poly(2-oxazoline)s based biomaterials: A comprehensive and critical update. *Biomaterials* **178**, 204-280, doi:10.1016/j.biomaterials.2018.05.022 (2018).
144 Kagiya, T., Narisawa, S., Maeda, T. & Fukui, K. Ring-opening polymerization of 2-substituted 2-oxazolines. *Journal of Polymer Science Part B: Polymer Letters* **4**, 441-445, doi:10.1002/pol.1966.110040701 (1966).
145 Aoi, K., Suzuki, H. & Okada, M. Architectural Control of Sugar-Containing Polymers by Living Polymerization - Ring-Opening Polymerization of 2-Oxazolines Initiated with Carbohydrate-Derivatives. *Macromolecules* **25**, 7073-7075, doi:DOI 10.1021/ma00051a056 (1992).
146 Zhang, N., Luxenhofer, R. & Jordan, R. Thermoresponsive Poly(2-Oxazoline) Molecular Brushes by Living Ionic Polymerization: Modulation of the Cloud Point by Random and Block Copolymer Pendant Chains. *Macromol Chem Phys* **213**, 1963-1969, doi:10.1002/macp.201200261 (2012).
147 Huber, S. & Jordan, R. Modulation of the lower critical solution temperature of 2-Alkyl-2-oxazoline copolymers. *Colloid Polym Sci* **286**, 395-402, doi:10.1007/s00396-007-1781-y (2008).
148 Moreadith, R. W. *et al.* Clinical development of a poly(2-oxazoline) (POZ) polymer therapeutic for the treatment of Parkinson's disease - Proof of concept of POZ as a versatile polymer platform for drug development in multiple therapeutic indications. *European Polymer Journal* **88**, 524-552, doi:10.1016/j.eurpolymj.2016.09.052 (2017).

149 Woodle, M. C., Engbers, C. M. & Zalipsky, S. New Amphipatic Polymer Lipid Conjugates Forming Long-Circulating Reticuloendothelial System-Evading Liposomes. *Bioconjugate Chem* **5**, 493-496, doi:DOI 10.1021/bc00030a001 (1994).
150 Glassner, M., Vergaelen, M. & Hoogenboom, R. Poly(2-oxazoline)s: A comprehensive overview of polymer structures and their physical properties. *Polym Int* **67**, 32-45, doi:10.1002/pi.5457 (2018).
151 Sramkova, P., Zahoranova, A., Kronekova, Z., Siskova, A. & Kronek, J. Poly(2-oxazoline) hydrogels by photoinduced thiol-ene "click" reaction using different dithiol crosslinkers. *J Polym Res* **24**, doi:ARTN 82 10.1007/s10965-017-1237-0 (2017).
152 Lorson, T. *et al.* A Thermogelling Supramolecular Hydrogel with Sponge-Like Morphology as a Cytocompatible Bioink. *Biomacromolecules* **18**, 2161-2171, doi:10.1021/acs.biomac.7b00481 (2017).
153 Jeon, O., Bin Lee, Y., Hinton, T. J., Feinberg, A. W. & Alsberg, E. Cryopreserved cell-laden alginate microgel bioink for 3D bioprinting of living tissues. *Mater Today Chem* **12**, 61-70, doi:10.1016/j.mtchem.2018.11.009 (2019).
154 Hoelzer, D. *et al.* Tumor targeting with pH-responsive poly(2-oxazoline)-based nanogels for metronomic doxorubicin treatment. *Oncotarget* **9**, 22316-22331, doi:10.18632/oncotarget.24806 (2018).
155 Hersel, U., Dahmen, C. & Kessler, H. RGD modified polymers: biomaterials for stimulated cell adhesion and beyond. *Biomaterials* **24**, 4385-4415, doi:10.1016/s0142-9612(03)00343-0 (2003).
156 Qu, C. C. *et al.* A thermosensitive RGD-modified hydroxybutyl chitosan hydrogel as a 3D scaffold for BMSCs culture on keloid treatment. *Int J Biol Macromol* **125**, 78-86, doi:10.1016/j.ijbiomac.2018.12.058 (2019).
157 You, Y. *et al.* Engineered cell-degradable poly(2-alkyl-2-oxazoline) hydrogel for epicardial placement of mesenchymal stem cells for myocardial repair. *Biomaterials*, 120356, doi:10.1016/j.biomaterials.2020.120356 (2020).
158 Kurzhals, S., Gal, N., Zirbs, R. & Reimhult, E. Controlled aggregation and cell uptake of thermoresponsive polyoxazoline-grafted superparamagnetic iron oxide nanoparticles. *Nanoscale* **9**, 2793-2805, doi:10.1039/c6nr08654c (2017).
159 Schmitz, M., Kuhlmann, M., Reimann, O., Hackenberger, C. P. & Groll, J. Side-chain cysteine-functionalized poly(2-oxazoline)s for multiple peptide conjugation by native chemical ligation. *Biomacromolecules* **16**, 1088-1094, doi:10.1021/bm501697t (2015).
160 Konieczny, S., Krumm, C., Doert, D., Neufeld, K. & Tiller, J. C. Investigations on the activity of poly(2-oxazoline) enzyme conjugates dissolved in organic solvents. *J Biotechnol* **181**, 55-63, doi:10.1016/j.jbiotec.2014.03.035 (2014).
161 Jordan, R., Graf, K., Riegler, H. & Unger, K. K. Polymer-supported alkyl monolayers on silica: Synthesis and self-assembly of terminal functionalized poly(N-propionylethylenimine)s. *Chemical Communications*, 1025-1026, doi:DOI 10.1039/cc9960001025 (1996).
162 Tauhardt, L., Kempe, K., Gottschaldt, M. & Schubert, U. S. Poly(2-oxazoline) functionalized surfaces: from modification to application. *Chemical Society Reviews* **42**, 7998-8011, doi:10.1039/c3cs60161g (2013).
163 Fik, C. P. *et al.* Telechelic Poly(2-oxazoline)s with a Biocidal and a Polymerizable Terminal as Collagenase Inhibiting Additive for Long-Term Active Antimicrobial Dental Materials. *Macromolecular Bioscience* **14**, 1569-1579, doi:10.1002/mabi.201400220 (2014).

164 Dworak, A. *et al.* Poly(2-substituted-2-oxazoline) surfaces for dermal fibroblasts adhesion and detachment. *J Mater Sci-Mater M* **25**, 1149-1163, doi:10.1007/s10856-013-5135-7 (2014).
165 Oleszko, N. *et al.* Controlling the Crystallinity of Thermoresponsive Poly(2-oxazoline)-Based Nanolayers to Cell Adhesion and Detachment. *Biomacromolecules* **16**, 2805-2813, doi:10.1021/acs.biomac.5b00745 (2015).
166 Hochleitner, G., Hummer, J. F., Luxenhofer, R. & Groll, J. High definition fibrous poly(2-ethyl-2-oxazoline) scaffolds through melt electrospinning writing. *Polymer* **55**, 5017-5023, doi:10.1016/j.polymer.2014.08.024 (2014).
167 Walach, W. *et al.* Processing of (Co)Poly(2-oxazoline)s by Electrospinning and Extrusion from Melt and the Postprocessing Properties of the (Co)Polymers. *Polymers (Basel)* **12**, doi:10.3390/polym12020295 (2020).
168 Moreadith, R. W. *et al.* Clinical development of a poly(2-oxazoline) (POZ) polymer therapeutic for the treatment of Parkinson's disease – Proof of concept of POZ as a versatile polymer platform for drug development in multiple therapeutic indications. *European Polymer Journal* **88**, 524-552, doi:https://doi.org/10.1016/j.eurpolymj.2016.09.052 (2017).
169 Yamada, N. *et al.* Thermoresponsive Polymeric Surfaces - Control of Attachment and Detachment of Cultured-Cells. *Makromol Chem-Rapid* **11**, 571-576 (1990).
170 Okano, T., Yamada, N., Sakai, H. & Sakurai, Y. A Novel Recovery-System for Cultured-Cells Using Plasma-Treated Polystyrene Dishes Grafted with Poly(N-Isopropylacrylamide). *J Biomed Mater Res* **27**, 1243-1251, doi:DOI 10.1002/jbm.820271005 (1993).
171 Yamato, M. *et al.* Thermo-responsive culture dishes allow the intact harvest of multilayered keratinocyte sheets without dispase by reducing temperature. *Tissue Eng* **7**, 473-480, doi:10.1089/10763270152436517 (2001).
172 Nishida, K. *et al.* Functional bioengineered corneal epithelial sheet grafts from corneal stem cells expanded ex vivo on a temperature-responsive cell culture surface. *Transplantation* **77**, 379-385, doi:10.1097/01.TP.0000110320.45678.30 (2004).
173 Kushida, A., Yamato, M., Isoi, Y., Kikuchi, A. & Okano, T. A noninvasive transfer system for polarized renal tubule epithelial cell sheets using temperature-responsive culture dishes. *Eur Cell Mater* **10**, 23-30; discussion 23-30 (2005).
174 Yamato, M. *et al.* Signal transduction and cytoskeletal reorganization are required for cell detachment from cell culture surfaces grafted with a temperature-responsive polymer. *J Biomed Mater Res* **44**, 44-52 (1999).
175 Shimizu, T. *et al.* Electrically communicating three-dimensional cardiac tissue mimic fabricated by layered cultured cardiomyocyte sheets. *J Biomed Mater Res* **60**, 110-117 (2002).
176 Ohashi, K. *et al.* Engineering functional two- and three-dimensional liver systems in vivo using hepatic tissue sheets. *Nat Med* **13**, 880-885, doi:10.1038/nm1576 (2007).
177 Gaertner, F. C., Luxenhofer, R., Blechert, B., Jordan, R. & Essler, M. Synthesis, biodistribution and excretion of radiolabeled poly(2-alkyl-2-oxazoline)s. *J Control Release* **119**, 291-300, doi:10.1016/j.jconrel.2007.02.015 (2007).
178 Hoogenboom, R. *et al.* Tuning the LCST of poly(2-oxazoline)s by varying composition and molecular weight: alternatives to poly(N-isopropylacrylamide)? *Chem Commun*, 5758-5760, doi:10.1039/b813140f (2008).
179 Luxenhofer, R. *et al.* Poly(2-oxazoline)s as polymer therapeutics. *Macromol Rapid Commun* **33**, 1613-1631, doi:10.1002/marc.201200354 (2012).

180 Cheon Lee, S., Kim, C., Chan Kwon, I., Chung, H. & Young Jeong, S. Polymeric micelles of poly(2-ethyl-2-oxazoline)-block-poly(epsilon-caprolactone) copolymer as a carrier for paclitaxel. *J Control Release* **89**, 437-446 (2003).
181 Dworak, A. *et al.* Poly(2-substituted-2-oxazoline) surfaces for dermal fibroblasts adhesion and detachment. *J Mater Sci Mater Med* **25**, 1149-1163, doi:10.1007/s10856-013-5135-7 (2014).
182 Boerman, M. A. *et al.* Synthesis of pH- and Thermoresponsive Poly(2-n-propyl-2-Oxazoline) Based Copolymers. *J Polym Sci Pol Chem* **54**, 1573-1582, doi:10.1002/pola.28011 (2016).
183 Schmidt, S. *et al.* Adhesion and Mechanical Properties of PNIPAM Microgel Films and Their Potential Use as Switchable Cell Culture Substrates. *Adv Funct Mater* **20**, 3235-3243, doi:10.1002/adfm.201000730 (2010).
184 Nakayama, M. *et al.* Thermoresponsive poly(N-isopropylacrylamide)-based block copolymer coating for optimizing cell sheet fabrication. *Macromol Biosci* **12**, 751-760, doi:10.1002/mabi.201200018 (2012).
185 Weydert, S. *et al.* Easy to Apply Polyoxazoline-Based Coating for Precise and Long-Term Control of Neural Patterns. *Langmuir* **33**, 8594-8605, doi:10.1021/acs.langmuir.7b01437 (2017).
186 Nash, M. E. *et al.* Straightforward, one-step fabrication of ultrathin thermoresponsive films from commercially available pNIPAm for cell culture and recovery. *ACS Appl Mater Interfaces* **3**, 1980-1990, doi:10.1021/am200204j (2011).
187 Noth, U., Tuli, R., Osyczka, A. M., Danielson, K. G. & Tuan, R. S. In vitro engineered cartilage constructs produced by press-coating biodegradable polymer with human mesenchymal stem cells. *Tissue Eng* **8**, 131-144, doi:10.1089/107632702753503126 (2002).
188 Cicha, I. *et al.* Pharmacological inhibition of RhoA signaling prevents connective tissue growth factor induction in endothelial cells exposed to non-uniform shear stress. *Atherosclerosis* **196**, 136-145, doi:10.1016/j.atherosclerosis.2007.03.016 (2008).
189 Ades, E. W. *et al.* HMEC-1: establishment of an immortalized human microvascular endothelial cell line. *J Invest Dermatol* **99**, 683-690 (1992).
190 Bloksma, M. M., Bakker, D. J., Weber, C., Hoogenboom, R. & Schubert, U. S. The Effect of Hofmeister Salts on the LCST Transition of Poly(2-oxazoline)s with Varying Hydrophilicity. *Macromol Rapid Commun* **31**, 724-728, doi:10.1002/marc.200900843 (2010).
191 Kostova, B., Ivanova, S., Balashev, K., Rachev, D. & Christova, D. Evaluation of poly(2-ethyl-2-oxazoline) containing copolymer networks of varied composition as sustained metoprolol tartrate delivery systems. *AAPS PharmSciTech* **15**, 939-946, doi:10.1208/s12249-014-0120-0 (2014).
192 Kim, S. J., Lee, K. J. & Kim, S. I. Thermo-sensitive swelling behavior of poly(2-ethyl-2-oxazoline)/poly(vinyl alcohol) interpenetrating polymer network hydrogels. *J Macromol Sci Pure* **A41**, 267-274, doi:10.1081/Ma-120028206 (2004).
193 Sancho, A., Vandersmissen, I., Craps, S., Luttun, A. & Groll, J. A new strategy to measure intercellular adhesion forces in mature cell-cell contacts. *Sci Rep* **7**, 46152, doi:10.1038/srep46152 (2017).
194 Kelly, A. M., Hecke, A., Wirnsberger, B. & Wiesbrock, F. Synthesis of poly(2-oxazoline)-based hydrogels with tailor-made swelling degrees capable of stimuli-triggered compound release. *Macromol Rapid Commun* **32**, 1815-1819, doi:10.1002/marc.201100409 (2011).

195 Dargaville, T. R., Hollier, B. G., Shokoohmand, A. & Hoogenboom, R. Poly(2-oxazoline) hydrogels as next generation three-dimensional cell supports. *Cell Adhes Migr* **8**, 88-93, doi:10.4161/cam.28205 (2014).
196 Ryma, M. *et al.* Easy-to-Prepare Coating of Standard Cell Culture Dishes for Cell-Sheet Engineering Using Aqueous Solutions of Poly(2-n-propyl-oxazoline). *ACS Biomaterials Science & Engineering*, doi:10.1021/acsbiomaterials.8b01588 (2019).
197 Escudero-Castellanos, A., Ocampo-Garcia, B. E., Dominguez-Garcia, M. V., Flores-Estrada, J. & Flores-Merino, M. V. Hydrogels based on poly(ethylene glycol) as scaffolds for tissue engineering application: biocompatibility assessment and effect of the sterilization process. *J Mater Sci-Mater M* **27**, doi:ARTN 176 10.1007/s10856-016-5793-3 (2016).
198 Hoffmann, J. *et al.* Blood cell and plasma protein repellent properties of star-PEG-modified surfaces. *J Biomater Sci Polym Ed* **17**, 985-996 (2006).
199 Luef, K. P. *et al.* UV-mediated thiol-ene click reactions for the synthesis of drug-loadable and degradable gels based on copoly(2-oxazoline)s. *Eur Polym J* **88**, 701-712, doi:10.1016/j.eurpolymj.2016.08.012 (2017).
200 Blöhbaum, J., Paulus, I., Pöppler, A.-C., Tessmar, J. & Groll, J. Influence of charged groups on the cross-linking efficiency and release of guest molecules from thiol–ene cross-linked poly(2-oxazoline) hydrogels. *Journal of Materials Chemistry B* **7**, 1782-1794, doi:10.1039/C8TB02575D (2019).
201 Park, B. J. *et al.* Cellular responses of vascular endothelial cells on surface modified polyurethane films grafted electrospun PLGA fiber with microwave-induced plasma at atmospheric pressure. *Surf Coat Tech* **205**, S222-S226, doi:10.1016/j.surfcoat.2010.07.087 (2010).
202 Groll, J., Ademovic, Z., Ameringer, T., Klee, D. & Moeller, M. Comparison of coatings from reactive star shaped PEG-stat-PPG prepolymers and grafted linear PEG for biological and medical applications. *Biomacromolecules* **6**, 956-962, doi:10.1021/bm049350u (2005).
203 Dalby, M. J., Gadegaard, N. & Oreffo, R. O. C. Harnessing nanotopography and integrin-matrix interactions to influence stem cell fate. *Nat Mater* **13**, 558-569, doi:10.1038/Nmat3980 (2014).
204 von Erlach, T. C. *et al.* Cell-geometry-dependent changes in plasma membrane order direct stem cell signalling and fate. *Nat Mater* **17**, 237-242, doi:10.1038/s41563-017-0014-0 (2018).
205 Brown, T. D. *et al.* Melt electrospinning of poly(epsilon-caprolactone) scaffolds: phenomenological observations associated with collection and direct writing. *Mater Sci Eng C Mater Biol Appl* **45**, 698-708, doi:10.1016/j.msec.2014.07.034 (2014).
206 Tourlomousis, F. *et al.* Machine learning metrology of cell confinement in melt electrowritten three-dimensional biomaterial substrates. *Microsyst Nanoeng* **5**, 15, doi:10.1038/s41378-019-0055-4 (2019).
207 Franz, S., Rammelt, S., Scharnweber, D. & Simon, J. C. Immune responses to implants - a review of the implications for the design of immunomodulatory biomaterials. *Biomaterials* **32**, 6692-6709, doi:10.1016/j.biomaterials.2011.05.078 (2011).
208 Martinez, F. O. & Gordon, S. The M1 and M2 paradigm of macrophage activation: time for reassessment. *F1000Prime Rep* **6**, 13, doi:10.12703/P6-13 (2014).
209 Sica, A. & Mantovani, A. Macrophage plasticity and polarization: in vivo veritas. *J Clin Invest* **122**, 787-795, doi:10.1172/JCI59643 (2012).

210 O'Brien, E. M., Risser, G. E. & Spiller, K. L. Sequential drug delivery to modulate macrophage behavior and enhance implant integration. *Adv Drug Deliv Rev* **149-150**, 85-94, doi:10.1016/j.addr.2019.05.005 (2019).
211 Luu, T. U., Gott, S. C., Woo, B. W., Rao, M. P. & Liu, W. F. Micro- and Nanopatterned Topographical Cues for Regulating Macrophage Cell Shape and Phenotype. *ACS Appl Mater Interfaces* **7**, 28665-28672, doi:10.1021/acsami.5b10589 (2015).
212 Jia, Y. *et al.* Nanofiber arrangement regulates peripheral nerve regeneration through differential modulation of macrophage phenotypes. *Acta Biomater* **83**, 291-301, doi:10.1016/j.actbio.2018.10.040 (2019).
213 Jin, G. *et al.* Electrospun three-dimensional aligned nanofibrous scaffolds for tissue engineering. *Mater Sci Eng C Mater Biol Appl* **92**, 995-1005, doi:10.1016/j.msec.2018.06.065 (2018).
214 Hochleitner, G. *et al.* Additive manufacturing of scaffolds with sub-micron filaments via melt electrospinning writing. *Biofabrication* **7**, 035002, doi:10.1088/1758-5090/7/3/035002 (2015).
215 Rajan, N., Habermehl, J., Cote, M. F., Doillon, C. J. & Mantovani, D. Preparation of ready-to-use, storable and reconstituted type I collagen from rat tail tendon for tissue engineering applications. *Nat Protoc* **1**, 2753-2758, doi:10.1038/nprot.2006.430 (2006).
216 Bloksma, M. M. *et al.* Poly(2-cyclopropyl-2-oxazoline): From Rate Acceleration by Cyclopropyl to Thermoresponsive Properties. *Macromolecules* **44**, 4057-4064, doi:10.1021/ma200514n (2011).
217 Bouten, P. J. M., Lava, K., van Hest, J. C. M. & Hoogenboom, R. Thermal Properties of Methyl Ester-Containing Poly(2-oxazoline)s. *Polymers-Basel* **7**, 1998-2008, doi:10.3390/polym7101494 (2015).
218 Demirel, A. L. *et al.* Revisiting the Crystallization of Poly(2-alkyl-2-oxazoline)s. *J Polym Sci Pol Phys* **54**, 721-729, doi:10.1002/polb.23967 (2016).
219 Glassner, M., Lava, K., de la Rosa, V. R. & Hoogenboom, R. Tuning the LCST of Poly(2-cyclopropyl-2-oxazoline) via Gradient Copolymerization with 2-Ethyl-2-Oxazoline. *Journal of Polymer Science Part a-Polymer Chemistry* **52**, 3118-3122, doi:10.1002/pola.27364 (2014).
220 Tenbrinke, G., Oudhuis, L. & Ellis, T. S. The Thermal Characterization of Multicomponent Systems by Enthalpy Relaxation. *Thermochim Acta* **238**, 75-98, doi:Doi 10.1016/S0040-6031(94)85207-3 (1994).
221 Wu, S. H., Wang, Y., Streubel, P. N. & Duan, B. Living nanofiber yarn-based woven biotextiles for tendon tissue engineering using cell tri-culture and mechanical stimulation. *Acta Biomaterialia* **62**, 102-115, doi:10.1016/j.actbio.2017.08.043 (2017).
222 Wu, Y., Wang, L., Guo, B. & Ma, P. X. Interwoven Aligned Conductive Nanofiber Yarn/Hydrogel Composite Scaffolds for Engineered 3D Cardiac Anisotropy. *ACS Nano* **11**, 5646-5659, doi:10.1021/acsnano.7b01062 (2017).
223 Sivalingam, G., Karthik, R. & Madras, G. Blends of poly(epsilon-caprolactone) and poly(vinyl acetate): mechanical properties and thermal degradation. *Polym Degrad Stabil* **84**, 345-351, doi:10.1016/j.polymdegradstab.2004.01.011 (2004).
224 McWhorter, F. Y., Davis, C. T. & Liu, W. F. Physical and mechanical regulation of macrophage phenotype and function. *Cell Mol Life Sci* **72**, 1303-1316, doi:10.1007/s00018-014-1796-8 (2015).

225 Chen, S. *et al.* Characterization of topographical effects on macrophage behavior in a foreign body response model. *Biomaterials* **31**, 3479-3491, doi:10.1016/j.biomaterials.2010.01.074 (2010).
226 Stewart, A. G., Thomas, B. & Koff, J. TGF-beta: Master regulator of inflammation and fibrosis. *Respirology* **23**, 1096-1097, doi:10.1111/resp.13415 (2018).
227 Witherel, C. E., Abebayehu, D., Barker, T. H. & Spiller, K. L. Macrophage and Fibroblast Interactions in Biomaterial-Mediated Fibrosis. *Adv Healthc Mater* **8**, e1801451, doi:10.1002/adhm.201801451 (2019).
228 Wang, T. T., Luu, T. U., Chen, A. R., Khine, M. & Liu, W. F. Topographical modulation of macrophage phenotype by shrink-film multi-scale wrinkles. *Biomater Sci-Uk* **4**, 948-952, doi:10.1039/c6bm00224b (2016).
229 Zheng, X. W. *et al.* Near-Infrared-Triggered Dynamic Surface Topography for Sequential Modulation of Macrophage Phenotypes. *Acs Appl Mater Inter* **11**, 43689-43697, doi:10.1021/acsami.9b14808 (2019).
230 Jia, Y. C. *et al.* Nanofiber arrangement regulates peripheral nerve regeneration through differential modulation of macrophage phenotypes. *Acta Biomaterialia* **83**, 291-301, doi:10.1016/j.actbio.2018.10.040 (2019).
231 Tien, J. Tissue Engineering of the Microvasculature. *Compr Physiol* **9**, 1155-1212, doi:10.1002/cphy.c180037 (2019).
232 Lee, V. K. *et al.* Creating perfused functional vascular channels using 3D bio-printing technology. *Biomaterials* **35**, 8092-8102, doi:10.1016/j.biomaterials.2014.05.083 (2014).
233 Pimentel, C. R. *et al.* Three-dimensional fabrication of thick and densely populated soft constructs with complex and actively perfused channel network. *Acta Biomater* **65**, 174-184, doi:10.1016/j.actbio.2017.10.047 (2018).
234 Milojevic, M. *et al.* Core/shell Printing Scaffolds For Tissue Engineering Of Tubular Structures. *J Vis Exp*, doi:10.3791/59951 (2019).
235 He, J. *et al.* Fabrication of nature-inspired microfluidic network for perfusable tissue constructs. *Adv Healthc Mater* **2**, 1108-1113, doi:10.1002/adhm.201200404 (2013).
236 Shang, L. *et al.* Micro/nanofabrication of brittle hydrogels using 3D printed soft ultrafine fiber molds for damage-free demolding. *Biofabrication* (2019).
237 Miller, J. S. *et al.* Rapid casting of patterned vascular networks for perfusable engineered three-dimensional tissues. *Nat Mater* **11**, 768-774, doi:10.1038/nmat3357 (2012).
238 Gelber, M. K., Hurst, G., Comi, T. J. & Bhargava, R. Model-guided design and characterization of a high-precision 3D printing process for carbohydrate glass. *Addit Manuf* **22**, 38-50, doi:10.1016/j.addma.2018.04.026 (2018).
239 Subbiah, T., Bhat, G. S., Tock, R. W., Pararneswaran, S. & Ramkumar, S. S. Electrospinning of nanofibers. *J Appl Polym Sci* **96**, 557-569, doi:10.1002/app.21481 (2005).
240 Bertassoni, L. E. *et al.* Hydrogel bioprinted microchannel networks for vascularization of tissue engineering constructs. *Lab Chip* **14**, 2202-2211, doi:10.1039/c4lc00030g (2014).
241 Litt, M., Rahl, F. & Roldan, L. G. Polymerization of Cyclic Imino Ethers .6. X-Ray Study of Some Polyaziridines. *J Polym Sci A2* **7**, 463-&, doi:DOI 10.1002/pol.1969.160070302 (1969).
242 Tait, A. *et al.* Biocompatibility of poly(2-alkyl-2-oxazoline) brush surfaces for adherent lung cell lines. *Biomaterials* **61**, 26-32, doi:10.1016/j.biomaterials.2015.04.059 (2015).

243 Oleszko, N. *et al.* Crystallization of Poly(2-isopropyl-2-oxazoline) in Organic Solutions. *Macromolecules* **48**, 1852-1859, doi:10.1021/ma502586x (2015).
244 Shive, M. S. & Anderson, J. M. Biodegradation and biocompatibility of PLA and PLGA microspheres. *Adv Drug Deliv Rev* **28**, 5-24, doi:10.1016/s0169-409x(97)00048-3 (1997).
245 Wan, Y. *et al.* Characterization of surface property of poly(lactide-co-glycolide) after oxygen plasma treatment. *Biomaterials* **25**, 4777-4783, doi:10.1016/j.biomaterials.2003.11.051 (2004).
246 Stobener, D. D., Hoppensack, A., Scholz, J. & Weinhart, M. Endothelial, smooth muscle and fibroblast cell sheet fabrication from self-assembled thermoresponsive poly(glycidyl ether) brushes. *Soft Matter* **14**, 8333-8343, doi:10.1039/c8sm01099d (2018).
247 Luo, J. *et al.* Inducing Macrophages M2 Polarization by Dexamethasone Laden Mesoporous Silica Nanoparticles from Titanium Implant Surface for Enhanced Osteogenesis. *Acta Metall Sin-Engl* **32**, 1253-1260, doi:10.1007/s40195-019-00926-y (2019).
248 Kaur, G. & Dufour, J. M. Cell lines: Valuable tools or useless artifacts. *Spermatogenesis* **2**, 1-5, doi:10.4161/spmg.19885 (2012).
249 Yamato, M., Kushida, A. & Okano, T. [Cell adhesion and detachment control toward cell sheet engineering utilizing temperature-responsive intelligent culture dishes]. *Tanpakushitsu Kakusan Koso* **45**, 1766-1772 (2000).

Appendix

A1. Abbreviations

^{1}H NMR	Proton nuclear magnetic resonance
2D	2-dimensional
3D	3-dimensional
AM	Additive manufacturing
ATP	Adenosine triphosphate
BSA	Bovine serum albumin
CD	Cluster of differentiation
CD_3CN	Deuterated acetonitrile
$CDCl_3$	Deuterated chlorofom
cDNA	Copy/complementary deoxyribonucleic acid
CO_2	Carbon dioxide
CytoD	Cytochalasing D
DAPI	4’,6-diamidino-2-phenylindole
DEX	Dexamethasone
DLP	Digital light processing
DMEM	Dulbecco’s Modifiend Eagle’s Medium
DMF	Dimethylformamide
DSC	Differential scanning calorimetry
ECM	Extracellular matrix
EDTA	Ethylenediaminetetraacetic acid
EGF	Epidermal growth factor
FCS	Fetal calf serum
FDA	Food and Drug Administration
FRESH	Freeform reversible embedding of suspended hydrogels
GelMA	Gelatin-methacryloyl
GPC	Gel permeation chromatography
HEPES	(4-(2-hydroxyethyl)-1-piperazineethanesulfonic acid)
HMEC-1	Human microvasular endothelial cell line

hMSCs	Human mesenchymal stem cells
HUVECs	Human umbilical vein endothelial cells
IL	Interleukin
L929	Murine fibroblast cell line
LatA	Latrunculin A
LCST	Lower Critical Solution Temperature
MeTos	methyl *p*-toluenesulfonate
MEW	Melt Electrowriting
PBS	Phosphate buffered saline
PCL	Polycaprolactone
P*cyclo*PrOx	Poly(2-*cyclo*propyl-2-oxazoline)
PEG	Polyethylenglycol
PEO	Polyethylene oxide
P*i*PrOx	Poly(2-*iso*propyl-2-oxazoline)
PLGA	Poly(lactid-co-glycolid)
PMMA	Polymethylmethacrylate
PNIPAM	Poly(N-isopropylacrylamide)
P*n*PrOx	Poly(2-*n*propyl-2-oxazoline)
POx	Poly(2-oxazoline)s
PS	Polystyrene
PVAc	Polyvinyl acetate
qPCR	Quantitative real-time polymerase chain reaction
RNA	Ribonucleic acid
RT	Room temperature
SEM	Scanning electron microscopy
SES	Solution electrospinning
SLA	Stereolithography
SLATE	Stereo Lithography Apparatus for Tissue Engineering
Tg	Glass transition temperature
TGF-β1	Transforming growth factor-beta 1
TNF-α	Tumor necrosis factor-alpha

UCST	Upper Critical Solution Temperature
UV	Ultraviolet
VE-Cadherin	Vascular endothelial cadherin
VEGF	Vascular endothelial growth factor

A.2 G-codes

Chapter 4:

```
G17 G21 G40 G49 G54 G80 G94 G91
m98 p1
m98 p6 l2
m98 p7
m30

o1
g1 x-10.000      y-10.000    f1500
g1 p1
m99

o2
g1   x-10.000    y0          f1500
g1   x0          y-0.250     f300
g1   x10.000     y0          f1500
g1   x0          y-0.250     f300
m99

o3
g1   x-10.000    y0          f1500
m99

o4
g1   x0          y10.000     f1500
g1   x0.250      y0          f300
g1   x0          y-10.000    f1500
g1   x0.250      y0          f300
m99

o5
g1   x0          y10.000     f1500
m99

o6
m98 p2 l20
m98 p3
m98 p4 l20
m98 p5
m99

o7
g1 x10.000       y-10.000    f1500
m99

o8
```

```
g4 p1
g1 x0.000      y5.000     f1500
g1 x-15.000     y0.000     f1500
g1 x0.000      y105.000     f1500
m99
```

Chapter 5:

```
G17 G21 G40 G49 G54 G80 G94 G91

m98 p1
m98 p2 l20
m98 p3


m30

o1
g1  x-5.000    y0         f300
m99

o2
g1  x0.000     y5.000      f300
g1  x1.500     y1.000      f300
g1  x0.000     y1.000      f300
g1  x-1.500    y1.000      f300
g1  x0.000     y5.000      f300

g1  x0.000     y-5.000     f300
g1  x-1.500     y-1.000      f300
g1  x0.000     y-1.000      f300
g1  x1.500     y-1.000      f300
g1  x0.000     y-5.000      f300

g1  x-4.000    y0         f300
m99


o3
g1  x0.000     y13.000     f300
g1  x85.000    y0.000      f1000
g1  x0.000     y7.000      f300
m99

G17 G21 G40 G49 G54 G80 G94 G91

m98 p1
m98 p2 l6
m98 p3
```

```
m30

o1
g1  x-5.000    y0        f300
m99

o2
g1  x-3.000    y0        f300
g1  x-1.000    y3.500    f300
g1  x-2.000    y0        f300
g1  x-0.000    y2.000    f300
g1  x-2.000    y0        f300
g1  x-0.000    y1.000    f300
g1  x-2.000    y0        f300
g1  x-0.000    y-1.000   f300
g1  x-2.000    y0        f300
g1  x-0.000    y-2.000   f300
g1  x-2.000    y0        f300
g1  x-1.000    y-3.500   f300
g1  x-3.000    y0        f300
g4 p0.5

g1  x3.000     y0        f300
g1  x1.000     y3.500    f300
g1  x2.000     y0        f300
g1  x0.000     y2.000    f300
g1  x2.000     y0        f300
g1  x0.000     y-1.000   f300
g1  x2.000     y0        f300
g1  x0.000     y1.000    f300
g1  x2.000     y0        f300
g1  x0.000     y-2.000   f300
g1  x2.000     y0        f300
g1  x1.000     y-3.500   f300
g1  x3.000     y0        f300
g4 p0.5


g1  x-3.000    y0        f300
g1  x-1.000    y3.500    f300
g1  x-2.000    y0        f300
g1  x-0.000    y-2.000   f300
g1  x-2.000    y0        f300
g1  x-0.000    y1.000    f300
g1  x-2.000    y0        f300
```

```
g1  x-0.000   y-1.000    f300
g1  x-2.000   y0        f300
g1  x-0.000   y2.000    f300
g1  x-2.000   y0        f300
g1  x-1.000   y-3.500    f300
g1  x-3.000   y0        f300
g4 p0.5

g1  x3.000    y0        f300
g1  x1.000    y3.500     f300
g1  x2.000    y0        f300
g1  x0.000    y-2.000     f300
g1  x2.000    y0        f300
g1  x0.000    y-1.000     f300
g1  x2.000    y0        f300
g1  x0.000    y1.000    f300
g1  x2.000    y0        f300
g1  x0.000    y2.000    f300
g1  x2.000    y0        f300
g1  x1.000    y-3.500    f300
g1  x3.000    y0        f300
g4 p0.5



g1  x-3.000   y0        f300
g1  x-1.000   y-3.500     f300
g1  x-2.000   y0        f300
g1  x-0.000   y2.000     f300
g1  x-2.000   y0        f300
g1  x-0.000   y1.000     f300
g1  x-2.000   y0        f300
g1  x-0.000   y-1.000    f300
g1  x-2.000   y0        f300
g1  x-0.000   y-2.000    f300
g1  x-2.000   y0        f300
g1  x-1.000   y3.500    f300
g1  x-3.000   y0        f300
g4 p0.5

g1  x3.000    y0        f300
g1  x1.000    y-3.500     f300
g1  x2.000    y0        f300
g1  x0.000    y2.000     f300
g1  x2.000    y0        f300
g1  x0.000    y-1.000     f300
g1  x2.000    y0        f300
```

```
g1  x0.000    y1.000    f300
g1  x2.000    y0        f300
g1  x0.000    y-2.000   f300
g1  x2.000    y0        f300
g1  x1.000    y3.500    f300
g1  x3.000    y0        f300
g4 p0.5


g1  x-3.000   y0        f300
g1  x-1.000   y-3.500   f300
g1  x-2.000   y0        f300
g1  x-0.000   y-2.000   f300
g1  x-2.000   y0        f300
g1  x-0.000   y1.000    f300
g1  x-2.000   y0        f300
g1  x-0.000   y-1.000   f300
g1  x-2.000   y0        f300
g1  x-0.000   y2.000    f300
g1  x-2.000   y0        f300
g1  x-1.000   y3.500    f300
g1  x-3.000   y0        f300
g4 p0.5

g1  x3.000    y0        f300
g1  x1.000    y-3.500   f300
g1  x2.000    y0        f300
g1  x0.000    y-2.000   f300
g1  x2.000    y0        f300
g1  x0.000    y-1.000   f300
g1  x2.000    y0        f300
g1  x0.000    y1.000    f300
g1  x2.000    y0        f300
g1  x0.000    y2.000    f300
g1  x2.000    y0        f300
g1  x1.000    y3.500    f300
g1  x3.000    y0        f300
g4 p0.5

g1  x0        y-15.000  f300
m99

o3
g1  x-20.000  y0        f300
g1  x0        y90.000   f300
m99
```

A.4 Publications and conference contributions

Publications

Matthias Ryma, Julia Blöhbaum, Raminder Singh, Ana Sancho, Jasmin Matuszak, Iwona Cicha, and Jürgen Groll, Easy-to-Prepare Coating of Standard Cell Culture Dishes for Cell-Sheet Engineering Using Aqueous Solutions of Poly(2-n-propyl-oxazoline), ACS Biomaterials Science & Engineering, Volume 5, Issue 3/ 1509–1517/2019

Oral presentations

- **Matthias Ryma**, Julia Blöhbaum, Jürgen Groll, Easy-to-prepare Poly(2-n-propyl-oxazoline) coatings of standard cell culture dishes from aqueous solutions for cell sheet engineering, Annual meeting of the German Society for Biomaterials (DGBM), 2017, Würzburg, Germany
- **Matthias Ryma**, Julia Blöhbaum, Christoph Böhm, Hatice Genc, Paul Dalton, Iwona Cicha, Jürgen Groll, Prevascularization of Tissue Engineered Constructs via Melt Electrowriting of Thermoresponsive Poly(2-Oxazoline)s, International Society for Biofabrication 2018, Würzburg, Germany
- **Matthias Ryma**, Tina Tylek, Julia Blöhbaum, Robin Fernandez, Jürgen Groll, Melt-Electrowritten 3D Scaffolds Based on Aligned Nano-Structured Microfibers for Topography-Mediated Immunomodulation of Human Macrophages, 30th Annual Conference of the European Society for Biomaterials in tandem with the 26th Annual Conference of the German Society for Biomaterials (DGBM), Dresden, Germany

Poster Presentations

Matthias Ryma, Julia Blöhbaum, Raminder Singh, Ana Sancho, Jasmin Matuszak, Iwona Cicha, Jürgen Groll, Aqueous Solutions of Poly(2-n-propyl-oxazoline): An Easy-to-prepare Coating of Standard Cell Culture Dishes for Cell Sheet Engineering, TERMIS 2018, Kyoto, Japan

A.5 Acknowledgement/Danksagung

Zunächst möchte ich Prof. Dr. Jürgen Groll danken, dass ich meine Dissertation am Lehrstuhl für Funktionswerkstoffe der Medizin und Zahnheilkunde absolvieren konnte. Die Interdisziplinarität am Lehrstuhl hat mich dazu gebracht, über den biologischen Tellerrand zu blicken und mir ein sehr breit gefächertes Wissen von 3D-Druck bis hin zur Polymerchemie und 3D-Zellkultur anzueignen. Besonders das eigenverantwortliche Forschen und Arbeiten hat mir Spaß gemacht.

Weiterhin möchte ich meinen Kollegen am gesamten Lehrstuhl danken.

Zunächst der Chefebene, der den gesamten Laden managed und sich im Laufe meiner Doktorarbeit sehr positiv enwickelt hat. An dieser Stelle möchte ich auch für die Möglichkeit danken, dass ich am Pontea Seminar teilnehmen konnte.

Als Nächstes möchte ich den Chemikern für ihre Unterstützung danken, besonders Julia Blöhbaum und Ilona Paulus, die mir immer wieder Material für meine Experimente zur Verfügung gestellt haben.

Außerdem danke ich allen aus der Biofabrikation für die Unterstützung beim MEW. Besonders hervorheben möchte ich den Trashtalk, der ohne Ali Nadernezhad und Christoph Böhm nicht möglich gewesen wäre.

Besonderen Dank verdient auch die Biogruppe. Vor allem möchte ich Katrin Schlegelmilch, Tina Tylek und Carina Blum danken, die mich vom Anfang bis zum Ende meiner Doktorarbeit begleitet haben und deren Gesellschaft mich immer wieder erfreute.

Vielen Dank an meine Freundin Kristina Andelovic, die mir während meiner Doktorarbeit immer wieder mit Rat und Tat zur Seite stand, und ohne die ich nie soweit gekommen wäre. Obwohl es manchmal nicht einfach mit mir sein kann, hast du zu mir gehalten und mein Leben sowohl beruflich, als auch privat sehr bereichert. Danke Maus! <3

Zuletzt möchte ich noch meiner Familie danken, die mir alle Möglichkeiten meiner beruflichen Karriere eröffnet hat. Danke Mama, Papa und Brudi für eure Unterstützung in allen Lebenslagen! Ich bin sehr froh, dass ich immer auf euch zählen kann! <3

A.6 Affidavit

I hereby confirm that my thesis entitled “Exploiting the Thermoresponsive Properties of Poly(2-oxazoline)s for Biofabrication” is the result of my own work. I did not receive any help or support from commercial consultants. All sources and / or materials applied are listed and specified in the thesis.

Furthermore, I confirm that this thesis has not yet been submitted as part of another examination process neither in identical nor in similar form.

Place, Date Signature

A.7 Eidesstattliche Erklärung

Hiermit erkläre ich an Eides statt, die Dissertation „Anwendung der Thermoresponsivität von Poly(2-oxazolin) für die Biofabrikation“ eigenständig, d.h. insbesondere selbständig und ohne Hilfe eines kommerziellen Promotionsberaters, angefertigt und keine anderen als die von mir angegebenen Quellen und Hilfsmittel verwendet zu haben.

Ich erkläre außerdem, dass die Dissertation weder in gleicher noch in ähnlicher Form bereits in einem anderen Prüfungsverfahren vorgelegen hat.

Ort, Datum Unterschrift